The Dissertation Committee for Rasha Huntoon El-Jaroudi
certifies that this is the approved version of the following dissertation:

III-V Optoelectronic Devices in the BGaInAs Material System

Committee:

Seth Bank, Supervisor

Ananth Dodabalapur

Tanya Hutter

Daniel Wasserman

Edward Yu

III-V Optoelectronic Devices in the BGaInAs Material System

by

Rasha Huntoon El-Jaroudi

Dissertation

Presented to the Faculty of the Graduate School of

The University of Texas at Austin

in Partial Fulfillment

of the Requirements

for the Degree of

Doctor of Philosophy

The University of Texas at Austin

December 2021

In memory of my strong-willed and fiercely-independent grandmothers, Afaf AbdelAziz and Zelma Huntoon.

Acknowledgments

I would like to sincerely thank my PhD supervisor, Dr. Seth Bank for his guidance, support, and encouragement through out my PhD process. My previous research experiences as a co-op student at the Georgia Teach RNOC, an REU at the University of New Hampshire, and a Fulbright fellow at Masdar Institute prepared me well for my PhD studies and I will be forever indebted to my many advisors, Dr. Russ Clark, Matt Sanders, Siva Jayaraman, Brian Davidson, and Dr. Ron Hutchins at Georgia Tech, Dr. Brian Calder at UNH, and Dr. Prashanth Marpu at Masdar Insitute.

I will be forever grateful for the hard work and support of LASE group members past and present. Many past group members have answered my calls when I had questions about the MBEs or needed advice navigating the PhD process including Erica (Krivoy) Davis and Rodolfo Salas. Thank you to Scott Sifferman, Nate Sheehan, Emily Walker, A.K. Rockwell, Stephen March, Qian Meng, Andrew McArthur, Corey White, Aaron Muhowski, Morgan Bergthold, Amberly Ricks, and Ellie Wang for their help maintaining the MBE systems. I am especially appreciative of Alec Skipper and Ashlee García who helped maintain Echo and put up with re-configuring Echo every maintenance we did together. Thank you to Dan Ironside and Kyle McNicholas for instilling in me a “healthy" paranoia towards the MBE systems. In addition Dan has been crucial in answering all of my very specific questions about solid-state engineering, best wind conditions for paddling Town Lake, and cats. I obviously have to acknowledge Kyle for the strong foundational knowledge of BGaAs growth he established in the group. I am also thankful for his guidance in safely maintaining Echo, safely maintaining and operating the boron e-beam, and safely using knives. I would not be the crystal grower, the Ohio State fan, nor the bourbon snob I am today without him. Thank you Andrew Briggs for being tall. But also thank you for your endless optimism, helping me with device fabrication, and being a patriots/TB12 fan. Lastly, thank you to my favorite LASE group member Leland Nordin for always being down for anything, whether it was lending a hand in non-standard maintenance or Austin adventures including ACL, SXSW, and anywhere there was free food, as well

as for introducing me to some of my now favorite things like good coffee, craft beer, and climbing.

I had the privilege of working with amazing collaborators through my work. I would like to thank Professor Robert Kudrawiec and his group for detailed PR measurements and analysis, especially Herbert Mączko. Additionally, I would like to thank Professor Joe Campbell's group for their photodiode fabrication and testing. I have enjoyed working with and learning from Andrew Jones and Adam Dadey. Professor Larry Lee's group proved critical in providing growth advice. I also am thankful for the hard work of the UVA Dev Hub, specially Nadim El-Jaroudi, G. Michael Fitzgerald, and Nathaniel Irwin who were willing to revamp the LASE database.

None of this work would have been completed without my extensive support system, and I am endlessly grateful to my friends and family for all of their patience and understanding over the past five years. I am so lucky to have such "fun" parents, as well as a brother and grandfather who are never boring. Finally, I would like to thank my fiancé and our cat, Pierogi, for their equal contribution to the work in this thesis.

University of Texas Land Acknowledgement

I would like to acknowledge that this work was completed on the Indigenous lands of Turtle Island, the ancestral name for what now is called North America. Moreover, I would like to acknowledge the Alabama-Coushatta, Caddo, Carrizo/Comecrudo, Coahuiltecan, Comanche, Kickapoo, Lipan Apache, Tonkawa and Ysleta Del Sur Pueblo, and all the Indigenous Peoples and communities who have been or have become a part of these lands and territories in Texas.

III-V Optoelectronic Devices in the BGaInAs Material System

Publication No. _____

Rasha Huntoon El-Jaroudi, Ph.D.
The University of Texas at Austin, 2021

Supervisor: Seth Bank

In this work, we investigate the potential of direct-bandgap, III-V materials for lattice-matched absorbers and emitters on silicon. Leveraging the small lattice constant of the boron pnictides, BGaInAs can be grown lattice-matched or nearly lattice-matched to Si; however, the difficult growth mechanics of elemental boron and the highly mismatched nature of BGaInAs have limited prior synthesis of this alloy to compositions outside those required for lattice-matched growth on Si and outside of technologically interesting wavelengths. Therefore, this work focuses on BGaInAs growth on GaAs. Focusing on GaAs reduces the simultaneous amount of boron and indium required to maintain lattice-matching or near lattice-matching as compared to Si. Here, we exploit the non-equilibrium growth properties of molecular beam epitaxy to simultaneously increase the incorporation of boron and indium - enabling the longest wavelength emission from BGaInAs, the first boron-containing active region electrically injected emitter, and all-BGaInAs photodetectors.

Our approach is the optimization of BGaInAs on GaAs, focusing on further extending emission wavelengths and increasing B, In concentrations in lattice-matched detectors in order to develop understanding of how increasing B concentrations (and requisite In concentrations) affect BGaInAs-based devices, thus providing a path towards lattice-matched optoelectronic devices on Si.

Contents

List of Figures

Chapter 1

Introduction

The realization of novel optoelectronic devices to address new application demands or reduce cost and increase manufacturing throughput of existing applications is often limited by fundamental material properties. Heteroepitaxy facilitates flexible device design, enabling a wide-range of applications. Devices are designed by integrating layers of varying alloy compositions and thicknesses to engineer the bandstructure of the material and meet the application demands. However, these designs are limited by the miscibility of alloys and the amount of strain that can be accommodated without incorporating device-killing defects. The investigation of new materials can overcome existing limitations in heteroepitaxial growth enabling new devices, which reduce the cost of existing applications and enable new applications. Similarly, the advancement of growth techniques to overcome miscibility gaps can extend the applicability of optoelectronic devices. This work focuses on one such material system, B-III-V alloys, and the process through which growth advancement can overcome previous limitations to realize new devices. These growth advancements have demonstrated the highest simultaneous incorporation of boron and indium in BGaInAs on GaAs and InP, the first light emitting diodes with a boron-containing active region, and the first all-BGaInAs photodiodes.

1.1 Lattice mismatch and epitaxial strain

The epitaxial integration of materials with different atomic spacing, or lattice constants, results in the introduction of strain as the atomic lattice of the epitaxial layer is distorted to that of the underlying substrate. Strain affects both the crystal quality and the band structure of the epitaxial layer. Therefore, the heterointegration of materials can be fundamentally limited by the

lattice-mismatch strain. This work focuses on the use of semi-infinite substrates, which is typical for semiconductor device growth. When growing on a semi-infinite substrate, the substrate is approximated as an infinitely thick layer, thus the atomic spacing of the epitaxial layer will be strained to match that of the substrate and the lattice-mismatch strain is accommodated by the epitaxial layers. This is a good approximation because substrates are on the order of $\sim$ 0.5 mm thick, while epitaxial layers are typically $\sim$ 1 μm thick. A few models describe the critical thickness of a material integrated on another material with a different lattice constant, which is the thickest a layer will remain strained to the substrate before the onset of plastic deformation or "relaxation". These models include Matthews-Blakeslee [1] and People and Bean [2]. Matthews-Blakeslee defines the critical thickness based on mechanical equilibrium, while People and Bean define the critical thickness based on energy equilibrium [1], [2]. In molecular beam epitaxy (MBE) growth, it is often observed that the theoretical critical thickness can be exceeded as shown in Figure 1.1 [3]. The oft-used example is the growth of AlAs on GaAs, where there is a small lattice mismatch but practically, an infinite amount of AlAs can be grown on GaAs without relaxation. The chosen method for measuring critical thickness can change the observed critical thickness. For example, X-ray diffraction (XRD) measures the average crystal composition and is less sensitive to relaxation than a more direct measurement of crystal quality or defects such as luminescence efficiency. As such an epitaxial layer may appear to be coherently strained in XRD, but a reduction in or loss of optical quality would suggest defect incorporation from strain relaxation.

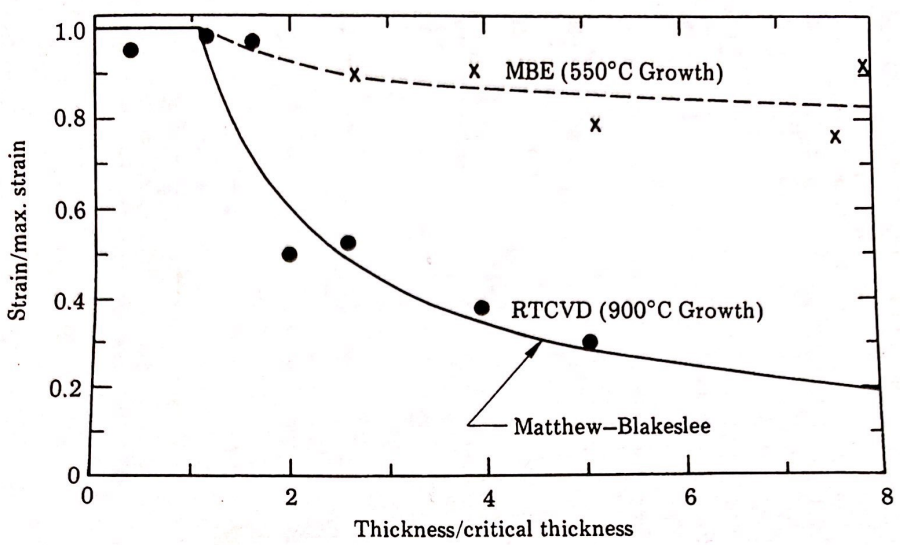

Figure 1.1: MBE growth can exceed critical thickness limit defined theoretically by Matthews-Blakeslee and experimentally by high temperature rapid-thermal chemical vapor deposition (RT-CVD) as shown in Ge_xSi_{1-x} films. Reproduced from [3]

As the strain increases, relaxation occurs through the formation of defects such as misfit and threading dislocations and misfit arrays increase. In practice, this limits mismatch strain to $< 1\%$ for layers thicker than ~ 100 nm. Figure 1.2 shows the bandgap and lattice constant of conventional III-V alloys. Commercially available substrates are highlighted in red and the approximate amount of strain that can be accommodated on these substrates is highlighted in gray. The amount of strain that can be accommodated has implications for the realization of optoelectronic devices as the integration of devices is limited to those with similar lattice constants. Additionally, local strain caused by the differences in the bond length of the atoms present in quaternary alloys can lead to local composition modulation [4]. This phenomenon was predicted from theory in dilute-nitride alloys [4] and has been observed experimentally [5].

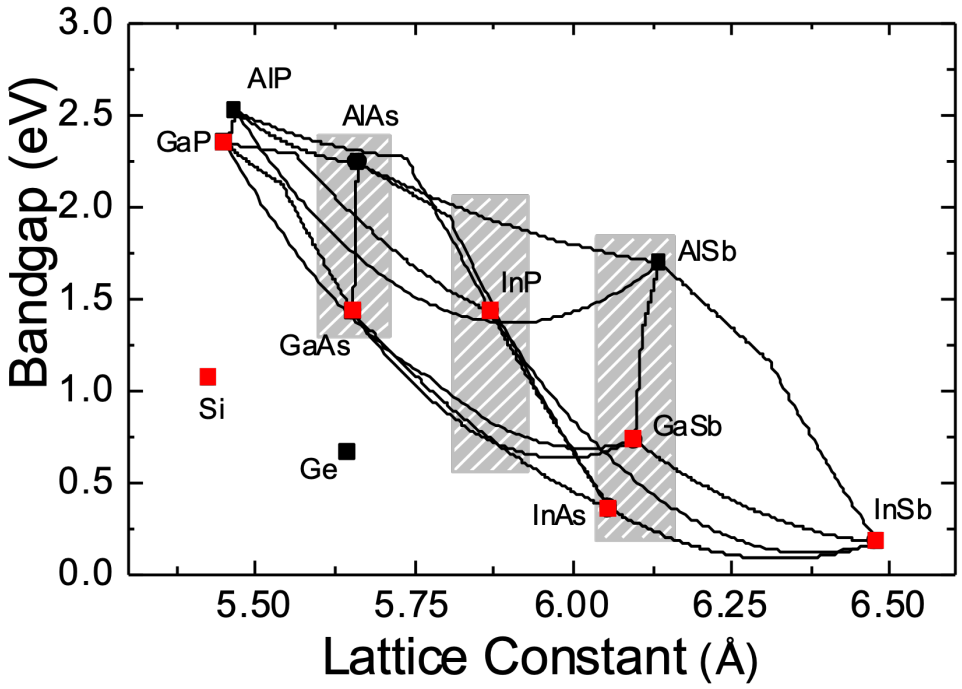

Figure 1.2: Bandgap versus lattice constant of conventional III-V materials. The gray boxes represent the approximate amount of lattice-mismatch that can be accommodated while maintaining high-quality coherently-strained films.

An additional consideration in heteroepitaxial growth is the effect of strain in the epitaxial layer on the band structure of the alloy as compared to the unstrained alloy, resulting in a change not only in the bandgap but also in the shape of the band edges. For example, in laser-related applications, the use of compressively strained QWs is preferred due to the beneficial change in valance band edge shape that increases hole confinement.

1.2 III-V optoelectronic devices

As shown in Figure 1.2, the fundamental band gaps of the III-V alloys cover a wide-range of wavelengths making them the ideal choice for optoelectronic devices across many applications. However, the large disparity in lattice-constant prevents arbitrary integration of these alloys for heterostructure device design. Furthermore, the bandgap type (direct or indirect) and band offset with respect to other materials in heteroepitaxial integration (type-I, type-II, type-III) complicate

heterostructure device design. These design limitations increase device cost, decrease device yield and ease of manufacturing and in some cases, completely prohibit the realization of devices with applications spanning telecommunications, quantum computing, and LiDAR.

1.2.1 Si-based III-V optoelectronic devices

A major limitation in the realization of inexpensive, efficient devices is the difficulty in integrating III-V optoelectronic devices with silicon. Si-based devices form the backbone of the current microelectronic infrastructure, as a result of their robust, high-yield and reliable fabrication and manufacturing processes. However, Si is a poor light emitter and absorber due to its indirect bandgap. The large difference in lattice constant between the conventional III-V alloys used for optoelectronic devices and Si results in defects as previously described. For this reason the monolithic integration of III-V materials on Si continues to be largely impractical for device design.

Photonic-integrated circuits (PICs) on Si will be essential for realizing smaller more efficient microelectronics; however, the realization of low-cost, high-performance Si PICs requires the integration of both lasers and photodetectors on Si. Furthermore, the monolithic integration of direct-bandgap materials on Si will enable high performance devices for applications beyond PICs including large-area photodetectors at eye-safe wavelengths expanding applications to self-driving cars, topological mapping, defense, and augmented reality.

Photonic-based quantum computing systems have emerged as an advantageous approach to quantum computing compared to other systems due to the large bandwidth for high data transmission capacity, high speed operation and the lack of requirement for vacuum or cooling systems [6]. Additionally, photonic quantum computers can capitalize on robust existing manufacturing technologies and ability to create photonic quantum states. For example, Kang *et al.* has demonstrated InP-based two polarization-entangled sources from a single chip [7]. However, key challenges remain limiting the realization of large-scale optical quantum computers, namely, the availability of high performance devices lattice-matched to Si.

The development of energy efficient devices has been crucial to avoiding the predicted doubling in data center energy usage to accommodate increased demand over the past decade [8], [9]; however, cooling and high power loss in the electrical links still account for significant energy usage [10], [11]. If the high power loss electrical links currently required to send information in Si-based devices were replaced with optical interconnects, smaller, more efficient devices could be realized [11]. Similarly, single-chip 2 μm LIDAR incorporating both light sources and single photon detectors

could overcome current limitations imposed by the use of Ge on Si [12].

1.2.2 GaAs-based devices

Near-infrared (NIR, 1-3 μm) emitters and detectors are important for a wide range of high-volume applications, such as telecomunications, optical data transmission in data centers, multi-junction solar cells, LiDAR, and facial recognition. GaAs-based devices are an obvious choice for these applications due to the low-cost and commerical availability of large GaAs substrates available. Additionally, GaAs-based vertical cavity surface-emitting lasers (VCSELs) offer the potential for a high manufacturing and testing throughput solution as they leverage the monolithic integration of AlGaAs-GaAs distributed Bragg reflectors and AlO_x native oxide technologies. However, few NIR active regions are available lattice-matched or nearly lattice-matched to GaAs. Existing NIR lasers for telecommunications have been demonstrated at 1.3 μm utilizing In(Ga)As quantum dots [13] or InGaNAs [14] active regions. InGaNAs lasers at 1.55 μm have also been demonstrated [15]. Unfortunately, the challenging growth of dilute-nitride alloys, as discussed in Section 2.2, has limited wide-spread commercial-availability of these devices.

1.2.3 Low-noise III-V avalanche photodiodes

Many of the applications operating in the near infrared, such as data centers, LiDAR, and telecommunications, require high sensitivity and high bandwidth photodetectors. Currently these applications are covered by the wide spectral range of III-V alloys. Solid-state photon detectors are typically p-n or p-i-n junctions, which operate under reverse bias. The photogenerated minority carriers then drift or diffuse into a high-field depletion region. Under moderate reverse bias, the photoresponse is proportional to the incident light; however, under larger reverse biases, the carriers impact ionize leading to internal avalanche multiplication gain, which can enable fast, high sensitivity avalanche photodiodes (APDs). Unfortunately, under these large reverse biases, the noise in the devices typically increases with increasing multiplication gain due to the stochastic nature of impact ionization. The additional noise from multiplication gain is commonly reported as the excess noise factor using the McIntyre noise model [16]. The excess noise factor versus multiplication gain for III-V alloys and other common APD materials is shown in Figure 1.4 [17]; most III-V materials have large excess noise factors, with InAs, which has an excess noise factor comparable to HgCdTe, being the most notable exception. Low-noise avalanche photodiodes have intrinsic material properties or epitaxial layer structure design that suppress hole or electron impact ionization allowing for higher

gains with less noise.

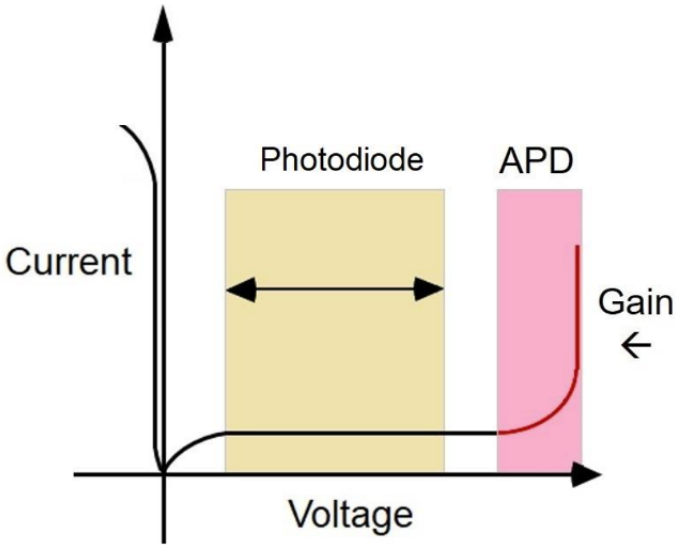

Figure 1.3: The current-voltage characteristics for p-i-n junction. While under moderate reverse biases, the p-i-n junctions behave as photodiodes with unity gain (yellow region), under large reverse biases, impact ionization leads to multiplication gain and the devices behave as avalanche photodiodes (red region).

.

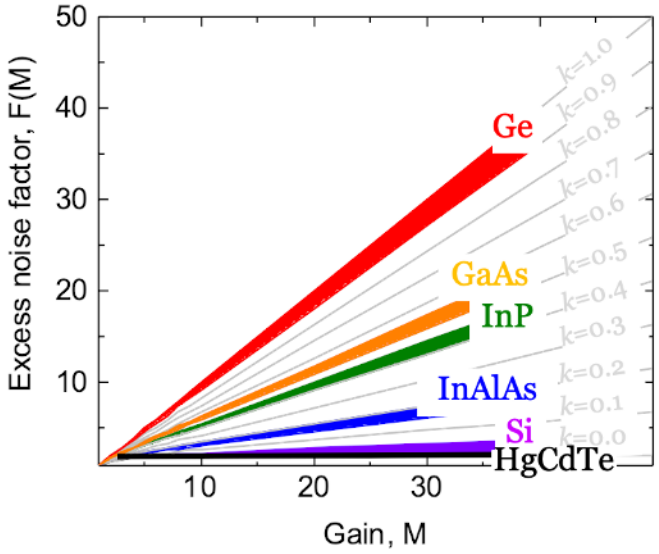

Figure 1.4: Excess noise factor versus multiplication gain for III-V alloys and common APD materials. Reproduced from [17]

.

HgCdTe is the most commonly used material for low noise APDs. HgCdTe detectors demonstrate high gain and low noise at low reverse bias [18]. However, their high cost, challenging synthesis and fabrication, as well as required cryogenic cooling complicate their use in many applications. There are few low-noise III-V alloys. The binary InAs, has low excess noise comparable to that of HgCdTe; however, its small bandgap results in high dark currents and tunneling at moderate biases, necessitating thick multiplication layers with low background carrier concentration, which have been challenging to realize [19]. Impact ionization engineering of III-V APDs has demonstrated significant reduction in device excess noise factors at the expense of limited multiplication gains [17]. Bandstructure engineering through the growth of digital alloys, or short period superlattices, has been shown to reduce excess noise in some III-V alloys, such as indium aluminum arsenide antimonide [20], but this approach is not universal and cannot be extended to all III-V alloys [21]. This work investigates B-III-V materials as a universal approach to reducing noise in avalanche photodetectors.

1.3 III-V highly-mismatched alloy-based optoelectronic devices

Alloys containing atomic constituents with large differences in size and/or electronegativity are considered highly-mismatched alloys. Highly-mismatched elements with conventional III-V alloys include boron, bismuth, and nitrogen. Dilute-bismide and dilute-nitride alloys have been more thoroughly investigated than the dilute borides. Both dilute bismides and dilute nitrides are highly mismatched in both size and electronegativity. Band anticrossing interactions in the conduction band in dilute nitrides and valence bands in the dilute bismides result in significant increase in bandgap reduction per percent incorporated mismatch constituent compared to conventional III-V alloys. This reduction in bandgap is often favorable as it extends the emission and absorption wavelength of conventional III-V alloys. In GaAs-based alloys, this reduction in bandgap increases the availability of lattice-matched or nearly lattice-matched NIR active regions. For example, the addition of Bi to GaAs results in a decrease of $\sim$ 88 meV per % Bi compared to a decrease of $\sim$ 16meV per % In [22]. However, the difficult growth mechanics of these alloys discussed in Chapter 2 have limited the amount of nitrogen or bismuth that can be incorporated and prevented their practical use in III-V optoelectronic devices.

1.3.1 Dilute-nitride GaAs-based optoelectronic devices

Dilute-nitride alloys have found application in both lasers and photodetectors. The addition of even dilute amounts ($\sim$ 1-2%) of nitrogen initially significantly reduced the optical quality, increasing the threshold current densities of the dilute nitride diode lasers [23]–[25]. However, through growth optimization, low threshold currents have been achieved in 1.5 μm InGaAsN diode lasers [23]. The demonstration of 1.55 μm VCSELs was possible with the addition of Sb as both a surfactant and alloy constituent to achieve desired device performance, but added further complications to the growth of high optical quality material [26]. Despite decades of extensive research, few dilute-nitride devices have matured to commercial products due to the complicated growth and poor reliability of the material.

Dilute-nitride alloys were also investigated for absorbing layers on GaAs. The addition of a fourth junction to GaAs and Ge -based multijunction solar cells, consisting of a lattice-matched materials with a bandgap of 1.0 eV offer comparatively increased efficiency [27]. At wider bandgaps, $\sim$ 1.15 eV, InGaAsN solar cells were demonstrated with nearly 100% internal quantum efficiency [28]. While, dilute nitride-based 1.0 eV bandgap materials require little In ($\sim$ 6-8%) due to band

anticrossing with N (only $\sim$ 2% required), similar to InGaAsN emitters, the increased nitrogen content degrades device performance [29]. Again, the material quality can be improved with the addition of antimony at higher nitrogen content [29].

1.3.2 Dilute-bismide GaAs-based optoelectronic devices

The introduction of Bi to GaAs-based alloys results in a rapid decrease per % Bi in bandgap due to band anticrossing in the valance band, analogous to the band anticrossing interaction in the conduction band with the addition of nitrogen to GaAs. However, unlike the addition of nitrogen which also decreases the lattice constant and thus decreases the lattice-mismatch of compressively strained layers with GaAs, the addition of bismuth increases the lattice constant, increasing the mismatch of compressively strained layers with GaAs. Although the challenging growth of high-quality dilute-bismide materials has increased the difficulty of realizing of Bi-III-V devices, room temperature LEDs [30]–[36] and lasers [37]–[39] have been demonstrated.

GaAs-based dilute-bismide photodetectors and photovoltaics are challenging because of the lattice-mismatch between dilute-bismide alloys and GaAs substrates. However, the lattice mismatch between $GaAs_{0.94}Bi_{0.06}$ is small and p-i-n structures showed the expected reduction in bandgap energy to almost 1 eV [40]. External quantum efficiency (EQE) measurements of GaAsBi diodes with up to 4% Bi showed a peak EQE of $< 10\%$ [41]. Despite the demonstration of dilute-bismide optoelectronics, the realization of commercially available devices is again limited by the challenging growth of these alloys as discussed in Chapter 2.

1.3.3 Highly-mismatched alloys for low-noise APDs

Highly-mismatched alloys have been investigated as alternative materials for low-noise multiplications layers in APDs. The asymmetric band anticrossing interaction (i.e. only the conduction band or the valence bands are perturbed) caused by the addition of nitrogen or bismuth has been considered as a potential avenue for reducing noise by suppressing impact ionization of one carrier type [42], [43]

In the dilute nitrides, Adams theorized that the valence band remaining unchanged with the addition of nitrogen would keep the hole impact ionization coefficient (β) unchanged, while the perturbed conduction band would increase the electron mass and electron scattering, significantly reducing the electron impact ionization coefficient (α) [42]. As shown in Figure 1.5(a), in GaInNAs APDs, the addition of 2% N resulted in no change in excess noise factor [44]. The addition of

3% and 4% nitrogen did result in a small increase in the excess noise factor of GaInNAs APDs under electron-injection, indicating that α decreased compared to β as expected. The realization of low-noise APDs under hole-injection could be possible if nitrogen incorporation increased the ratio of β to α more rapidly. However, realizing low noise dilute-nitride APDs would require higher N incorporation, such that the difficulty in incorporating N currently makes the realization of low-noise dilute-nitride APDs impractical.

Similar to the dilute nitrides, the addition of bismuth perturbs the valence band, increasing the valence band spin-orbit splitting. Liu *et al.* recently demonstrated low-noise dilute bismide APDs, where the addition of Bi suppresses hole impact ionization [45]. As expected, the electron impact ionization remained unchanged with the addition of Bi, resulting in a reduction in excess noise [45]. The reduction in noise with increasing bismuth incorporation suggests a materials solution for low noise APDs. However, the large size of the bismuth atom, which increases device strain, and difficulty in incorporating more than 5% bismuth may limit the ultimate performance of these devices. The difficulty in synthesizing the B-III-V alloys has limited the understanding of the effect of B incorporation on bandstructure and has limited the experimental measurement of the effect of B incorporation on excess noise factor in B-III-V APDs. However, Lindsay *et al.* theorized that the addition of B may decrease the excess noise in APDs through pertubation of the conduction band [43], motivating our investigation of the noise performance B-III-V APDs.

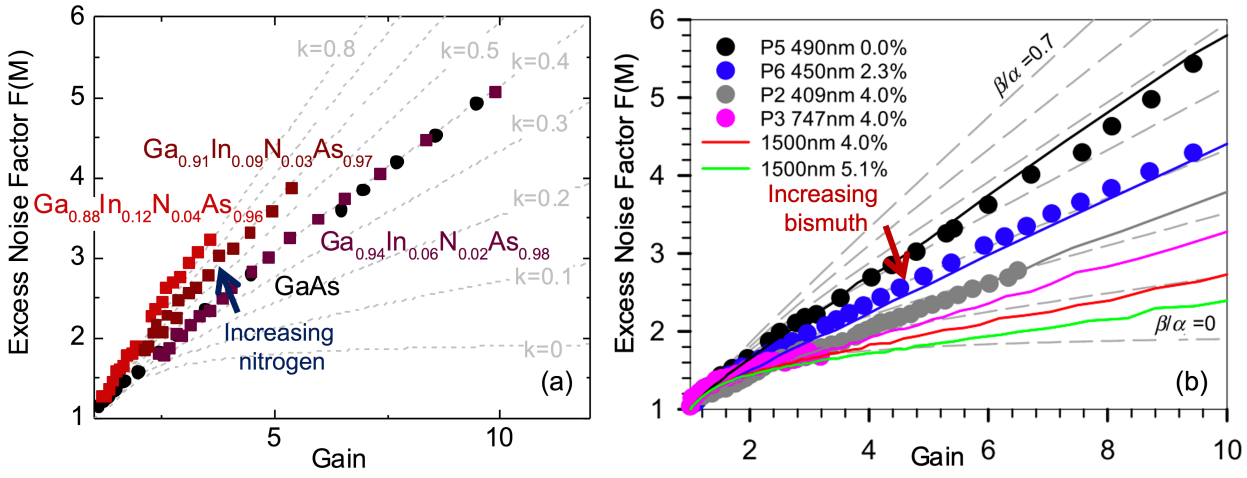

Figure 1.5: Measured excess noise factor versus multiplication gain for (a) GaInNAs [44] and (b) GaAsBi [45] avalanche photodiodes. The change in excess noise factor as nitrogen increases is too small to realize low-noise dilute-nitride APDs. The excess noise factor in GaAsBi decreased with increasing bismuth incorporation indicating a potential path to a materials-based method for low noise APDs. Reproduced from [44], [45]

1.4 Previous demonstrations of B-III-V alloys

The epitaxial growth of boron containing alloys is quite challenging due to the high melting point and low vapor pressure of boron, the thermodynamically stable sub-pnictide phase of B-V materials [46], [47], and the large lattice mismatch between B-V binaries and conventional substrates [46]. Until recently, where 18% B was demonstrated in BGaAs through optimized MBE growth [48], demonstrations of the ternary alloy BGaAs were limited to B concentrations of about $\sim$ 8% by both MOCVD [49] and MBE [50]. In BGaInAs, as with other highly-mismatched alloys, the Gibbs free-energy of mixing increases as the In and B concentrations are increased, limiting the range of thermodynamically stable alloy compositions [51]. As a result, the growth of the quaternary BGaInAs has been limited to even smaller boron concentrations, $\leq$ 4% [52]. The difficulty in synthesizing B-III-V alloys has limited the understanding of fundamental properties, (e.g. bandgap, bandbowing) even for the binary BAs. Theoretical values for the direct bandgap of the binary BAs range from 1 eV to 6 eV as shown in Figure 1.6 [53]–[63]. Therefore, there is little understanding of the effects of boron incorporation on many properties of B-III-V alloys. The significant disparity in

reported values of the BAs direct bandgap energy leads to a large variation in the predicted cutoff wavelengths available on Si and GaAs with B-III-V alloys as seen in Figure 1.7. The growth of B-III-V alloys is discussed further in Section 2.2. Recent advancements in BGaAs growth, discussed in Section 2.2 have enabled more thorough investigation of the bandgap and bandbowing of BAs and BGaAs. In collaboration with Robert Kudrawiec's group at Wroclaw University of Science and Technology, we found that the BAs direct bandgap was 5.8 eV and the BGaAs bandbowing was 3.39 [48], [64].

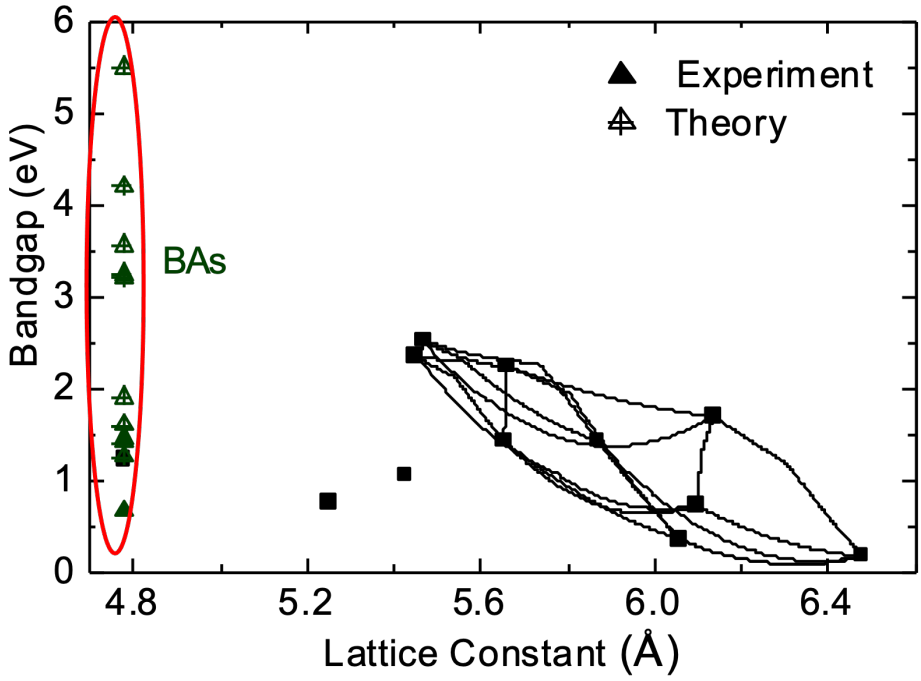

Figure 1.6: Theoretical and experimental BAs and B-III-V bandgaps. The large variation in estimated bandgaps necessitates further investigation to predict direct bandgaps available lattice-matched to Si [53]–[63]. Reproduced from [48].

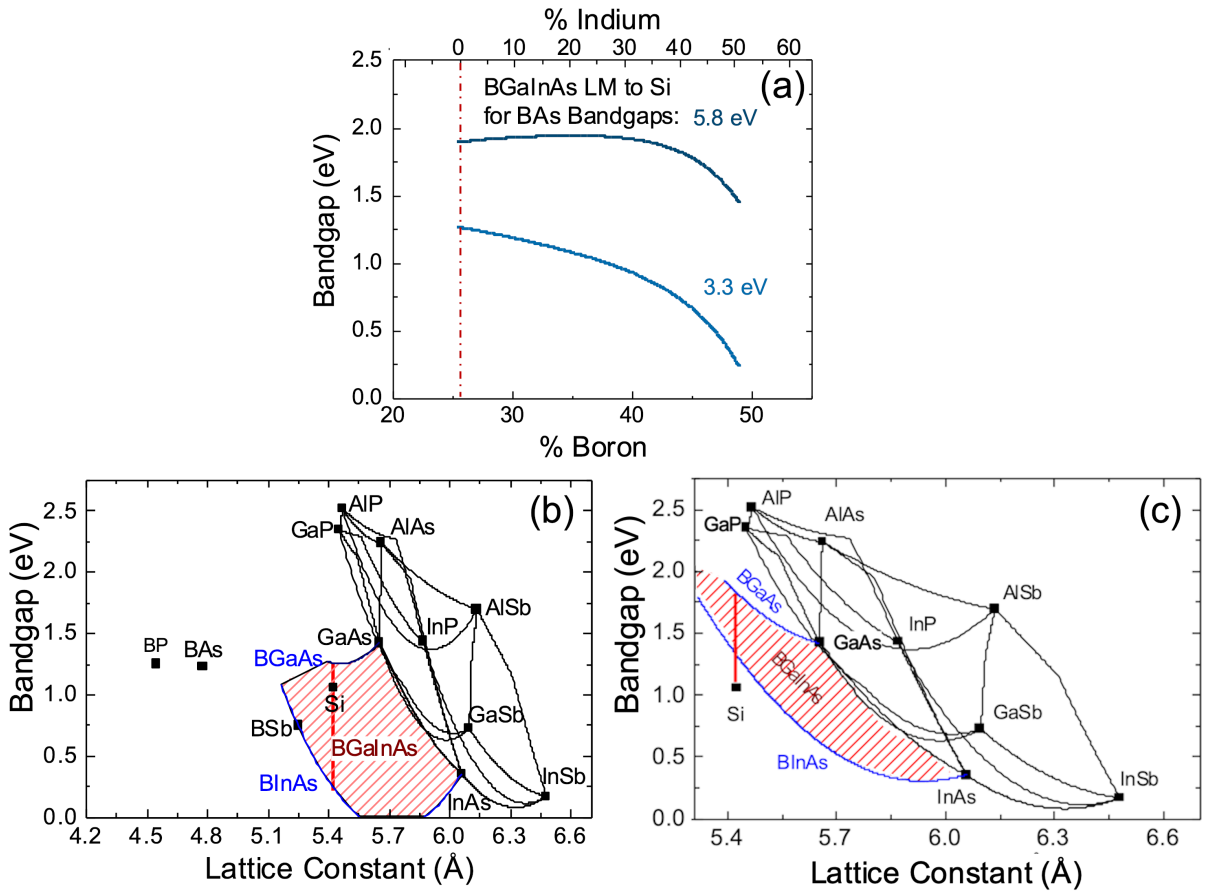

Figure 1.7: (a) Predicted BGaInAs bandgaps for lattice-matched alloy compositions on Si for a BAs bandgap of 5.8 eV (dark blue line) and 3.3 eV (light blue line).Theoretical bandgaps for BGaAInAs alloys using predicted direct bandgaps of (b) 3.3 eV and (c) 5.8 eV.

1.4.1 Previous B-III-V emitters

The potential for the realization of B-III-V emitters as sources at telecommunication wavelengths of 1.3 μm and 1.55 μm has been previously established by [52], [65]. Previous demonstration of photoluminesence from B-III-V alloys include BGaAs films [48], [60], [65]–[70], BGaInAs films and quantum wells (QW) [67], [69], [71], and BInAs quantum dots (QD) [72]. Room-temperature photoluminesence of BGaAs has been rarely reported [67]. The difficulty in simultaneously incorporating B and In in BGaInAs has limited the emission wavelength of BGaInAs QWs to < 1.2 μm, shorter than the 1.3 and 1.55 μm wavelengths required for the applications discussed in Section 1.2. Previous reports of temperature-dependent photoluminesence from BGaInAs QWs observed a deviation from the parabolic dependence of bandgap on temperature described by the Varshni equation.

Compared to an InGaAs QW of similar In concentration (Figure 1.8(a)) where the bandgap versus temperature dependence follows the relationship defined by the Varshni equation, in the bandgap versus temperature relationship of the BGaInAs QW (Figure 1.8(b)) a constant peak wavelength with decreasing temperature or even an "S-shaped" dependence have been reported [69], [73], [74]. These reports suggested the deviation from the Varshni equation resulted from the formation of B-B clusters or localized defects in the BGaInAs material [69], [73], [74]. Fortunately, this deviation is not intrinsic to the B-III-V material system, but rather innate to unoptimized growth of these materials as this work will demonstrate. Importantly, as shown in Figure 1.8(c), Wang *et al.* demonstrated improved optical quality over InGaAs control structures with the addition of B, demonstrating that the addition of B does not inherently degrade the optical quality of the material [71].

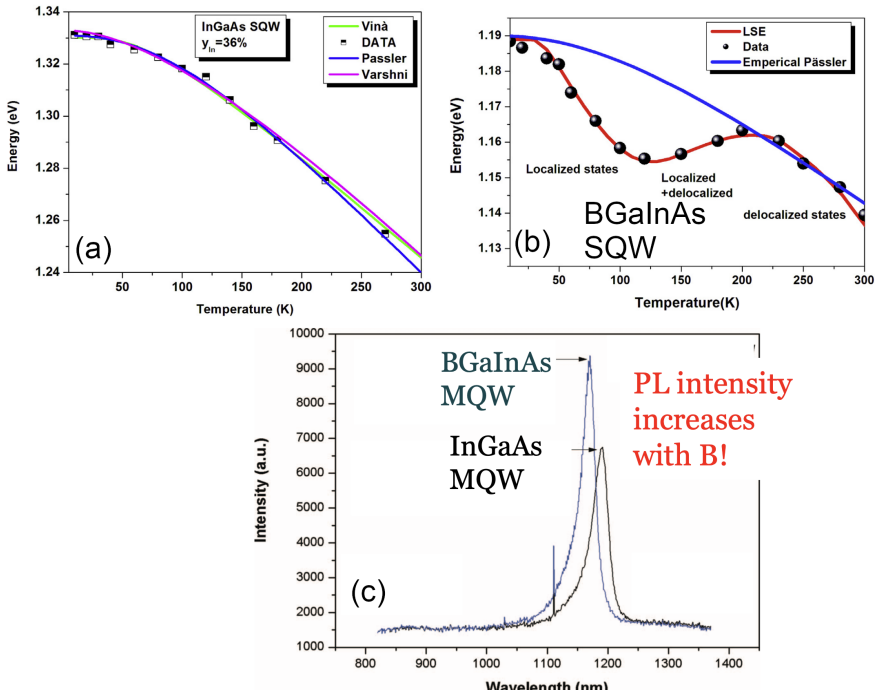

Figure 1.8: Hidouri et al. demonstrated in temperature-dependent PL that the peak energy versus temperature relationship of (a) an InGaAs QW followed the Varshni equation [73]. (b) However, a comparable BGaInAs QW demonstrated an S-shaped deviation from the Varshni equation [73]. (c) Wang *et al.* demonstrated an increase in PL intensity with the addition of B compared to a boron-free InGaAs MQW, indicating that the addition of boron does not preclude high optical quality material [71]. Reproduced from [71], [73].

1.4.2 Previous B-III-V optoelectronic devices

Geisz et al. investigated BGaInAs for the development of lattice-matched active regions in multijunction III-V solar cells [52]. The challenge in simultaneously incorporating B and In limited the achievable composition to $B_{0.03}Ga_{0.91}In_{0.06}As$, which has shorter cutoff wavelengths than the 1 eV cutoff necessary to significantly improve the efficiency of multi-junction solar cells [52]. Geisz *et al.* observed a significant decrease in the internal quantum efficiency (IQE) with the addition of boron as compared to InGaAs and GaAs photovoltaic cells as shown in Figure 1.9(a) [52]. The decrease in IQE was partially attributed to the diborane source used for the MOCVD growth [52]. McNicholas demonstrated prototype BGaAs p-i-n junctions to investigate the effect of adding boron on photodiode EQE [48]. The higher B % p-i-n junction had lower EQE as shown in Figure 1.9(b), which may be due to increased B % or defects resulting from the increase in tensile strain [48].

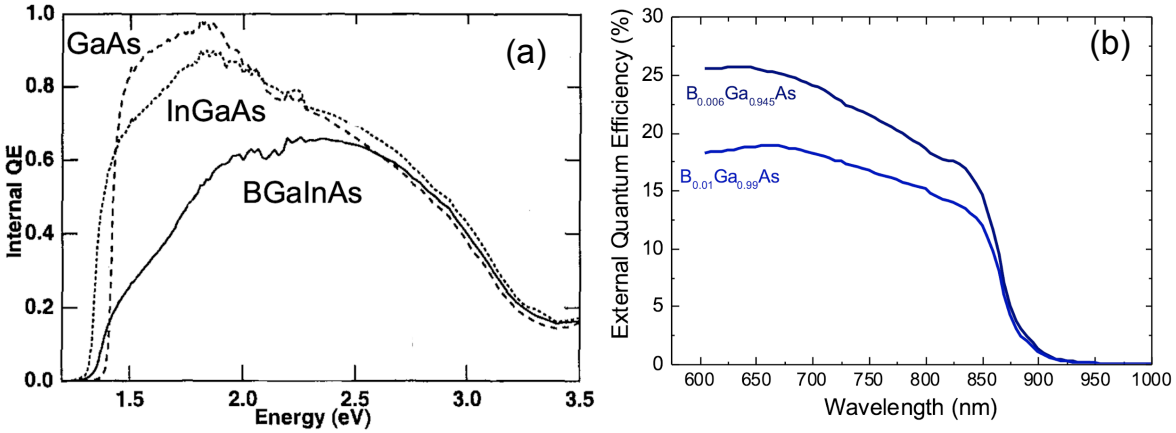

Figure 1.9: Previous investigation of B-III-V absorbing layers showed a decrease in quantum efficiency with increasing B concentrations. (a) The addition of boron severely decreased the IQE of solar cells [52]. (b) The EQE of BGaAs p-i-n junction photodiodes decreased when the boron concentration was increased from 0.6% to 1% [48]. Reproduced from [48], [52].

1.5 Organization of dissertation

This dissertation discusses the demonstration of optoelectronic devices using B-III-V epitaxial layers, including the first demonstration of BGaInAs active region light-emitting diodes and the first all-BGaInAs avalanche photodiodes. Molecular beam epitaxy, the growth technique through which these materials were grown, is discussed in detail in Chapter 2. The characterization methods

critical to this work are discussed in Chapter 3. The growth of these alloys and the method through which we optimized their growth to improve their optical quality are discussed in Chapter 4. Chapter 5 discusses the growth and properties of the B-III-V optoelectronic devices demonstrated in this work. Finally, Chapter 6 presents a summary and conclusion of this work.

Chapter 2

Molecular beam epitaxy

2.1 Introduction

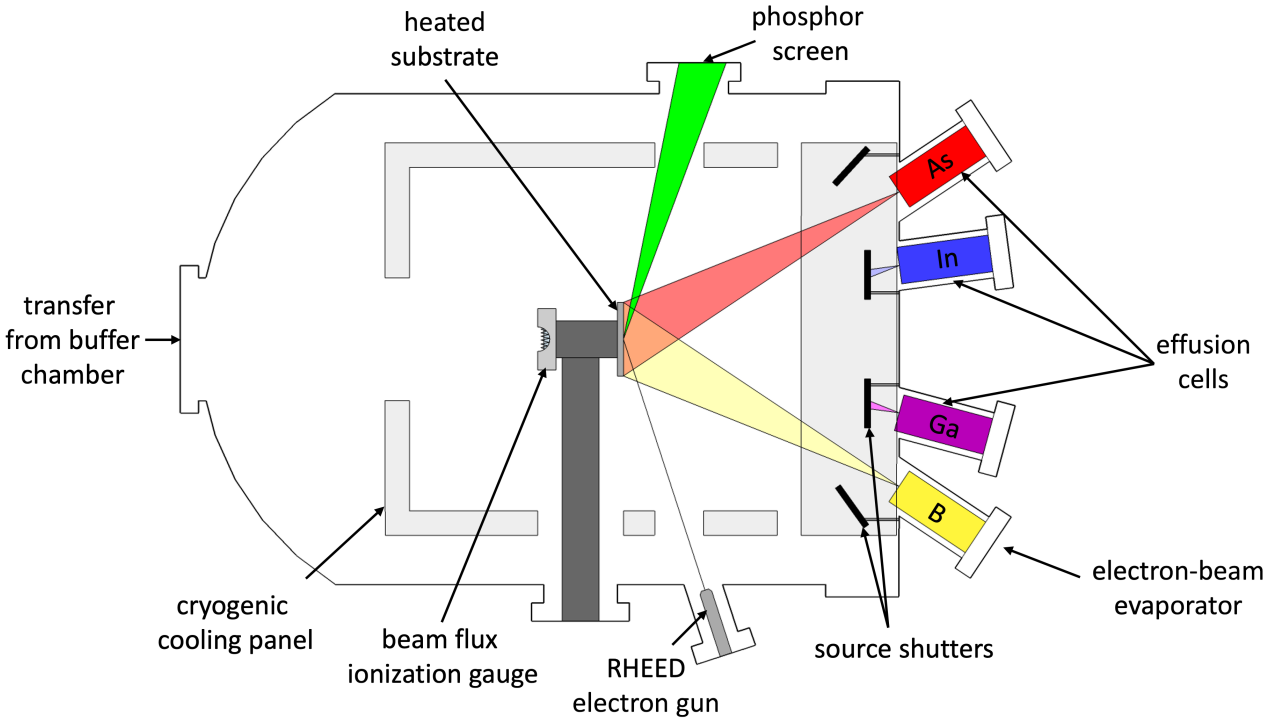

Figure 2.1: Molecular beam epitaxy (MBE) growth chamber.

Molecular beam epitaxy (MBE) is a crystal growth technique often used for the production of semiconductor materials and device structures. In solid-source MBE, high-purity sources are sublimated or evaporated towards a heated, rotating substrate. Rotation of the substrate during growth allows

for uniform deposition over the substrate. The sublimated atomic flux is blocked or allowed by *in situ* shutters providing submonolayer control of the epilayer thickness and composition. The MBE system is operated at ultra-high vacuum (UHV) $\sim 10^{-10}$ Torr. The advantages of MBE include low impurity levels due to the high vacuum system and high purity sources used, as well as precise control over the composition and structure of the epitaxial materials. The independent control over growth parameters granted by MBE allows for manipulation of the epilayer surface kinetics, enabling synthesis of materials that are of thermodynamically unfavorable at equilibrium conditions, as discussed in Section 2.1.1.

An additional benefit of MBE is the use of *in situ* measurement tools enabled by UHV growth conditions. In the systems used for this project, reflection high energy electron diffraction (RHEED) is used to characterize epilayer crystalline quality during growth. Prior to growth, beam equivalent pressure (BEP) measurements from the effusion cells used for growth are taken by measuring the difference in pressure readings with the source shutter opened and closed of an ion gauge mounted in the beam path. These measurements allow for a relationship between BEP and atomic flux to be established such that epilayers with a target composition and thickness can be repeatedly grown.

Ultra-high vacuum growth provides for long mean-free paths of the atoms, and in conjunction with the high purity source material used, reduces the incorporation of impurities in the epitaxial material. Vacuum is maintained through the use of cryogenic and ion pumps as well as a liquid nitrogen-cooled cyropanel surrounding the inside of the system. Substrates are loaded and outgassed in a loading chamber before being moved to a buffer chamber where the substrates are outgassed again prior to being moved to the growth chamber. Substrates are outgassed again inside the growth chamber before being rotated to face the sources. After the oxide on the substrate is thermally removed, a buffer layer is grown to form a good epitaxial template away from the substrate interface prior to the epitaxial layers of interest.

The main MBE system used in this work was an EPI MOD Gen II, which is a vertical reactor with eight cell ports. Dual-zone Sumo effusion cells were used to sublimate/evaporate Ga, In, and Bi. A dual-zone valved cracker was used for sublimating As_2 and a dual-zone valved GaP decomposition cell was used to sublimate P_2. Originally, a custom-made two-crucible cell, "dual-dopant," designed by MBE Komponenten was used for Si and Be sublimation and an additional Veeco dual-dopant cell was required for GaTe evaporation. Recently, a three-crucible cell "triple-dopant," custom made by MBE Komponenten, was used for deposition of all three dopant materials. The substrate is positioned such that it is in the center of the atomic beam paths of the eight cells.

The cells are heated to sublimate/evaporate the desired atomic flux, shutters mounted in front of the cells are manipulated to block or not block the atomic beam fluxes directed at the substrate. The substrate is heated to control the surface kinetics as described in Section 2.1.1.

This work used two molecular beam epitaxy systems for the devices discussed in Section 5.1; the systems are connected with a buffer chamber such that samples can be transferred between systems *in situ*. The second MBE system was equipped with an aluminum cell, which is necessary for the AlGaAs cladding layers in the electroluminescence structures. The second MBE has deep upward looking dopant cells for Be, Si, and Te doping and a Veeco dual-dopant cell for Si and Be doping. Dual-zone Sumo effusion cells were used to sublimate/evaporate Ga and Al. Only the base filament of the Al cell was powered in order to prevent Al from "creeping" up the crucible.

2.1.1 Surface kinetics in MBE

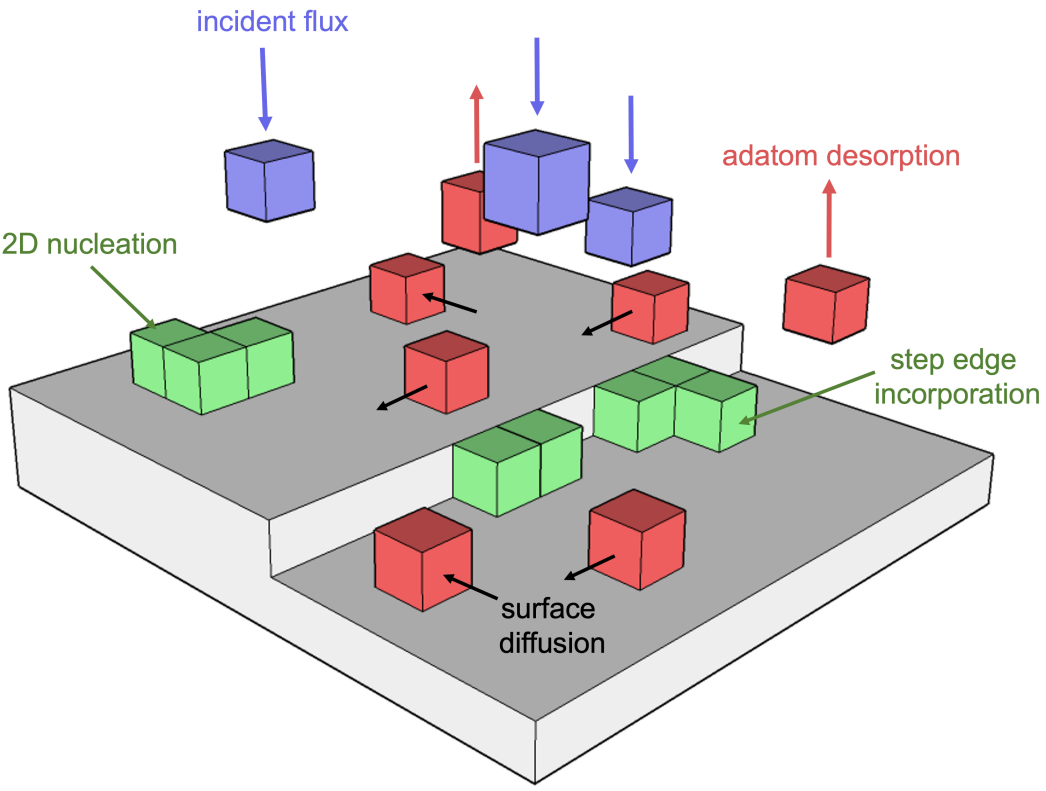

Figure 2.2: Adatom surface processes during MBE growth.

In MBE growth, the precise control of adatom surface kinetics promotes uniform high-quality growth of epitaxial layers. The importance of surface thermodynamics on the synthesis of random alloys

is demonstrated by the lack of compositional clustering in III/V alloys [75], [76] and becomes even more critical in the growth of thermodynamically unfavorable materials and structures. The surface kinetics in MBE are controlled by manipulating the growth rate, growth temperature, group-V/group-III flux ratio, and presence of a surfactant. Low growth temperatures and high growth rates are shown to promote random alloys and facilitate growth within the instability range [76].

Growth rate

Growth rate has been shown to have an effect on the formation of ordered structures [75]. Reducing the growth rate provides the atoms at the surface more time to rearrange in ordered structures at the surface [75] and interaction between the surface atoms and the previously deposited monolayers closest to the surface [77]. Faster growth rates reduce the time for rearrangement, and therefore,the number of epitaxial layers involved in rearrangement. Jasik *et al.* observed the dependence of growth rate on photoluminesence (PL) intensity in InGaAs QWs [78]. The PL intensity increased with increasing growth rate, to an optimal point, after which it decreased as the growth rate increased [78].

Growth temperature

The MBE growth (substrate) temperature that promotes layer-by-layer growth rather than islanding growth is dependent on the material system. Alloys composed of group-III elements with high desorption temperatures, such as Al and Ga, are typically grown at higher temperatures than elements with lower desorption temperatures, such as In. For example, typical AlAs or GaAs growth temperatures are around 580 °C, while typical InGaAs temperatures are around 470 °C. Low growth temperatures can be used to overcome alloy miscibility gaps as they reduce the surface mobility of atoms, reducing their ability to form ordered structures during growth [75].

Group-V overpressure

Typical III-V MBE is performed in the group-III limited growth regime where an excess of group-V atoms is supplied. The probability of adatom incorporation or "sticking coefficient" of group-III elements is ~ 1, while group-V elements have a sticking coefficient < 1 with excess group-V elements desorbing from the epitaxial surface. Therefore, excess group-V is supplied in order to promote 1:1 III:V incorporation and to prevent group-V or group-III vacancies. Adatom surface diffusion lengths are affected by the amount and type of arsenic supplied. Increasing the arsenic overpressure

increases surface diffusion [79]–[81] and the use of dimeric arsenic rather than tetrameric arsenic (As_2 instead of As_4) similarly decreases diffusion lengths [82]–[85]. At typical growth temperatures, unincorporated arsenic desorbs from the surface; however, at low growth temperatures, $\leq$ 400 °C, excess As is incorporated as interstitial or antisite defects, degrading material and optical property [78], [86]. Therefore, at low growth temperatures, balancing the As/III flux ratio to prevent As vacancies while also preventing excess As incorporation becomes critical [5], [87], [88].

Surfactant-mediated growth

Another method for altering adatom surface diffusion in MBE is the use of surfactants to modify the epitaxial growth kinetics [89]–[91]. As defined by Copel *et al.* a surfactant is an element that when supplied during growth is mobile enough to preferentially segregate to the epilayer surface instead of incorporating into the epilayer [89]. However, some material systems include elements that behave both as a lattice-constituents and as surfactants [26], [29], [92]. The method through which a surfactant promotes layer-by-layer growth remains to be fully clarified. Copel *et al.* described one potential mechanism for reduction in adatom surface diffusion length compared to a "clean" substrate; on a clean substrate, the atom is free to move until it is impeded by a step edge or defect [89]. When a surfactant is introduced, the added layer formed by accumulated surfactant atoms reduces the distance before atom diffusion is impeded [89]. However, surfactants are reported to both decrease [90], [93], [94] and increase [90], [95] adatom surface diffusion length. The effects of the surfactant on adatom diffusion, and ultimately epitaxial layer quality, are dependent on the surfactant used, the material system, and the lattice-mismatch between the epitaxial layers and the substrate. Massies *et al.* qualified the difference between surfactants that increase or decrease the surface diffusion length as non-reactive surfactants, which are surfactant atoms that occupy interstitial sites and reactive surfactants, where surfactant atoms occupy substitutional sites [90]. Hetereoepitaxy with a large lattice-mismatch often leads to a transition from layer-by-layer growth to islanding growth when the film approaches a critical thickness corresponding to the onset of plastic deformation [89], [90]. The use of surfactants has been shown to increase the critical thickness in InGaAs grown on GaAs [89], [96], [97]; however, surfactants useful in homoepitaxial growth do not necessarily behave the same in heteroepitaxial growth [98]. As discussed in Section 2.2.3, the work presented in this thesis used bismuth as a surfactant, which has previously been demonstrated to increase N incorporation and improve surface quality in dilute-nitride alloy growth [99].

2.2 MBE growth of highly-mismatched alloys

The large differences in size and electronegativity in highly-mismatched alloys reduce the solid solubility of the highly-mismatched constituent, necessitating the use of non-equilibrium growth techniques, such as molecular beam epitaxy (MBE), in order to overcome thermodynamic solubility limitations and synthesize high quality epilayers. Even with non-equilibrium growth processes, the incorporation of the highly-mismatched constituent requires precise control of the adatom surface kinetics, such that incorporation of even the dilute concentrations can be challenging. The dilute nitrides (InGaAsN and related alloys) and dilute bismides (InGaAsBi and related alloys) are both highly-mismatched alloy families, which demonstrate challenging synthesis and severe reduction in material quality with increasing mismatched constituent incorporation [100]–[102]. The large miscibility gap and the poor material quality of high concentration dilute nitrides and dilute bismides has thus far limited their widespread use in optoelectronic devices. The "favorable" band anticrossing effects that modify the energy band structure of these alloys and reduce alloy energy bandgap simultaneously increase alloy scattering effects, fundamentally limiting the carrier mobility in these materials [103]–[106]. Additionally, the high likelihood of point defects resulting from miscibility limits in highly-mismatched alloys further contributes to the reduction in carrier mobility through perturbation of the energy band structure from anticrossing interaction with isolated defect states [104], [107] and reduce carrier lifetimes, greatly degrading device performance. Boron-III-V alloys are also classified as highly mismatched alloys given the large atomic size difference between boron and conventional group-III and group-V elements, despite a smaller difference in electronegativity in comparison to the dilute nitrides [54]. While the dilute borides are not predicted to benefit from the same band anticrossing as in the dilute nitrides, higher concentrations of boron can be incorporated in InGaAs than nitrogen [54] potentially enabling a broad range of accessible energy gaps through alloying. The growth advancements previously demonstrated in other highly-mismatched alloys, as described below, established a framework for developing a highly kinetically-limited growth regime for B-III-V MBE growth.

2.2.1 Dilute-bismide growth

The incorporation of bismuth into conventional alloys has proven to be extremely challenging, requiring growth with near unity III/V flux ratios [108], [109] and low growth temperatures [109], [110] for bismuth incorporation to occur. According to the growth model developed by Lu *et al.*,

a bismuth atom will either incorporate into the film, evaporate from the film, or form a Bi droplet at the surface, [109] requiring control of the growth kinetics in order to promote Bi incorporation into the film rather than its evaporation or formation of Bi droplets. Ptak *et al.* demonstrated that the formation of surface droplets could be suppressed by controlling the growth regime such that complete incorporation of the bismuth flux occurred [111].

Growth growth of dilute bismides near stoichemetry is required to promote Bi incorporation because under typical group-V rich growth, the lack of group-V sites for Bi to bond to Ga in results in Bi atoms behaving as non-binding surfactants, segregating to the surface, and eventually desorbing from the epilayer [108]. Under III-rich growth, the formation of surface droplets was observed, which is suggestive of phase separation due to the immiscibility of Ga and Bi [108]. Therefore, the III/V flux ratio needs to be optimized to allow for Bi incorporation without promoting surface droplets, severely complicating the growth of these alloys. The growth temperature of dilute-bismide alloy growth is similarly important. At a fixed Bi BEP and Ga/As flux ratio, the incorporated Bi % decreases as the substrate temperature is increased [110].

2.2.2 Dilute-nitride growth

As with the dilute bismides, MBE-growth optimization of dilute-nitride alloys has demonstrated the necessity to carefully control growth kinetics in order to promote high-quality dilute-nitride material and devices. The substitutional incorporation of nitrogen is challenging with deviations from unity sticking observed at higher nitrogen concentrations [112]. The use of Bi as a surfactant in InGaAsN QWs was shown to increase nitrogen incorporation and increase photoluminesence intensity [99]. As the nitrogen content is increased, the growth window narrows significantly degrading device performance [26]. Growth temperature was found to be one of the most important factors in promoting high-quality dilute-nitride growth [15]. Additionally, the use of antimony as as surfactant and lattice-constituent and deflection plates to prevent nitrogen plasma damage were essential to improving dilute nitride growth and extending the wavelength accessible on GaAs-based emitters [26].

2.2.3 Dilute-boride growth

Prior to the work done by McNicholas, the incorporation of B in III-V alloys had been severely limited by its complicated growth [48]. Previous investigations of the ternary alloy BGaAs focused on increasing the B concentration through control of the surface kinetics in both MBE growth [50], [113],

[114] and MOCVD growth [65], [68], [115]. Increased boron incorporation with decreasing substrate temperature has been observed in both MBE [50] and MOCVD [65], [68], [115] grown material. Groenert *et al.* noted the importance of growth temperature on B incorporation and the deviation from substitutional incorporation under unoptimized growth conditions [50]. Additionally, Groenert *et al.* observed a boron incorporation dependence on group-V overpressure [50]. Ptak *et al.* observed an increase in B incorporation with increasing Bi surfactant flux, establishing the importance of surfactant mediated epitaxy using Bi for high-quality B-III-V growth [113]. Detz *et al.* observed increased substitutional B incorporation with increasing growth rate and an accompanying reduction in RMS roughness as measured with atomic force microscopy (AFM) [114]. Phase segregation has often been observed in BGaAs films grown under unoptimized growth conditions [114], [115]. Despite the growth advancements demonstrated in previous investigations of BGaAs, boron incorporation remained limited to $\sim 8\%$ in BGaAs films grown on GaAs by both MBE [50] and MOCVD [68].

Demonstration of a unity substitutional growth regime for BGaAs

McNicholas demonstrated a unity substitutional growth regime, combining disparate observations in the literature discussed above [50], [113], [114], that promoted substitutional incorporation of boron through control of the surface kinetics [48]. In order to exceed the limited boron incorporation previously demonstrated and prevent surface segregation of boron, a boron electron-beam source was used. Low growth temperatures, previously identified as a critical parameter in other highly-mismatched alloys including the dilute borides, were used to reduce the surface mobility of B adatoms and increase miscibility. High group-V overpressure and Bi as a surfactant were also used to prevent B segregation. On GaAs, up to 12% boron was incorporated in coherent (not relaxed) BGaAs films [66]. Transferring this growth regime to GaP substrates, which decreases the lattice-mismatch between substrate and epitaxial BGaAs film, McNicholas demonstrated B incorporation up to 18%, far exceeding previous demonstrations of B incorporation in the literature [48]. The first BGaAs/GaP QWs grown on GaP/Si templates were grown, demonstrating the potential for B-III-V integration on Si [48]. This unity substitutional incorporation regime enables a repeatable calibration of B flux as a function of e-beam power using HR-XRD measurements of the boron concentration in BGaAs films as discussed in Section 4.1.

Previous BGaInAs growth

As discussed in detail in Chapter 1, previous demonstrations of BGaInAs growth has thus far been limited to MOCVD growth of alloys with $\leq$ 4 % B [52], [69]. Very little investigation and optimization of the BGaInAs growth kinetics had been reported especially via MBE. This work extends the growth regime established by McNicholas for BGaAs growth on GaAs to the quaternary alloy BGaInAs with a focus on optimizing growth conditions to realize high optical quality material for optoelectronic device applications.

Chapter 3

Characterization Methods

3.1 Photoluminescence

Photoluminesence measurements were performed to compare the spontaneous emission from quantum wells (QW) and films with and without boron, as well as the peak wavelength of emission from these samples. Comparing the intensity of spontaneous emission across samples can be used to understand the material quality and is a good approximation of the eventual device quality. In addition to measuring the emission wavelength, photoluminesence is more sensitive to defects than x-ray diffraction measurements making it a critical tool for optimizing the MBE growth regime for materials used in light emitting devices. In this work, samples were optically pumped with a 532 nm laser and their spectral response was then measured as described below.

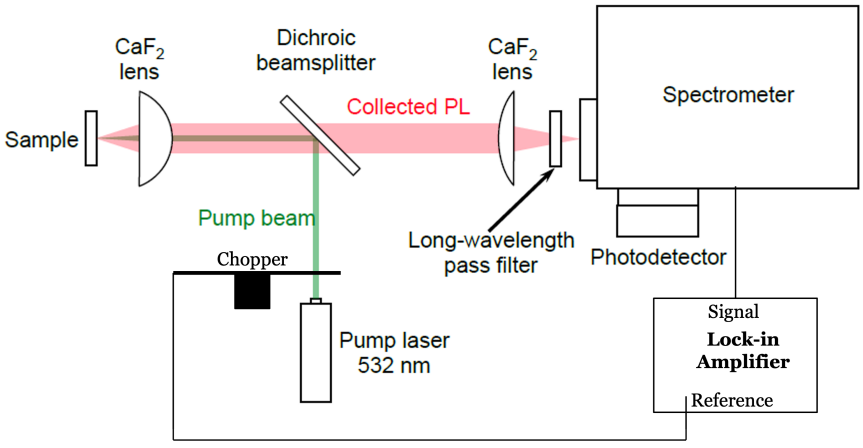

Figure 3.1: Schematic of the photoluminescence setup used for this work.

Each sample was optically excited at 532 nm by a chopped frequency doubled laser Nd:YAG,

allowing for measurements of samples with band gaps less than 2.3 eV. The pump laser light is absorbed in the top $\sim$ 100 nm of the epitaxial layers, creating electron-hole pairs, which relax to the conduction and valence minimum and maximum before recombining. When the electron-hole pairs radiatively recombine, the resulting photons are collected. The light emitted is passed through a grating spectrometer and the intensity at the wavelength of interest is measured by a single-channel photodiode using a lock-in amplifier, enabling the determination of PL intensity versus wavelength. This work focused on measuring room temperature emission < 1.5 μm using a thermoelectrically-cooled InGaAs photodiode. The laser power was maintained at $\sim$ 100 mW at the sample surface for every measurement and a control sample was measured every time in order to facilitate direct comparison between measured samples. The relative intensities of light emitted from the samples allow for qualitative assessment of how efficiently the samples emit light. When comparing samples of similar composition and layer structure, higher intensities indicate less loss due to nonradiative recombination pathways in the material and therefore higher quality material.

The temperature-dependent PL measurements discussed in Section 4.3 were performed by our collaborators in Professor Robert Kudrawiec's group at Wroclow University of Science and Technology who have the ability to cool samples to 0 Kelvin. The Varshni equation defines the variation in bandgap of semiconductor materials with temperature as shown in Equation 3.1, where E_g, the bandgap of a semiconductor at a temperature T, is a function of the bandgap at 0 K and material-specific constants α and β [116]. Variation from the Varshni equation at low temperatures is often indicative of carrier localization [117], [118] and can be an indicator of poor crystalline quality and ultimately, device quality [119].

$$E_g = E_0 - \alpha T^2/(T + \beta) \tag{3.1}$$

3.2 High-resolution X-ray diffraction

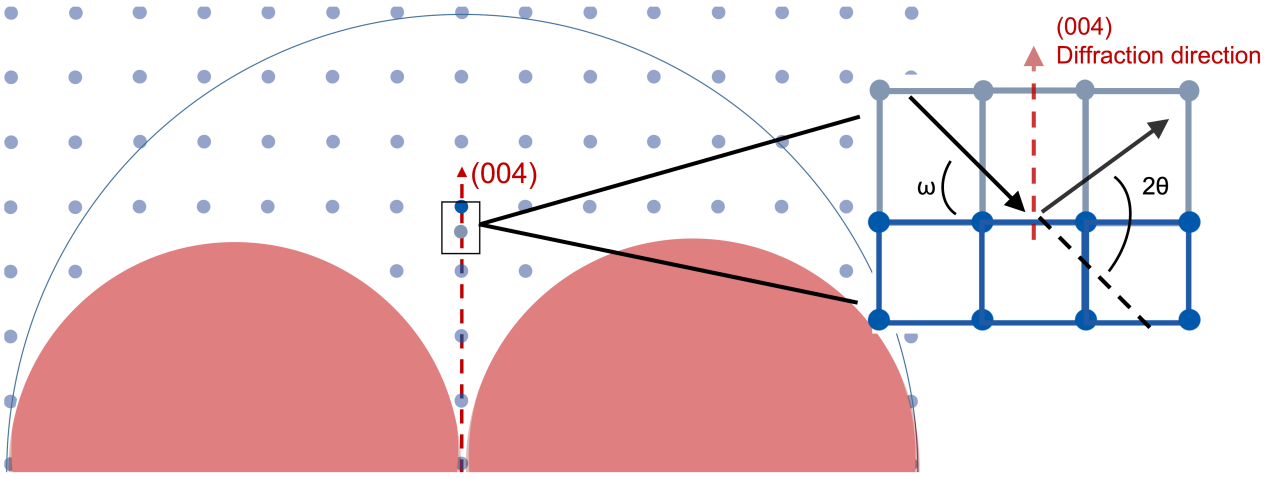

Figure 3.2: Reciprocal space of substrate lattice (dark blue circles - left) and real space of substrate lattice (dark blue lattice - right). X-ray diffraction conditions for coupled ω-2θ in reciprocal space (left) and real space (right) are shown.

High-resolution X-ray diffraction (HR-XRD) was used in this project to characterize the structural properties of (B)GaInAs films and QWs. In HR-XRD, the intensity of scatter x-rays is measured as a function of diffraction angle. Bragg's law defines the conditions for constructive interference of the x-rays scattering from the atomic layers in the crystal; the diffraction x-ray intensities are at their highest when the conditions of Bragg's law are met. This work used coupled ω-2θ scans to measure the intensity of diffraction as a function of the Bragg diffraction angle. ω-2θ scans maintain a single diffraction vector, thus allowing for the measurement of the spacing of atomic planes in a single direction. ω is defined as $\frac{1}{2}2\theta$. ω-2θ measurements were performed about the (004) direction to measure the out-of-plane lattice constants of the epitaxial films and QWs. Constructive interference of x-rays reflected at the interfaces of epitaxial layers produces finite thickness fringes in addition to the substrate and epitaxial layer peaks allowing for determination of layer thicknesses in heteroepitaxial structures. The presence of finite thickness fringes necessitates abrupt uniform epitaxial interfaces providing a qualitative metric for evaluating epitaxial layer crystalline quality.

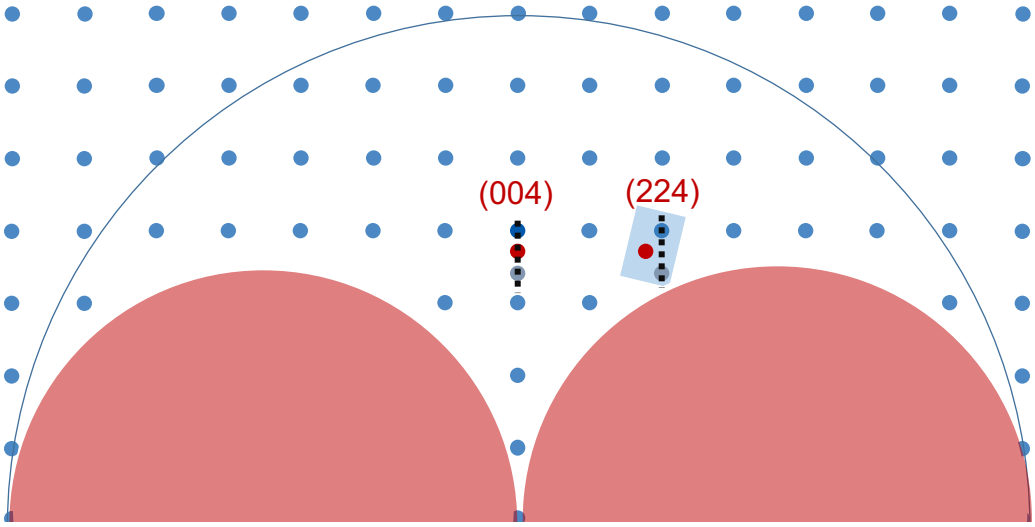

Figure 3.3: Reciprocal space of substrate lattice (dark blue circles), coherently-strained epitaxial layer (light blue circles), and relaxed epitaxial layer (red circle). Peaks along the ω-2θ line of the substrate (004) direction (black dotted line) probe only the out-of-plane lattice constant. To characterize the epitaxial strain and relaxation in layers, asymmetrical reciprocal space maps (RSMs) in the (224) direction use multiple ω-2θ scans incrementing ω to measure diffraction from the relaxed epitaxial layer peak to the coherently-strained epitaxial peak as they no longer lie along the same ω-2θ line. A typical RSM coverage area is shown in the blue box.

ω-2θ scans allow for the characterization of layer thickness, lattice-constant, and, using Vegard's Law, alloy composition of coherently-strained epitaxial layers. Characterizing the strain in epitaxial layers requires the use of asymmetric reciprocal space maps (RSMs) which can be used to measure both the in-plane and out-of-plane lattice constants of the epitaxial layers. A series of ω-2θ scans are performed incrementing ω to create a "map" of reciprocal space containing both the substrate peak and the relaxed epitaxial layer peak. In the (00x) direction only out-of-plane lattice constants are measured and the relaxed epitaxial layer peaks would lie on the same line as the substrate peak. Therefore, asymmetric RSMs are performed in the (224) or $(\bar{2}\bar{2}4)$ directions to measure both the in-plane and out-of-plane lattice spacing. Relaxation of the epitaxial layer shifts the relaxed layer peak off of the measured ω-2θ line of the substrate peak. Meanwhile, the layer peak of a epitaxial layer coherently strained to the substrate will remain on the same line as the substrate peak. Both coherent and relaxed layer peaks are measured with asymmetric RSMs allowing for characterization of relaxation in the epitaxial layers.

3.3 Photoreflectance

The photoreflectance measurements discussed in this work were performed in collaboration with Professor Robert Kudrawiec's group at Wroclow University of Science and Technology.

Photoreflectance was used to measure the interband transitions of BGaInAs QWs and films on GaAs and BGaInAs. Photoreflectance (PR) is a characterization technique that measures the wavelength-dependent change in reflectivity of a sample to investigate the bandstructure of the material. The photoreflectance experimental set-up used for this work is shown in Figure 3.4. Photoreflectance uses a laser to generate electron-hole pairs, which modulates the internal electric field in the sample, and a separate lamp that is separately filtered to change its wavelength in order to measure the wavelength-dependency of the reflectivity. A monochromater and lock-in detector referenced to the modulation frequency of the laser (to reduce system noise) are used to measure the signal. The shape of the measured ΔR/R (or the change in reflectance divided by the baseline reflectance) versus the wavelength can be used to measure optical transitions in the material. Photoreflectance is sensitive to inhomogeneity in the alloy, which results in broadening of the PR resonances [64].

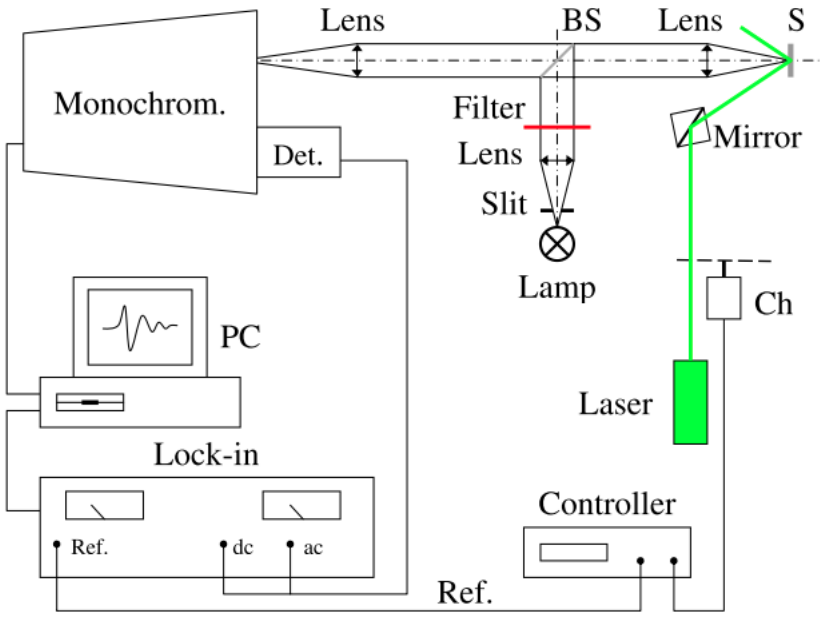

Figure 3.4: Schematic of the photoreflectance experimental set up used for this work. Reproduced from [120]

3.4 Avalanche photodiode characterization

The BGaAs and BGaInAs photodiode fabrication and characterization discussed in this work was performed by Professor Joe Campbell's group at the University of Virginia. A brief discussion of the methods used by our collaborators at UVA are described here; a more detailed discussion can be found in [121].

External quantum efficiency (EQE) is the ratio of collected photo-excited electrons to the number of incident photons. The measurements were performed with a broadband laser-driven light source coupled to a monochromator as shown in Figure 3.5. The use of monochromator allows for isolating narrow-band regions of the light source in order to accurately measure the EQE versus wavelength. The APD photoresponse was measured with a lock-in amplifier and compared to that of a NIST-traceable calibrated Si photodetector in order to determine the efficiency as shown in Equation 3.2.

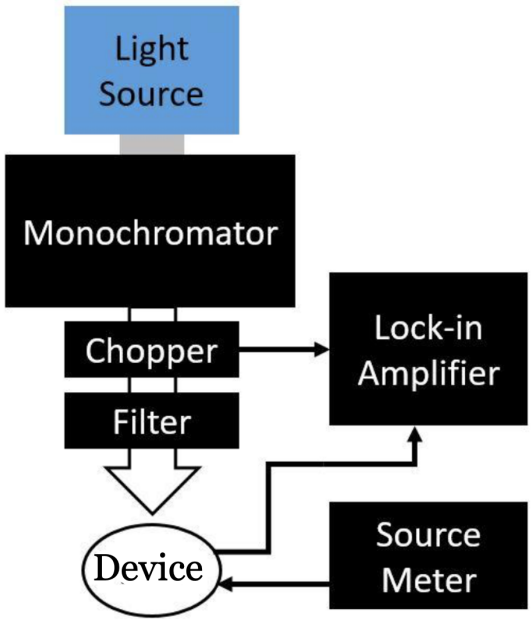

Figure 3.5: External quantum efficiency measurement setup used for measuring the EQE of BGaAs and BGaInAs photodiodes discussed in this work. Reproduced from [121].

$$EQE_{device} = EQE_{known} \frac{I_{photo,device}}{I_{photo,known}} \tag{3.2}$$

It is important that the EQE is measured at the bias where the device exhibits unity gain (rather than at a bias that results in multiplication gain) in order to accurately measure the EQE of the device. Due to the non-ideal photocurrent response exhibited by the devices studied here, the non-ideal photocurrent was fit following the method established by Woods *et al.* [122] to determine the multiplication gain. The measured EQE was then normalized to account for the gain at the bias of the measurement if it was not unity.

The measured photocurrent from a photodiode is the sum of the current resulting from photogenerated carriers and the dark generation of carriers. The multiplication gain of an APD is defined as a ratio of the photocurrent when the device is biased in the region where multiplication gain from impact ionization is taking place to the photocurrent when the device has unity gain or is in the ordinary photodiode region.

3.4.1 Excess noise measurements

As discussed in Chapter 1, excess noise in avalanche photodiodes typically increases with multiplication gain, except in a few low-noise materials or devices. In this work, our collaborators at University of Virginia measured the excess noise of BGaInAs photodiodes in order to understand how the addition of boron affects excess noise.

In avalanche photodiodes, the McIntyre local field model shown in Equation 3.3 [16] defines the excess noise factor *F(M)* as a function of the multiplication gain, M, and k, which is ratio of impact ionization coefficients α and β. The impact ionization coefficients, α and β, are approximated as the inverse of the average length before impact ionization of electrons and holes respectively.

$$F(M) = kM + (1-k)(2 - \frac{1}{M}) \tag{3.3}$$

Reducing the increase in excess noise factor as multiplication gain increases requires reducing k. As $k = min(\frac{\alpha}{\beta}, \frac{\beta}{\alpha})$ such that $k \leq 1$, reducing k requires $\beta \ll \alpha$ or $\alpha \ll \beta$.

Noise power measurements

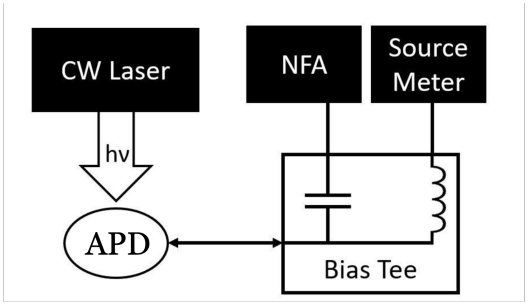

Figure 3.6: Noise power measurement system used for measuring noise power and determining the excess noise factor versus multiplication gain for BGaInAs materials. Reproduced from [121].

Noise power measurements were taken with a noise figure analyzer (NFA) relative to a calibrated noise source. The system set-up is shown in Figure 3.6 was used to measure the noise power and determine the excess noise factor versus gain for BGaInAs APDs [121]. The local field model of noise spectral density, S, defines the relationship between noise spectral power and multiplication gain as defined in Equation 3.4. R is the total impedance of the system. First, the noise power is measured at the unity gain point, where $M = 1$ and $F(M) = 1$ to determine S_0 as defined in Equation 3.5.

$$S_N = 2qIRM^2F(M) \tag{3.4}$$

$$S_0 = 2qIR \tag{3.5}$$

To determine *F(M)* as a function of M, subsequent measurements are performed for $M > 1$. Light and dark measurements are performed at the measurement frequency and substracted from each other to define N_p at the measurement frequency. The excess noise can then be calculated from the measured noise spectral power as defined in Equation 3.6. Finally, plotting excess noise versus multiplication gain allows for extracting the k value of the measured device.

$$F(M) = \frac{S_N}{S_0 M^2} = \frac{N_{p,N}}{N_{p,0}M^2} \tag{3.6}$$

3.5 Hall measurements

Hall measurements were performed in order to determine the carrier density and mobility in films. Hall measurements in the Vander Pauw configuration provide a simple method for measuring the doping concentration in uniform semiconductor film with contacts in the corners as shown in Figure 3.7. Hall measurements depend on a uniform film

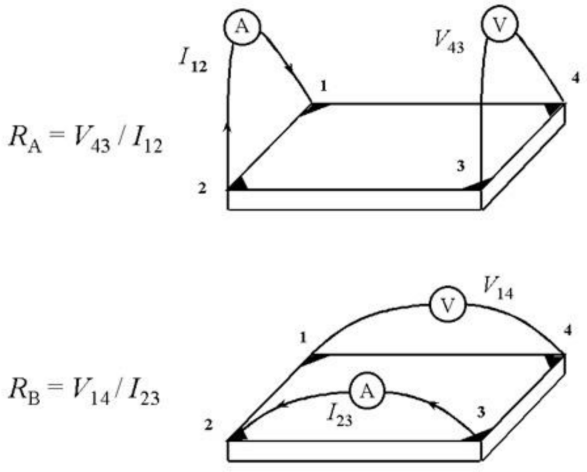

Figure 3.7: The sample set up for Van Der Pauw Hall measurements. Reproduced from [123]

The Van der Pauw technique allows for the determination of the mobility and sheet density (and thus carrier density). This technique assumes a uniform sample [123], [124]. As shown in

Figure 3.7, four small contacts are placed at the corner of a square sample in order to determine the resistances R_A (from Equation 3.7) and R_B (from Equation 3.8) by supplying a current across two contacts and measuring the voltage across the other two contacts (i.e. supplying a current from 1 to 2 and measuring the voltage across 3 to 4). As shown in Equation 3.9, the sheet resistance (R_s) can then be determined fromR_A and R_B.

$$R_A = V_{43}/I_{12} \tag{3.7}$$

$$R_B = V_{14}/I_{23} \tag{3.8}$$

$$e^{-\pi R_A/R_s} + e^{-\pi R_B/R_s} = 1 \tag{3.9}$$

Additionally the Hall voltage (V_H) can be calculated by measuring the voltage across diagonal contacts under a known magnetic field (B). The Hall voltage allows for the calculation of the sheet density n_s (Equation 3.10) and subsequently the bulk carrier density (n or p) given a known conducting layer thickness (Equations 3.11 and 3.12). As shown in Equation 3.13, the Hall mobility, μ, can be calculated from the sheet resistance and sheet density.

$$n_s = \frac{IB}{q|V_H|} \tag{3.10}$$

$$n = \frac{n_s}{d} \tag{3.11}$$

$$p = \frac{p_s}{d} \tag{3.12}$$

$$\mu = \frac{1}{qn_sR_s} \tag{3.13}$$

Chapter 4

Growth of B-III-V alloys

4.1 Unity substitutional incorporation growth regime

The growth of high-quality material by MBE necessitates unity substitutional incorporation, such that every incorporated atom is incorporated on a lattice site. Previous investigations of highly-mismatched alloys have demonstrated that precise control of growth parameters is critical to the promotion of substitutional incorporation of highly-mismatched constituent, requiring a highly kinetically-limited growth regime as described in Chapter 2.2.3. Under unoptimized BGaAs growth as observed by Groenert *et al.* excess boron was incorporated interstitially [50]. McNicholas *et al.* similarly noted a rough surface in atomic force microscopy (AFM) scans of BGaAs films under unoptimized growth suggesting preferential surface accumulation of B [66]. The kinetically-limited growth regime demonstrated by McNicholas *et al.* to promote substitutional B incorporation in BGaAs was confirmed by Rutherford backscattering spectrometry (RBS) performed by Evans Analytical Group, which indicated $\geq 99\%$ substitutional B in a $B_{0.17}Ga_{0.83}As$ film. As substitutional incorporation indicates that nearly every boron atom is incorporated at a lattice site and assuming that the incorporation of Ga does not change with the addition of B, the boron atomic flux can be calculated *ex situ* through dynamic X-ray scattering simulations of HR-XRD ω-2θ measurements. As shown in Figure 4.1, the substitutional incorporation of boron introduces tensile strain in the BGaAs epilayer resulting in a linear relationship between out-of-plane lattice constant as measured by HR-XRD ω-2θ scans (Figure 4.1(a)) and the increasing B ion intensity measured by SIMS in BGaAs films for BGaAs films with varying B concentrations (Figure 4.1(b)) [66].

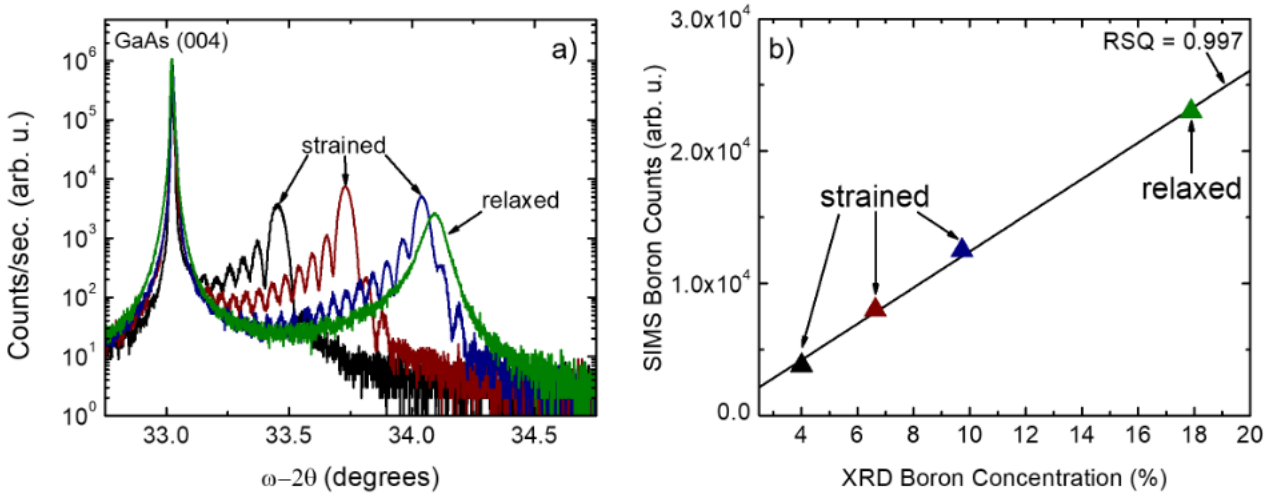

Figure 4.1: (a) HR-XRD ω-2θ diffraction measurements from 100 nm $B_xGa_{1-x}As$/GaAs heterostructures with B concentrations spanning coherent (black, red, blue) and structurally degraded (green) compositions. (b) B secondary ion yield in SIMS versus apparant B concentration determined from HR-XRD measurements shown in (a). Reproduced from [66].

4.1.1 Investigation of unity substitution in BGaInAs alloys

Extending this growth regime to the quaternary BGaInAs alloy decouples the alloy bandgap from the lattice constant, enabling strain-engineering of emitters and absorbers on GaAs over a range of technologically interesting wavelengths while maintaining a fixed lattice constant. However, the addition of In increases the difference in lattice constants of the constituent binary components, which is thought to increase the enthalpy of mixing as compared to the In-free alloy, resulting in a more limited growth regime for high quality epitaxial layers [76]. Therefore, we first investigated if the highly kinetically-limited growth regime for BGaAs maintains unity substitutional incorporation of B with the addition of In. To do so, we grew BGaInAs quantum wells (QW) with $\sim 30\%$ In and varying B concentrations on GaAs substrates.

Determining the elemental composition of quaternary alloys with conventional XRD measurements is not trivial because many alloy compositions can share a common lattice constant. Precise control of quaternary BGaInAs alloy composition requires pre-growth calibration of In, Ga, and B fluxes versus cell temperatures (for In, Ga) and electron-beam power (for B) using a combination of *in situ* beam-equivalent pressure (BEP) measurements and post-growth HR-XRD ω-2θ scans. To calibrate the In and Ga incorporation rate, InGaAs/GaAs superlattices (SL) were grown varying the In cell temperature (or BEP). The incorporated In and Ga fluxes were calibrated to pre-growth *in situ* BEP measurements of the In and Ga effusion cells using dynamic X-ray scattering

simulations to determine the alloy composition and thickness from HR-XRD ω-2θ measurements of the SL samples (Figure 4.2(a)). Owing to the near unity substitutional incorporation of these elements under group-III limited growth regimes [82], we assumed that the incorporation of Ga and In did not change with the addition of B and used these flux calibrations to control the In:Ga flux ratios during the growth of quaternary BGaInAs alloys. Eutectic reactions between elemental boron and the tungsten filament of the ionization gauge [125] used for BEP measurements precludes *in situ* BEP measurements of the B evaporator. Instead, a series of BGaAs films were grown with varying e-beam power and dynamic X-ray scattering simulations of HR-XRD ω-2θ measurements were used to determine the substitutional incorporation of B. The Arrhenius relationship between incorporated B flux (measured by HR-XRD) and B e-beam evaporator power observed in BGaAs alloys enabled calibration of B flux as a function of evaporator power prior to growth (Figure 4.2(b)). This relationship was maintained across multiple days as shown in Figure 4.2(b). Furthermore, an Arrhenius relationship was observed between incorporated B flux (measured by HR-XRD) and B e-beam evaporator power in BGaInAs QWs (Figure 4.2). Similar to the method demonstrated in the dilute nitrides by Spruytte *et al.* and extended for BGaAs by McNicholas *et al.*, we grew BGaInAs QWs (structure shown in Figure 4.3(a)) with an In:Ga flux ratio of 31:69 varying the B evaporator power. We observed a linear relationship between measured incorporated B in HR-XRD (ω-2θ scans shown in Figure 4.3(b)) and the B secondary ion yield (Figure 4.3(c)) measured by secondary mass spectrometry (SIMS) in our quaternary BGaInAs alloys, consistent with near unity substitutional B incorporation with the addition of In, validating the assumptions outlines above. Specifically, we confirmed that the unity substitution incorporation growth regime was maintained with the addition of indium allowing for the use of dynamic X-ray scattering simulations of HR-XRD ω-2θ measurements to determine the substitional B incorporation and motivating the investigation of the effects of B incorporation on optical quality and the potential for strain-engineering high quality extended wavelength emitters and absorbers on GaAs.

4.2 Extending the wavelength to 1.3 μm on GaAs

Leveraging our prior growth optimization of BGaAs to increase boron concentration from 8% to 18%, we focused on investigating the potential for strain engineering highly-compressively strained InGaAs on GaAs with the addition of B. To begin, our efforts centered on the extension of the highly kinetically-limited growth regime using fast growth rates, low substrate temperature, high

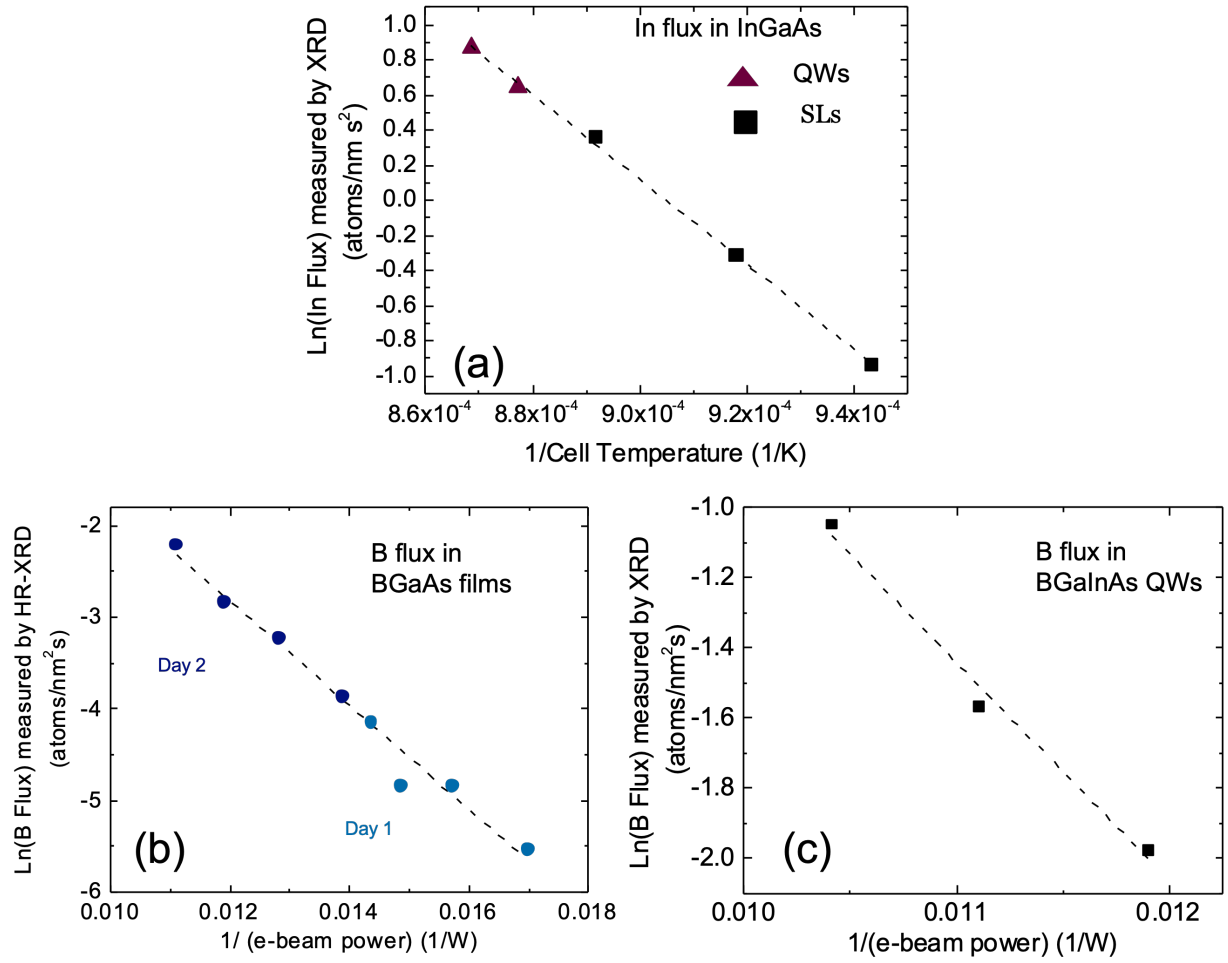

Figure 4.2: (a) The expected Arrhenius relationship between In flux measured by HR-XRD ω-2θ scans and cell temperature was observed in InGaAs/GaAs SLs and QWs. (b) A consistent Arrhenius relationship between B flux measured by HR-XRD ω-2θ scans and e-beam power was observed in BGaAs films grown on consecutive days. (c) An Arrhenius relationship between B flux measured by HR-XRD assuming a fixed In:Ga flux ratio and e-beam power was observed in BGaInAs QWs.

As/III flux ratios, and Bi as a surfactant to maintain high material quality as we increased the In concentration in BGaInAs in order to extend the emission wavelength accessible on GaAs. As discussed in section 4.1, we first grew BGaInAs QWs on GaAs with shorter wavelengths than the target 1.3 μm emission wavelength to understand how adding boron affected the structural and optical quality of the material. As shown in Figure 4.3(b) good structural quality was observed in HR-XRD ω-2θ measurements. Photoluminesence (PL) shown in Figure 4.3(d), measured from the $In_{0.31}Ga_{0.69}$ As QW, the $B_{0.03}Ga_{0.67}In_{0.3}As$ QW, and the $B_{0.07}Ga_{0.64}In_{0.29}As$ QW structures shown in Figure 4.3(a), showed a $\sim$ 2x improvement in PL intensity with the addition of 3% B and a small

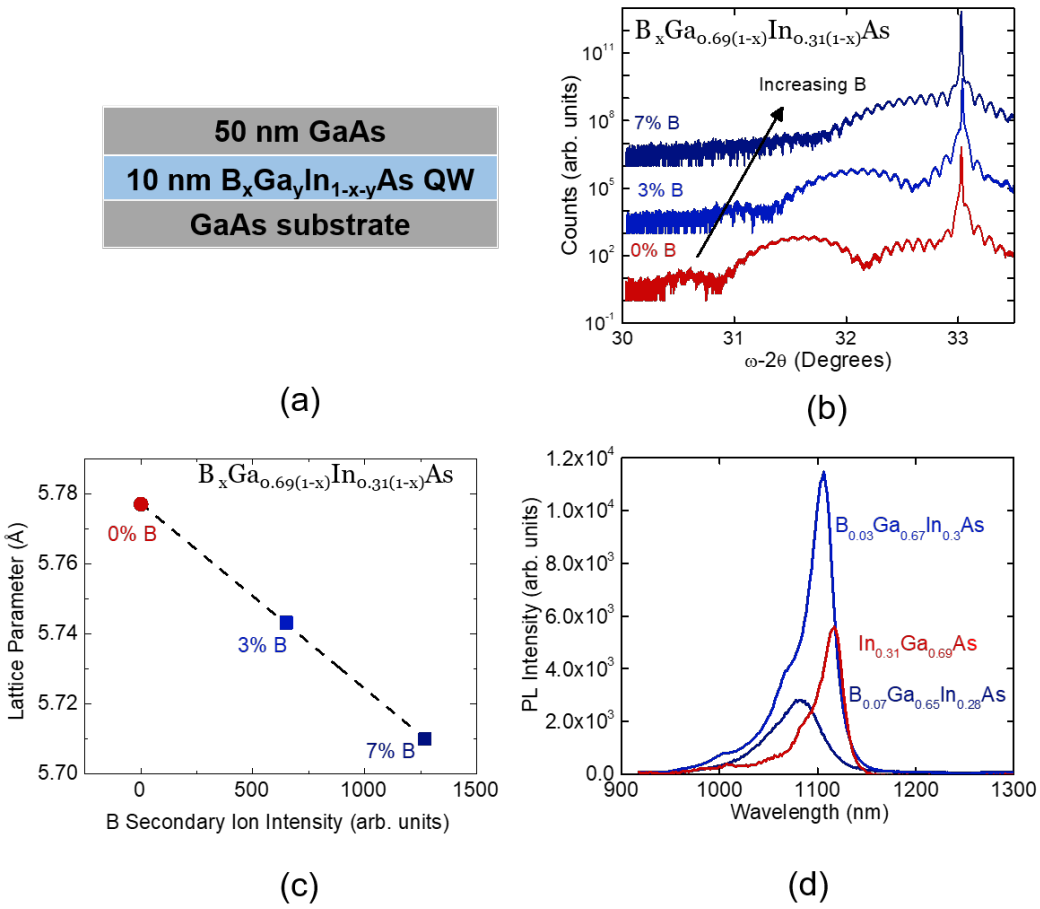

Figure 4.3: (a) Thin BGaInAs QW PL structures were grown on GaAs substrates. (b) HR-XRD ω-2θ scans of $B_xGa_{0.69(1-x)}In_{0.31(1-x)}As$ QWs show good structural quality. (c) The linear relationship between the lattice parameter measured by HR-XRD and B secondary ion intensity of $B_xGa_{0.69(1-x)}In_{0.31(1-x)}As$ QWs suggests unity substitutional incorporation is maintained with the addition of In. (d) Photoluminescence measurements of $B_xGa_{0.69(1-x)}In_{0.31(1-x)}As$ QWs show an increase in PL intensity with the addition of 3% B followed by a decrease in PL intensity with the addition of more boron.

blueshift in wavelength, demonstrating that the addition of boron does not inherently preclude high optical quality material, and may in fact, be used to improve the optical quality of near-IR emitters on GaAs. However, when increasing the B concentration to 7%, we observed a decrease in PL intensity as well as broadening of the PL emission spectrum. As shown in Figure 4.3(b), the strain in the QW was decreased with the addition of B as expected, suggesting the improvement in PL intensity was simply due to a reduction in crystalline defects from the decrease in compressive strain in the BGaInAs QW. The subsequent reduction in PL intensity with more boron may indicate a "boron-penalty" similar to the reduction in material quality observed in the dilute-nitrides [25] and

dilute-bismides [126].

Our approach to extend the wavelengths available on GaAs was similar to that of Tansu *et al.*, [127] we first increased the In concentration in InGaAs QWs on GaAs until no PL was observed ($>$ 40% In). We then added B to this InGaAs alloy in order to reduce the compressive strain in the QWs and recover optical quality material. Figure 4.4 shows the effects of increasing indium and boron concentration on the structural and optical quality of (B)GaInAs quantum wells. As shown in the HR-XRD ω-2θ scans of the B(Ga)InAs QWs (red curve in Figure 4.4(a)), increasing the indium concentration resulted in a reduction in crystalline quality with complete loss of previously well-defined finite thickness fringes, as well as broadening of the QW peak. This loss of structural quality was accompanied by a loss of optical quality as seen in Figure 4.4(b). The addition of 1% to 4% boron reduced the compressive strain in the material as indicated by the shift of the QW peak to larger diffraction angles with increasing B. The recovery of well-defined thickness fringes and QW peaks suggests improved structural quality. In PL, optical quality was recovered and the desired wavelength extension to 1.3 μm was observed (Figure 4.4(b)). The higher In and B concentrations accessible with our growth regime enabled us to exceed the 1.2 μm peak emission wavelength demonstrated by Wang *et al.* [71]. However, unlike Wang *et al.*, we observed a decrease in optical quality with the addition of boron as compared to the $In_{0.4}Ga_{0.6}As$ QW. This reduction in PL intensity with the addition of 2% B was not as severe as that observed in the dilute nitrides, where even 1% nitrogen significantly degraded the optical quality of the material [25], [128]. As the B concentration was further increased, we observed a decrease in the PL intensity, suggesting an inherent "boron penalty" and similar to the decrease in PL intensity observed at shorter wavelengths.

4.3 Growth advancement for improved optical quality

As we moved our focus to larger In:Ga flux ratios, we continued to observe a decrease in PL intensity as well as a broadening of the PL emission spectrum. The growth optimization discussed here focused on BGaInAs QWs as thin BGaInAs QW layers typically do not exceed the critical thickness for relaxation, allowing for increased B or In concentrations without degradation of material quality from strain relaxation. These structures broaden the range of alloys that can be grown pseudomorphically, allowing us to grow non-lattice-matched alloys while optimizing the growth with direct measurement of optical quality using photoluminesence. Photoluminescence of BGaInAs QWs with a In:Ga flux ratio of $\sim$ 44:56 grown using the growth regime optimized for BGaAs growth (blue

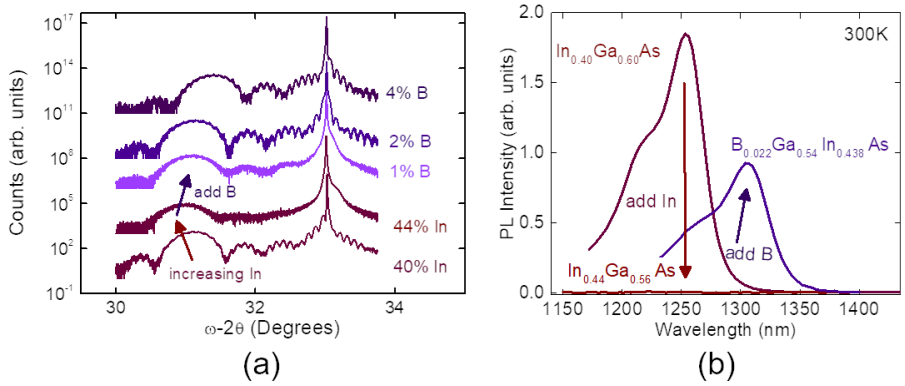

Figure 4.4: (a) HR-XRD ω-2θ scan of (B)GaInAs QWs on GaAs. A loss of well-defined finite thickness fringes and well-defined QW peak was observed as the In concentration was increased. With the addition of B, the recovery of thickness fringes and well-defined QW peak suggests improved structural quality from the reduction in strain. (b) PL of the (B)GaInAs QWs on GaAs targeting 1.3 μm emission. Increasing the In concentration in the InGaAs QW resulted in complete loss of PL intensity. With the addition of $\sim$ 2% B, a strong emission peak at 1.3 μm was observered.

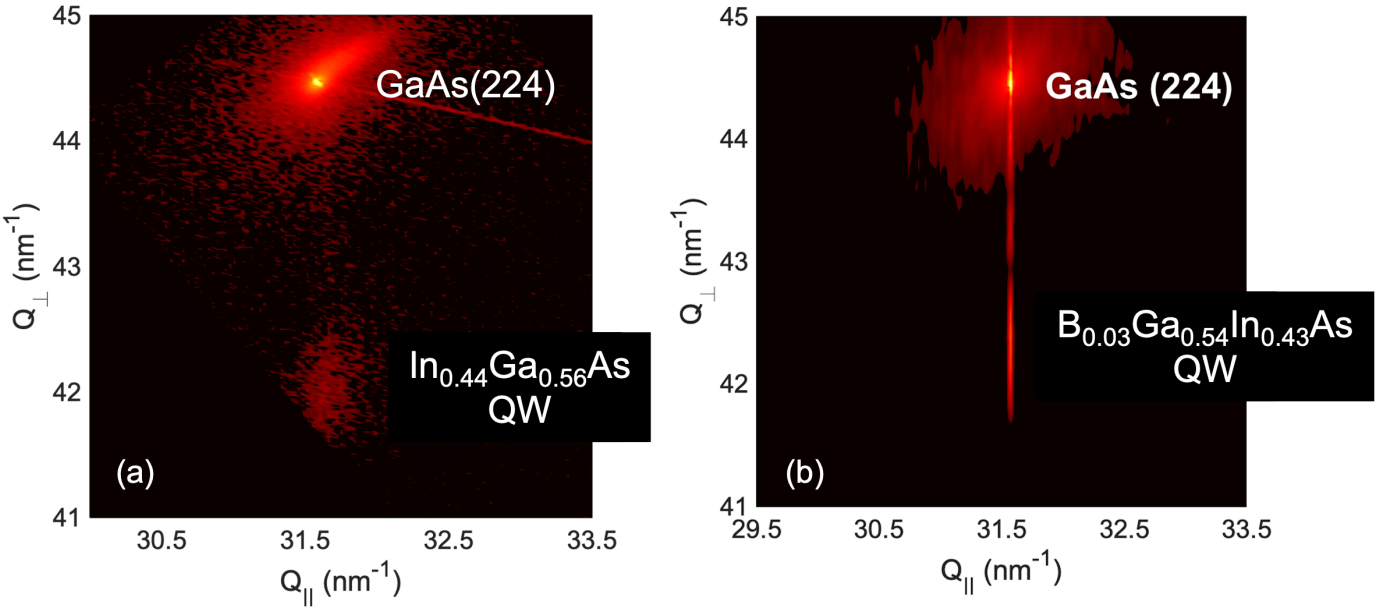

Figure 4.5: (a) Reciprocal space map of $In_{0.44}Ga_{56}As$ QW. In good agreement with HR-XRD ω-2θ scan of the $In_{0.44}Ga_{56}As$ QW, the QW peak is not coherently-strained to the GaAs substrate. (b) Reciprocal space map of $B_{0.03}Ga_{0.54}In_{0.43}As$ QW shows that the QW layer is coherently strained to the GaAs substrate, demonstrating that strain-engineering is possible with the addition of boron.

curves of Figure 4.7(a)) show a decrease in PL intensity with increase B concentration.

The previous investigations of B-III-V growth optimization focused primarily on improving the structural quality and increasing the boron concentration through careful control of the growth

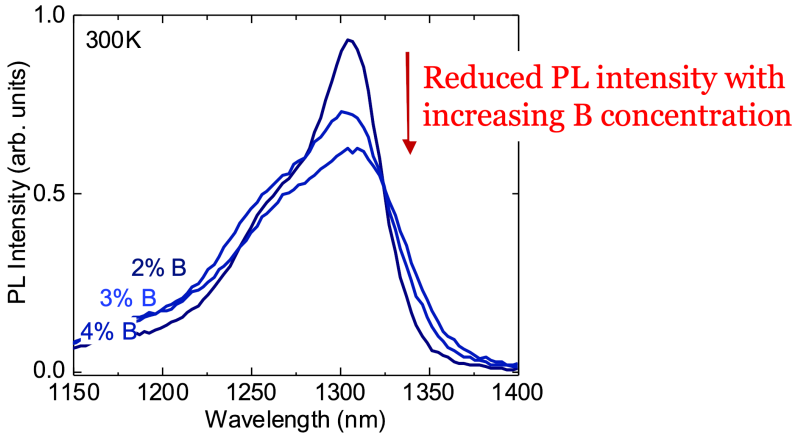

Figure 4.6: PL intensity decreased with increasing boron incorporation suggestive of an inherent B penalty

regime. In order to improve the optical quality of the material, we broadened our characterization of these alloys to focus not only on maintaining good structural quality and promoting boron incorporation, but also on preventing the incorporation of PL-degrading defects.

4.3.1 Growth rate

Epilayer growth rate has been shown to affect both the surface roughness and structural quality of BGaAs alloys [114]. However, the influence of growth rate on optical quality of B-containing alloys has not been studied in detail. Here, we investigate the effects of BGaInAs growth rate on the optical quality of the material. We grew BGaInAs QW structures, maintaining an In:Ga flux ratio of $\sim$ 44:56, with peak emission wavelengths of $\sim$ 1.3 μm, and varying the B concentration at BGaInAs growth rates of 2 Å/s and 2.8 Å/s. As shown in Figure 4.7, reducing the growth rate from 2.8 Å/s to 2 Å/s resulted in an increase in peak PL intensity ($\sim$2x) at boron concentrations of 2% and 4% B indicating that the BGaInAs growth rate can significantly affect the luminescent efficiency of the layer. Additionally, the initial dependence of PL intensity on B concentration observed at higher growth rates seems to be mitigated at slower growth rates. In other words, the perceived "B penalty" at the faster growth rates, was less significant at the slow growth rates. Previous studies as discussed in Chapter 2, suggest that epitaxial growth kinetics extend beyond the immediate sample surface, with rearrangement of atoms occurring between the surface and top 4-10 atomic layers during MBE growth [129], [130]. The number of monolayers participating in rearrangement may be dependent on MBE growth parameters [82]. Here, we believe that the slower growth rate may

allow more time for favorable rearrangement of adatoms, potentially mitigating the formation of B-related point defects [60], which could impact the material optical quality at quantities below the detection limit of structural characterization techniques such as HR-XRD. Further investigation is required to fully understand the influence of growth rate on the formation of B related point defects.

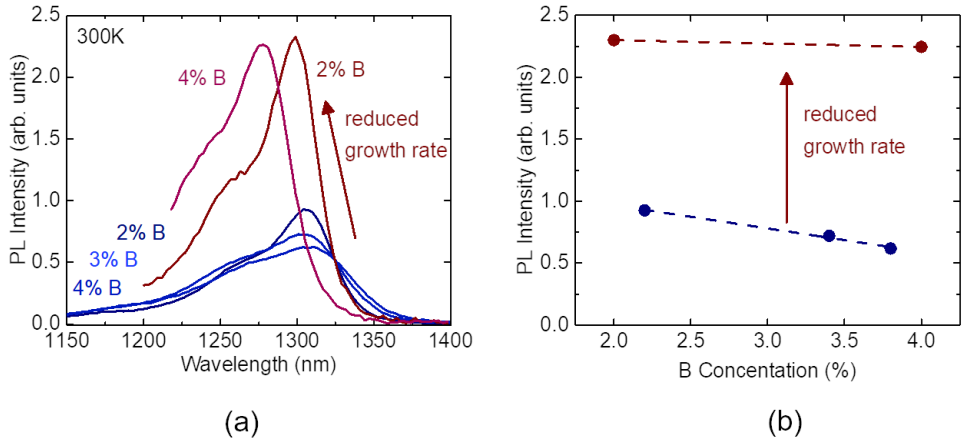

Figure 4.7: (a) Reducing the BGaInAs growth rate increased the PL intensity by > 2x. (b) The B "penalty" observed at faster growth rates, with the addition of just 2% B decreasing the PL intensity by half, is less severe at slower growth rates.

4.3.2 Growth temperature

Growth temperature has been identified as a crucial growth parameter for boron incorporation in the dilute borides [50], [66], [113], as well as for promoting good structural and/or optical quality material in other highly-mismatched alloy growth, including in the dilute bismides [111] and dilute nitrides [88]. In the dilute borides, lower growth temperature results in increased substitutional B concentrations [50], [66], [113], and improved structural quality [66]. Investigating the impact of substrate temperature during growth, we grew a series of BGaInAs QW structures maintaining an In:Ga flux ratio of $\sim$ 44:56. As shown in Figure 4.8(a), the loss of well-defined finite thickness fringes in HR-XRD scans as the substrate growth temperature was increased to $\geq$ 400 °C is indicative of degraded structural quality at elevated growth temperatures. Unsurprisingly, the loss of structural quality was mirrored in the optical quality ofthe material and no measurable PL was observed in samples grown at temperatures $\geq$ 400 °C (4.8(b)). We found that 380 °C was the ideal growth temperature for BGaInAs QWs emitting at $\sim$ 1.3 μm.

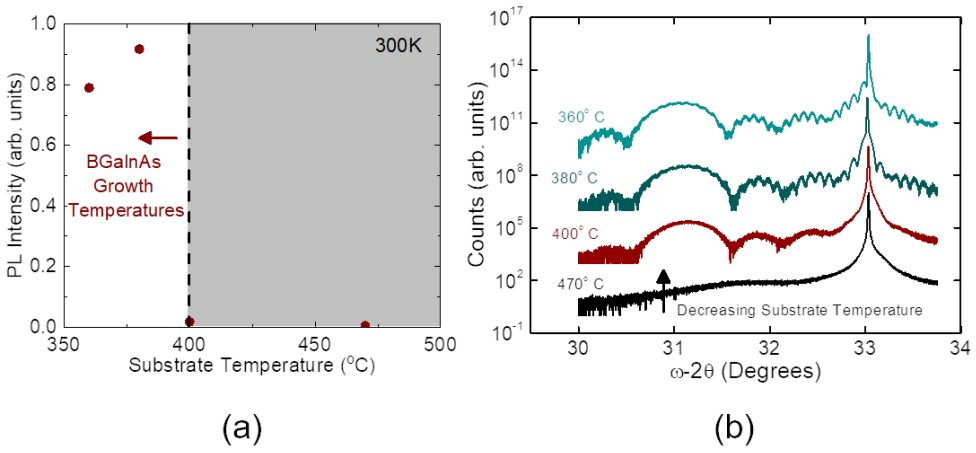

Figure 4.8: (a) Photoluminesence intensity v. growth temperature for BGaInAs QWs emitting at 1.3 μm. Poor optical quality is observed at growth temperatures greater than 380 °C. (b) HR-XRD ω-2θ scan of BGaInAs grown between 360°C to 470 °C. Above 380 °C, the loss of thickness fringes suggests poor crystalline quality.

4.3.3 Group-V/group-III flux ratio

Building on the improvements in optical quality observed at slower growth rates, we sought to optimize the V/III flux ratio to further improve the optical quality of BGaInAs emitters. As with the alloy growth rate and growth temperature, previous investigations of V/III flux ratio in B alloy growth have primarily focused on promoting substitutional B incorporation, with virtually no reports of the impact of V/III flux ratio on optical quality of BGaInAs emitters. BGaInAs QW structures were grown with constant Ga, In, and B fluxes and the As_2/III flux ratio was varied from approximately 1-3. In Figure 4.9(a), HR-XRD ω-2θ measurements of the QW structures grown with as As_2/III flux ratio > 1 showed clear QW layer diffraction peaks with pronounced finite thickness fringes from both the QW and GaAs barrier, indicating high structural quality. Groenert *et al.* previously demonstrated increased substitutional B incorporation in BGaAs films with increasing As_4/III flux ratio [50]. Contrary to the findings of Groenert *et al.* for BGaAs films [50], we noted a small decrease in ($\sim 5\%$) in B incorporation with increasing As_2 overpressure as seen in Figure 4.9(b) (samples were grown out of order to control for small variations in the B flux). We employed Bi as a surfactant, a lower growth temperature, and As_2 rather than As_4. Lower growth temperatures [84] and an As_2 (instead of As_4) overpressure [85], [86] have been shown to decrease adatom surface migration, which may explain the differences observed here. Further investigation is necessary to fully clarify how the As_2/III ratio affects the substitutional B incorporation in BGaAs and BGaInAs

alloys under these growth conditions.

Additionally, as shown in Figure 4.9(c), despite the consistent high structural quality observed in HR-XRD, varying the As/III flux ratio significantly impacted the QW PL intensity. At low substrate temperatures, such as those required for BGa(In)As growth, high As/III flux ratios promote As-related point defects, which behave as non-radiative recombination centers, decreasing the direct band-to-band recombination of carriers and reducing the optical quality of the material [86]. Because low substrate temperatures are necessary to promote substitutional incorporation of B in BGaInAs alloys, the As/III over-pressure needs to carefully be balanced such that enough As is supplied to avoid group-V site vacancies while also minimizing the formation of As-related point defects from excess As_2 [82]. Our PL measurements indicated that an As/III flux ratio of $\sim$ 2x (BEP ratio of $\sim$ 10x) resulted in the highest photoluminesence intensity. Previous investigations of GaAs and AlGaAs alloys grown by MBE had similarly found peak luminescence efficiencies are achieved with an As/III flux ratio of $\sim$ 2 [82], [131]–[133].

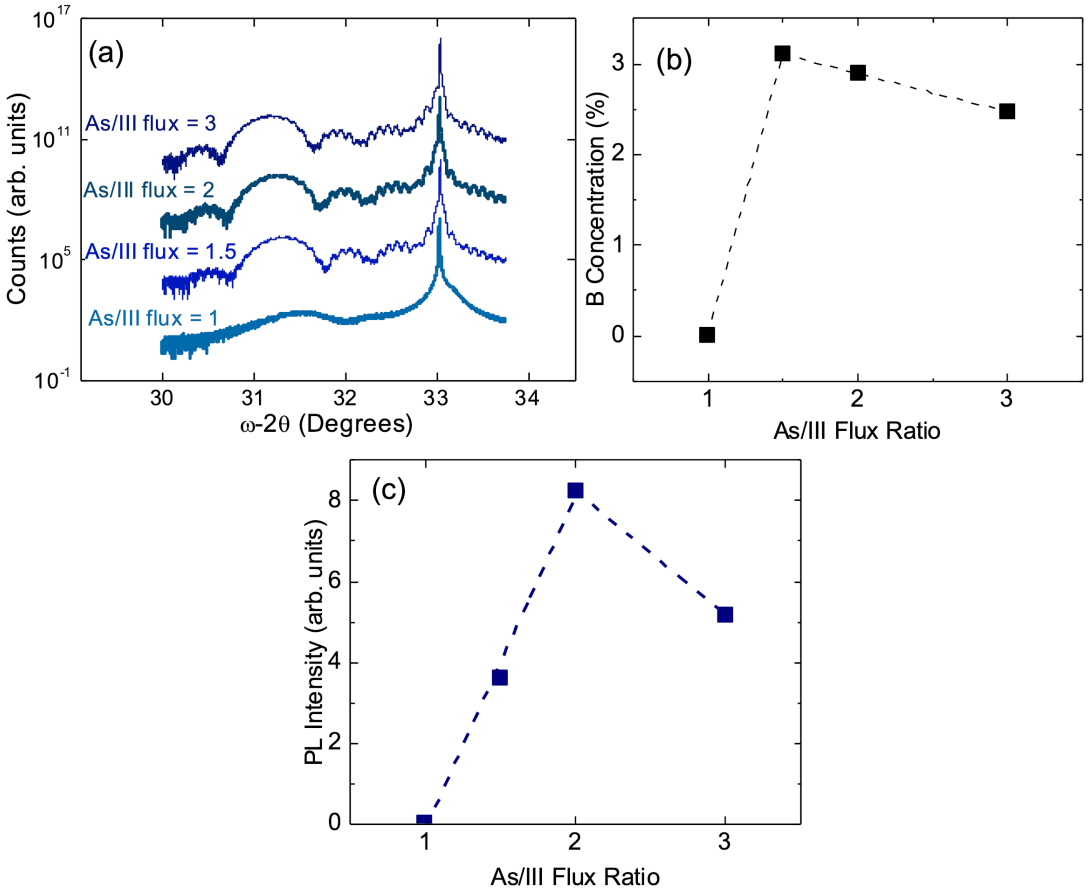

Figure 4.9: (a) HR-XRD ω-2θ scan of $B_xGa_{0.56(1-x)}In_{0.44(1-x)}$ varying the As_2/III flux ratio. Poor crystal quality is observed at an As_2/III flux ratio of 1. (b) The measured B concentration slightly decreased with increasing As/III flux ratio. (c) Photoluminesence intensity of $B_xGa_{0.56(1-x)}In_{0.44(1-x)}$ varying the As_2/III flux ratio. An As_2/III flux ratio > 1 was required for obtaining measurable PL and an As/III flux ratio of 2 produced the highest optical quality material.

4.3.4 Optimized growth conditions

Combining these disparate growth optimizations, we grew a QW structure with a BGaInAs growth rate of 2 Å/s, a growth temperature of 380 °C, and an As_2 flux ratio of ~ 2. As shown in Figure 4.10, this growth optimization demonstrated a 10x improvement in PL over a control sample grown with similar B concentration under the initial BGaAs growth conditions using a fast growth rate of 2.8 Å/s, a growth temperature of 380 °C, and an As_2 flux ratio of 3. Also shown in Figure 4.10, this growth optimization facilitated improvement in the BGaInAs optical quality such that

the B-containing QW grown under these conditions demonstrated increased PL efficiencies (∼3x) compared to the reduced In concentration ($In_{0.40}Ga_{0.60}As$) QW. The growth optimization at 1.3 μm demonstrated that control of growth kinetics is critical for improving the optical quality of BGaInAs alloys. These results demonstrate that BGaInAs alloys not only enable wavelength extension of emitters on GaAs, but also improved optical quality at extended wavelengths.

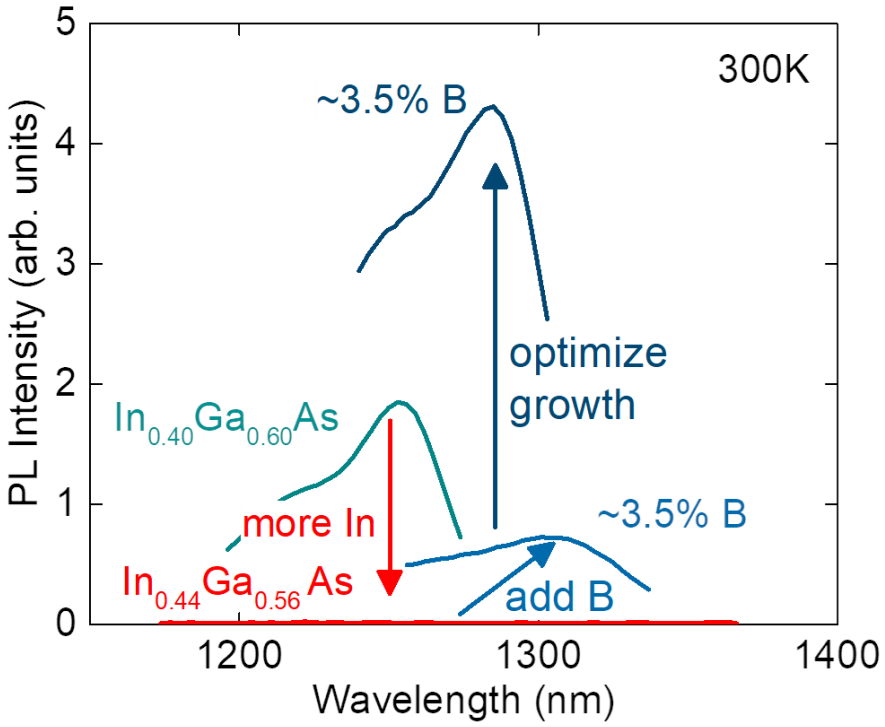

Figure 4.10: Through growth optimization of the BGaInAs growth rate, substrate temperature, and As/III flux ratio, we have demonstrated increased PL intensity compared to both the BGaInAs QW under unoptimized growth conditions and the InGaAs QW.

High angle annular dark-field scanning transmission electron microscopy (HAADF-STEM) and electron dispersion spectroscopy (EDX), performed by Larry Lee's group at the University of Illinois at Urbana-Champaign, of a BGaInAs QW emitting at 1.3 μm grown under the optimized growth regime also indicated good structural quality as shown in Figure 4.11.

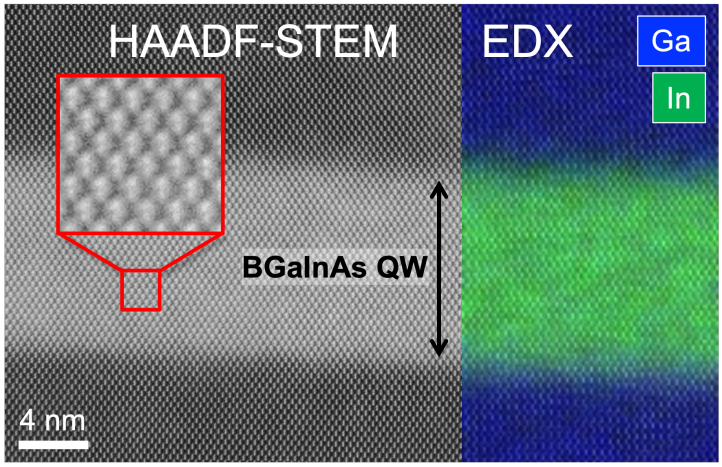

Figure 4.11: High-angle annual dark-field scanning transmission electron microscopy and electron dispersion spectroscopy of a BGaInAs QW performed by Larry Lee's group at UIUC.

4.3.5 Comparison of optimized growth in $B_x(Ga_{0.6}In_{0.4})_{1-x}As$ QWs

At an In:Ga flux ratio of $\sim$ 44:56, we were not able to grow a high-quality boron-free InGaAs QW on GaAs due to relaxation of the QW layer from the large amount of compressive strain in the epitaxial layer. The highest In concentration InGaAs QW we were able to grow without observing structural degradation and loss of optical quality material was a In:Ga flux ratio of $\sim$ 40:60. The challenge in growing GaAs-based InGaAs QWs at even this In concentration or emission wavelength has been well established [127], [134]. To facilitate direct comparison with high-quality InGaAs control QW structures, we grew BGaInAs QWs at an In:Ga flux ratio of $\sim$ 40:60, with boron concentrations ranging from 1% to 5% B. We observed comparable PL intensities from the low B concentration ($<$ 2% B) and boron-free PL structures. At 2% B, we noted a significant improvement in PL intensity ($\sim$ 3x). However, that PL improvement degraded as the boron concentration was increased to 5% resulting in a similar PL intensity as the boron-free QW. Previous reports of BGaInAs QW structures have suggested that bron-related defect states may lead to localization of carriers at low temperatures, resulting in an "S"-shaped dependence on the bandgap with temperature [73]. In temperature-dependent PL performed by Robert Kudrawiec's group at the Wroclaw University of Science and Technology, we observed good agreement with the Varshni equation for BGaInAs alloys with B concentrations $<$ 5%. However, at 5% B we noted a small deviation below 100 K suggestive of localization or inhomogeneity in the QW due to increased defects, indicating that further growth advancements may be necessary for increasing B concentrations. These results demonstrate that

the addition of B does not inherently cause the "s-shape" and localization reported by Hidouri *et al.* [73]. Rather, good quality boron-containing alloy material is possible through optimization of the growth regime.

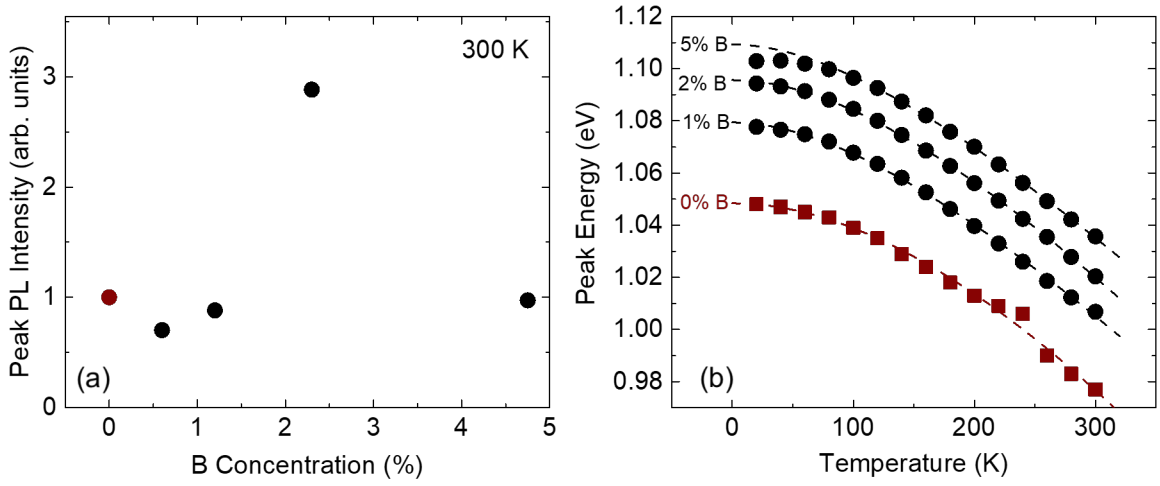

Figure 4.12: (a) Peak PL intensity v. B concentration for a fixed In:Ga flux ratio of 40:60. We observed comparable PL between the boron-free InGaAs QW (red dot) and the $< 2\%$ B BGaInAs QWs. At 2% B we observed the highest PL intensity and at 5% we observed a degradation in PL intensity to that of the InGaAs QW. (b) Temperature-dependent photoluminesence of (B)InGaAs QWs (performed by our collaborators in Robert Kudrawiec's group) with a In:Ga flux ratio of 40:60 and B concentrations of 0%, 1%, 2%, and 5%. A good fit with Varshni's equation is observed for the QWs with 0-2% B. Small deviation from Varshni's equation at 5% B is suggestive of localization.

4.3.6 As-grown emission beyond 1.3 μm

A thorough understanding of the B-miscibility gap in BGaInAs alloys is essential for identifying prospective device applications for these alloys as extended wavelength emitters/absorbers on GaAs. Additionally, given that 25% B is necessary to lattice-match these alloys to Si, establishing the miscibility limits of B in BGaInAs is also critical for evaluating the potential of these materials for the realization of lattice-matched, direct-gap III-V alloys on Si. To further probe the miscibility limit of B in BGaInAs, we grew BGaInAs QW structures simultaneously increasing the In:Ga flux ratio, and the B flux, while maintaining the growth conditions optimized at 1.3 μm (380 °C substrate temperature, Bi as a surfactant, As_2 flux ratio of $\sim$ 2 and a GaAs growth rate of $\sim$ 2 Å/s). As

shown in Figure 4.13(a), increasing the In:Ga flux ratio to 53:47 from 44:56 resulted in broadening of the BGaInAs QW layer peak as well as disappearance of finite thickness fringes in HR-XRD ω-2θ scans indicating structural degradation despite the use of our previously optimized growth regime. Consistent with reports of growth optimization in the dilute nitrides [135] and dilute bismides [111], the optimal growth window for substitutional boron incorporation appears to narrow and/or shift as the In or B concentration is increased and the alloy becomes more highly mismatched. Returning to the growth regime optimized by McNicholas to increase substitutional B incorporation beyond the dilute limit in BGaAs (growth rate of $\sim$ 2.8 Å/s, growth temperature of 380 °C, As/III flux ratio of $\sim$ 3), we found that decreasing the growth temperature of BGaInAs QWs to 360 °C with an In:Ga ratio of 53:47 to 360 °C resulted in increased substitutional B incorporation and good structural quality as shown in Figure 4.13(b). Photoluminesence of these QWs (Figure 4.13(c)) showed an extension of the emission wavelength to 1.4 μm, consistent with the 1.3 μm emission from the BGaInAs QW with a In:Ga flux ratio of 44:56 and the 1.25 μm emission from the InGaAs QW with an In:Ga flux ratio of 40:60. However, these samples show a large reduction in PL intensity (over 2 orders of magnitude) compared to the BGaInAs QW optimized for emission at 1.3 μm. The observed sensitivity of structural quality to substrate growth temperature with increasing In/B concentration further emphasized the importance of substrate temperature on BGaInAs alloy quality, and indicates that substrate temperature is a good starting point for optimization of yet to be explored alloys with different simultaneous In and B concentrations.

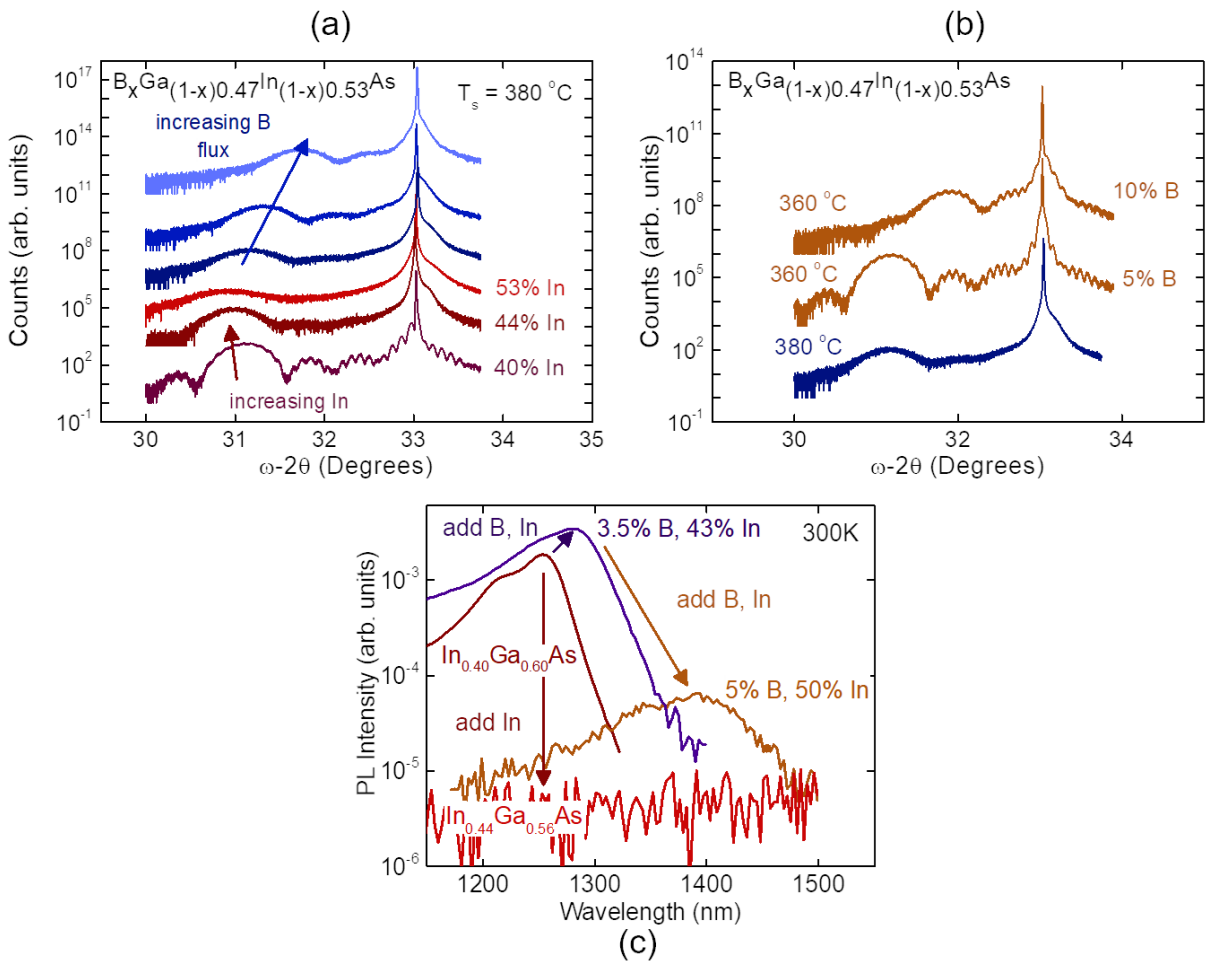

Figure 4.13: (a) HR-XRD ω-2θ scans of (B)GaInAs QWs. As anticipated, increasing the In:Ga ratio to 53:47 resulted in poor structural quality in the InGaAs QW. Despite the use of the BGaInAs growth regime optimized at lower In:Ga flux ratios. (b) HR-XRD ω-2θ of BGaInAs QWs grown with the same In:Ga flux ratio at varying substrate temperatures. Decreasing the substrate temperature promotes substitutional incorporation of B, with up to 10 % incorporation demonstrated. (c) Increasing the In:Ga flux ratio resulted in an extension of the PL emission wavelength to 1.4 μm.

4.4 B-III-V alloys on InP

The emission and cutoff wavelengths of InP-based emitters and absorbers are limited by the amount of epitaxial strain that can be accommodated, similar to GaAs-based emitters and absorbers. The addition of boron to InGaAs alloys again offers a method for strain-engineering these alloys to extend the emission and absorption wavelengths available on InP. The bandgaps of BGaInAs alloys,

predicted from theory, lattice-matched to InP are shown in Figure 4.14. Unlike InGaAs on GaAs, InGaAs can be grown lattice-matched to InP, increasing the flexibility of B and In concentrations by reducing the amount of B necessary to strain-engineer InGaAs alloys on InP.

As discussed in Section 4.3, we were able to demonstrate luminescence and wavelength extension in BGaInAs QW structures at higher In and B concentrations on GaAs (In:Ga flux ratio of 53:47 and 5% B). However, the PL intensity was significantly reduced compared to the lower In and B concentration BGaInAs QWs (In:Ga flux ratio of 44:56 and B concentrations $\leq 4\%$). Moreover, in photoreflectance measurements of the higher In and B concentration BGaInAs QWs on GaAs, no PR resonances were observed, suggesting poor material. To investigate alloy properties including structural quality, bandstructure, and optical quality, we investigated the growth of BGaInAs on InP.

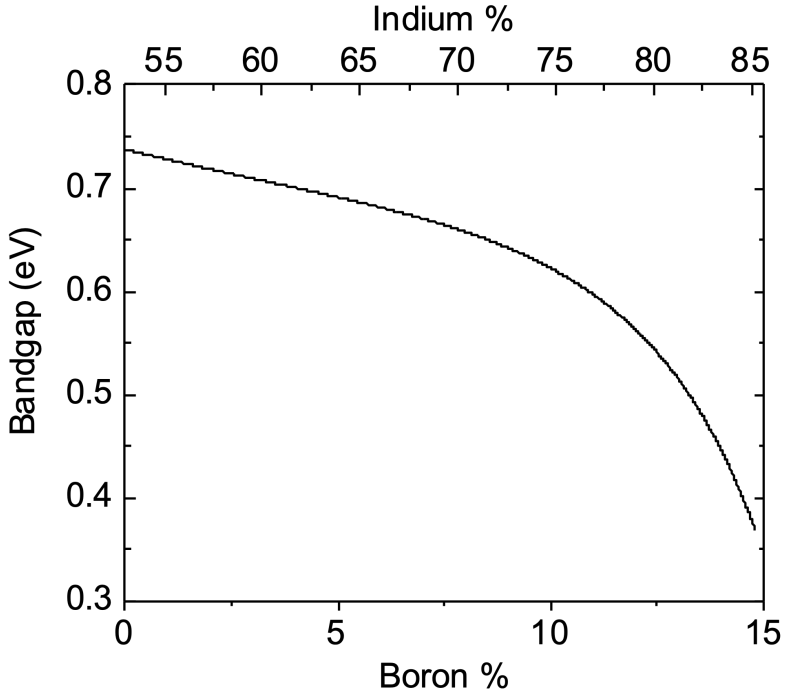

Figure 4.14: Estimated bandgaps for BGaInAs lattice-matched to InP assuming a BAs direct bandgap of 5.8eV.

Growth of InP-based BGaInAs alloys

Transitioning our growth regime to InP substrates, we were able to reduce the impact of epitaxial strain on the material quality, while maintaining and even increasing the In concentration. Similar

to the method described in Section 4.2, we focused on optimizing the growth to increase the incorporation of B and In simultaneously. We first grew InGaAs films (with In concentrations between 41% and 56%) on InP. The InP oxide was removed using a P_2 overpressure and an InP buffer was grown at 400 °C. The InGaAs films were grown at 400 °C with a As/III flux of 3 and a InGaAs growth rate of $\sim$ 2.8 Å/s. Good structural quality and photoluminesence were observed from the InGaAs films. Then, BGaInAs films on InP were grown maintaining the growth temperature of 400 °C with an As/III flux of 3 and a BGaInAs growth rate of $\sim$ 2.8 Å/s. As shown in Figure 4.15, the addition of 2% B to an InGaAs film with an In:Ga ratio of 56:44 resulted in the expected change in strain from compressive to tensile, demonstrating the potential for strain-engineering InGaAs emitters and absorbers on InP in order to realize longer cutoff and emission wavelengths.

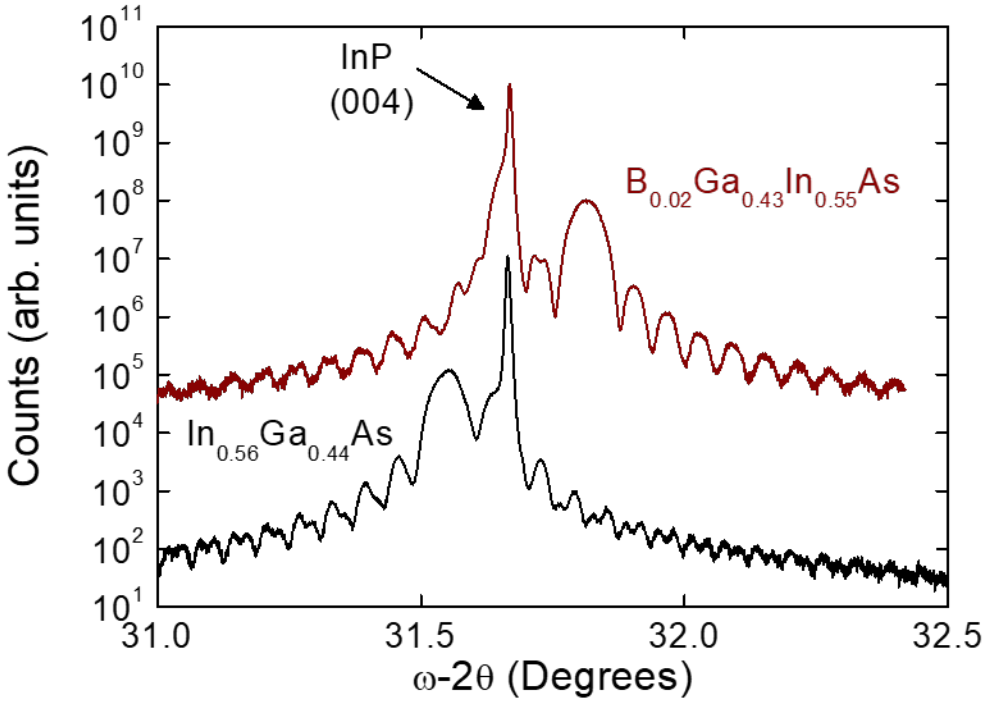

Figure 4.15: HR-XRD ω-2θ InGaAs film on InP (black) and BGaInAs film on InP (red). The transition from compressive to tensile strain demonstrated the ability to strain engineer InGaAs films on InP with the addition of B.

Photoluminescence and photoreflectance of BGaInAs films on InP

Unfortunately, no photoluminescence was observed from the BGaInAs films on InP. Improved photoreflectance was observed compared to the BGaInAs QWs grown on GaAs. However, compared to the InGaAs films on InP, broadening in the PR signal was observed, indicating poorer material quality compared to the born-free material. In PR, we observed a blueshift in bandgap with boron as expected from the predictions from Kudrawiec *et al.* and McNicholas [48], [64] as shown in Figure 4.16. Future investigation of these alloys should focus on optimizing the growth regime to recover optical quality material in a similar method to the one discussed in Section 4.3 and improved material quality for PR measurements. Specifically we believe focusing on growth temperature optimization would be the next logical step, given the increased sensitivity to growth temperature as the alloy becomes more highly-mismatched with the addition of B and In.

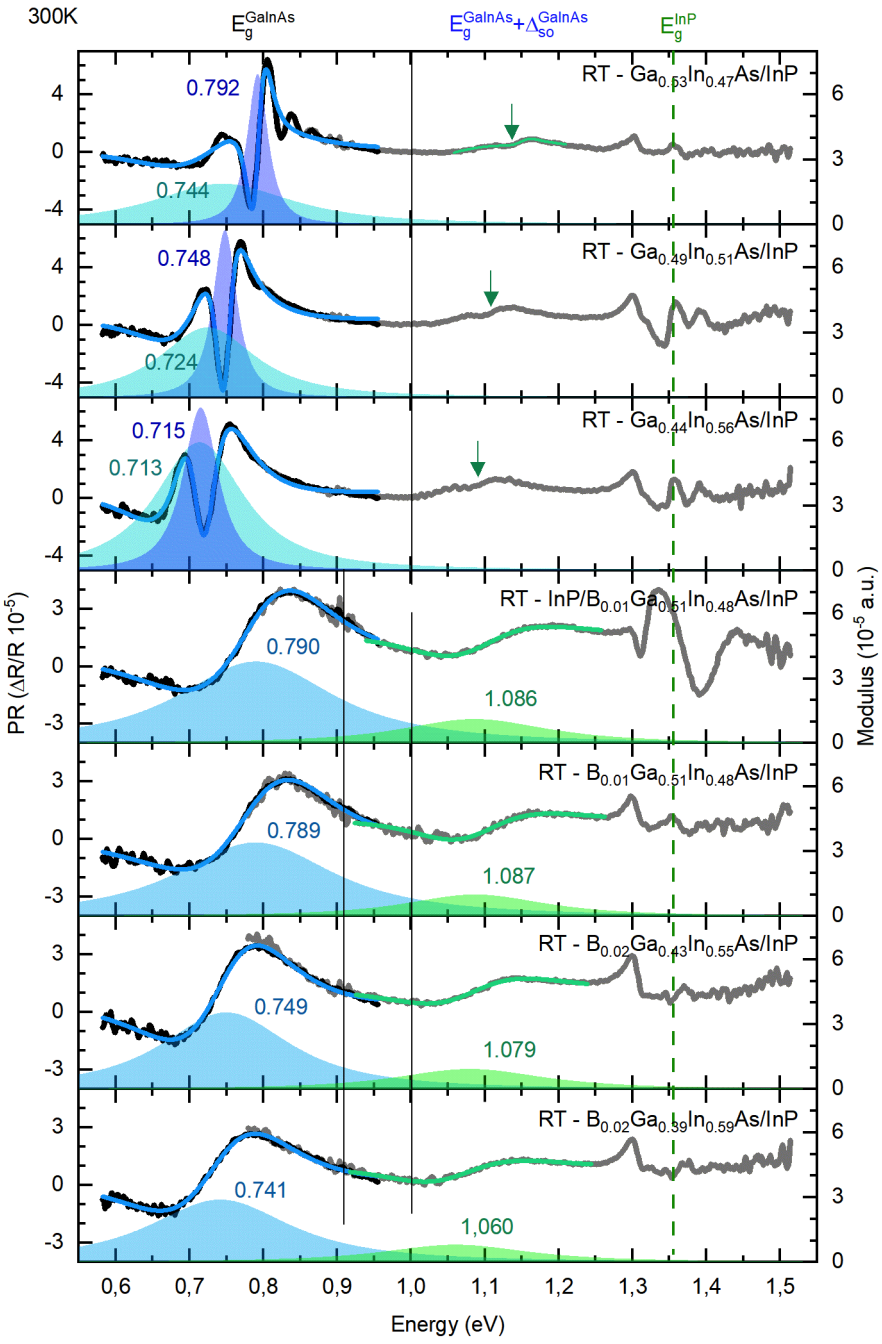

Figure 4.16: PR measurements, performed in collaboration with Professor Robert Kudrawiec's group, of (B)GaInAs films on InP. The broadening in the boron-containing films indicates poor material quality. However, the spectral features were defined enough that bandgap energies could be calculated from these measurements.

4.5 Dopant incorporation in B-III-V alloys

Potential B-III-V device applications require an understanding of dopant activation and carrier dynamics in BGaAs and its related alloys. Previous investigations of B-III-V alloys have observed unintentional p-type doping [60], [114], a reduction in dopant incorporation/activation, and a reduction in carrier mobility [136]. Geisz *et al.* observed reduced dopant incorporation in photovoltaic detectors in both p-type and n-type $B_{0.03}Ga_{0.91}In_{0.06}As$ regions grown by metal organic chemical vapor deposition (MOCVD) compared to boron-free alloys [52]. Previous n-type doping of B-III-V alloys with silicon has been reported in MOCVD-grown BGaInAs alloys with lower carrier concentrations and mobilities comparable to similarly grown GaAs [52], [136].

Investigating the effects of boron incorporation in the ternary alloy BGaAs demonstrated little to no effect on p-type dopant activation with increasing B content. However, McNicholas observed no dopant activation when Si-doping BGaAs films [48]. Instead, the use of Te as an n-type dopant was required [48]. McNicholas also found that increasing the B concentration resulted in a decrease in n-type carrier concentration and carrier mobility as shown in Figure 4.17(a) [48]. This effect is similar to that observed in the dilute nitrides [136]. However, the reduction in carrier concentration per percent highly-mismatched constituent was not as severe [48]. The addition of indium with a constant B concentration of $\sim 1.25\%$ to form BGaInAs demonstrated no significant reduction in electron carrier concentration nor mobility as shown in Figure 4.17(b) [48], in good agreement with theoretical predictions [43]. The consistent carrier activation and mobility observed in n-type BGaInAs films with varying In concentrations suggests that n-type doping BGaInAs alloys with Te would not have the same carrier concentration dependency on alloy composition as observed in the ternary alloy BGaAs.

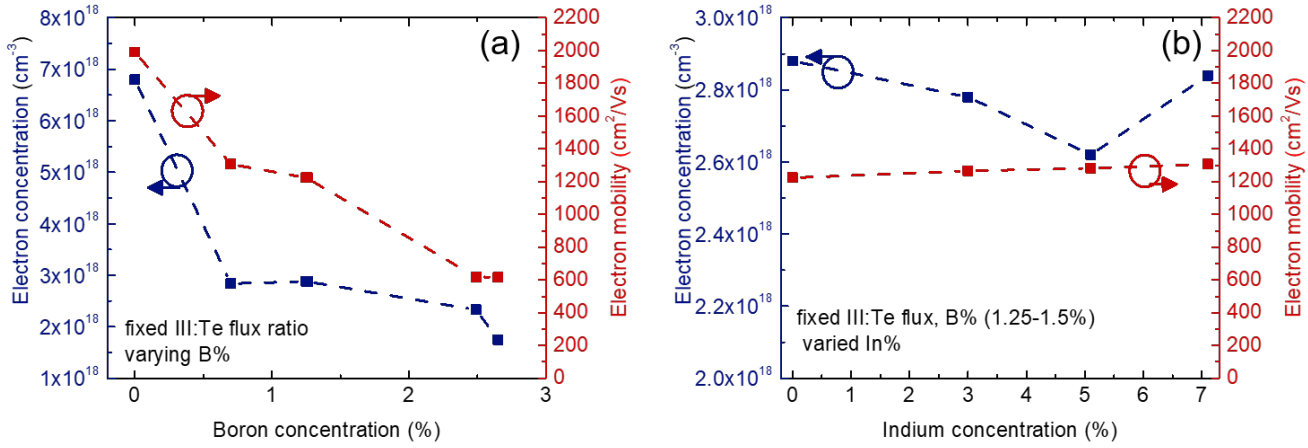

Figure 4.17: (a) The measured electron carrier concentration and mobility decreased with increasing B in BGaAs films with a fixed group-III/Te flux ratio. (b) The measured electron carrier concentration and carrier mobility was consistent in BGaInAs films with a fixed B concentration and fixed group-III/Te flux ratio. Reproduced from [48].

Expanding this initial work to more thoroughly examine doping of BGaInAs alloys, we focused on BGaInAs alloy compositions lattice-matched to GaAs. We grew 250 nm BGaInAs films on GaAs using Be as a p-type dopant and Te as a n-type dopant. We observed only a small reduction in p-type dopant activation with increasing B concentration, similar to p-type doping of BGaAs (Figure 4.18(a)). However, in contrast to previous reports, we noted a reduction in n-type carrier activation and electron mobility with increasing B and In concentrations as shown in Figure 4.18(b). As discussed in Section 4.3, as the alloy becomes more highly mismatched, the growth of high crystalline quality material requiring further optimization of the growth regime. Here, we found that reducing the growth temperature overcame the reduction in carrier activation and mobility observed at high B and In concentrations as indicated by the red circle in Figure 4.18(b). Teubert *et al.* observed localized B impurity states below the conduction band edge in n-type $B_{0.03}Ga_{0.91}In_{0.06}As$ films as indicated by the reduction in free carrier concentration under hydrostatic pressure [136]. Tellurium is a shallow donor, sitting $\sim$ 30 meV below the conduction band edge [137]. One potential cause for the reduction in dopant activation we observed under unoptimized growth conditions may be increased electron trapping in B cluster states below the conduction band edge. Similar to the improvements observed in optical quality through growth optimization, improved growth conditions may reduce or eliminate these B-cluster states, reducing

electron trapping, and increasing the free carrier concentration.

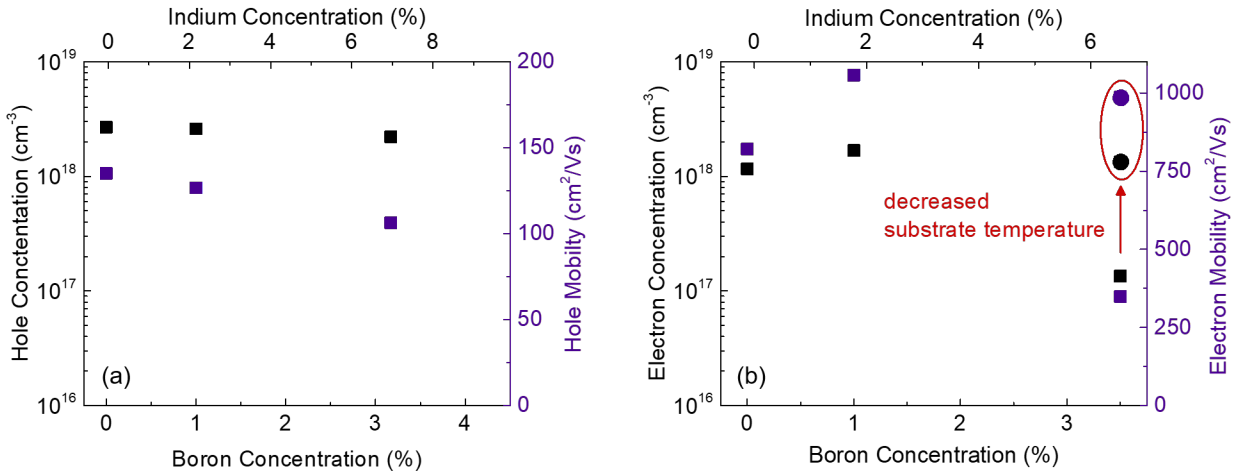

Figure 4.18: Carrier concentration and carrier mobility from Hall measurements of (a) p-type and (b) n-type doped BGaInAs alloys with compositions lattice-matched to GaAs. We observed a small reduction in carrier activation and carrier mobility with increasing B, In concentrations in the p-type, Be-doped, samples. In n-type samples, Te-doped, we observed a significant reduction in n-type carrier concentration at higher B, In concentrations. By reducing the substrate temperature during growth (circled in red), we were able to mitigate the deliterius effects of B incorporation on dopant activation and electron mobility, resulting in virtually no reduction in n-type carrier concentration nor electron mobility.

Chapter 5

B-III-V based optoelectronic devices

5.1 Prototype BGaInAs light-emitting diodes

To demonstrate the potential for B-containing optoelectronic devices, we grew an electroluminescence structure (EL) with a BGaInAs QW emitter active region n- and p- type AlGaAs contact layers as shown in Figure 5.1(a). The light-output versus input current (L-I) curve and the emission spectrum are shown in Figure 5.1(b). The demonstration of electroluminescence from this structure confirmed that the addition of B is not a fundamental impediment to devices. The EL structure shown in Figure 5.1(a) was chosen as it is a common structure for GaAs-based edge emitting lasers with an appropriate waveguide for lasing at 1.3 μm (the total thickness of the GaAs waveguide is $\sim \lambda/4$). However, no lasing was observed from these devices. As discussed in Section 5.1.1, the growth of this structure required multiple *in situ* transfers of the sample between MBE systems. The lack of lasing may not be a fundamental BGaInAs material property, but rather caused by these transfers or the optical quality of the MBE system equipped with boron and used to grow the active region of the EL structure. Further investigation is necessary to clarify the lack of lasing from this material.

This section is adapted from a previously published paper: R.H. El-Jaroudi, K.M. McNicholas, A.F. Briggs, S.D. Sifferman, L. Nordin, S.R. Bank,"Room-temperature photoluminescence and electroluminescence of 1.3-μm-range BGaInAs quantum wells on GaAs substrates," *Applied Physics Letters*, vol. 117, no. 2, p. 021102, 2020, doi: 10.1063/5.0011147. My contributions to this work included material/device design, growth, fabrication and characterization.

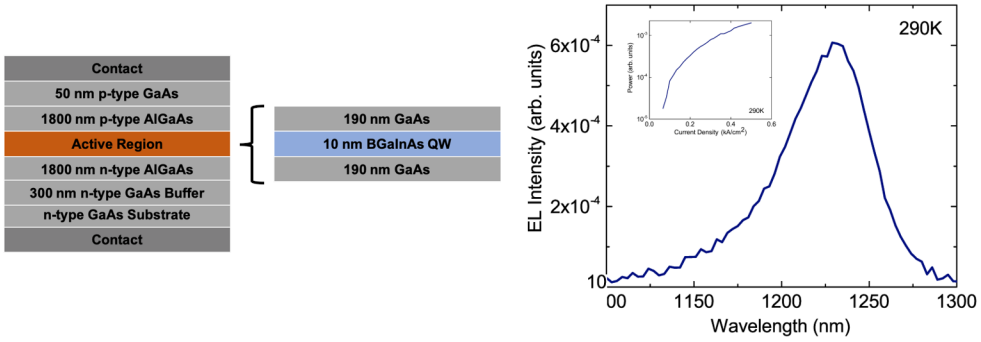

(a) (b)

Figure 5.1: (a) Epitaxial layer structure of the EL device structure with a BGaInAs QW active region. (b) L-I curve (inset) and emission spectra (at J=0.5kA/cm$^(2)$) of the electrically injected emitter BGaInAs active region. While the nominally identical composition PL structure, $B_{0.02}Ga_{0.55}In_{0.43}As$, emitted at 1.3 μm, a blueshift in wavelength to $\sim$ 1.24 μm was observed

5.1.1 Growth of the electroluminescence structures

As discussed in the previous section, we demonstrated 1.3 μm peak emission with as-grown, thin QW structure designed for PL measurements. To demonstrate EL devices emitting at 1.3 μm, we first grew n-type cladding layers on the Al-equipped MBE system, which is attached *in situ* to the B-equipped MBE system. After the growth of the AlGaAs layer, a 55 nm GaAs capping layer was grown. The sample was then cooled to room temperature under an As_2 overpressure. The sample was kept under an As_2 overpressure for an hour to deposit an As cap, which protects the surface from contamination during transfer between the two growth chambers. The sample was then transferred into the MBE system with the boron e-beam source for the growth of the GaAs waveguides and BGaInAs QW. Prior to the growth of the GaAs and BGaInAs layers, the As cap was thermally desorbed by heating the sample to the GaAs growth temperature (580 °C) under an As_2 overpressure. The sample was then cooled to the BGaInAs growth temperature of 380 °C. The target composition of the BGaInAs QWs was $B_{0.02}Ga_{0.55}In_{0.43}As$; the same composition that showed peak PL emission around 1.3 μm in the QW PL structures. After the growth of the GaAs waveguide, the sample was then As capped again before being transferred back to the Al-containing system. The As cap was removed under an As_2 overpressure as the sample was heated to the GaAs and AlGaAs layer growth temperature of 580 °C. A p-type AlGaAs layer was grown and then a p-type GaAs capping layer. Electroluminescence was measured at room temperature using a thermoelectrically-cooled, butt-coupled, InGaAs detector. The devices were electrically-driven

under pulsed conditions with a 1% duty cycle.

5.1.2 Wavelength shift with unintentional annealing during growth

As mentioned above, the active region of the EL structure was nominally identical to the 1.3 μm QW PL structures discussed in Section 4.3. However, the EL structure emission spectra exhibited blue-shifting to a peak emission wavelength of 1.25 μm. Through investigation of the effects of annealing on emission wavelength, we demonstrated this blueshift is due to unintentional annealing of the active region during the growth of the top cladding layer.

In situ and *ex situ* annealing

During the growth of III-V alloys, the optimal substrate temperature is material-dependent. Growth of III-V heteroepitaxy devices often requires substrate temperature changes for each material. Due to the low diffusion lengths of aluminum, high growth temperatures ($\geq$ 550 °C) are required to promote high quality material growth. The LEDs discussed in Section 5.1 use AlGaAs cladding layers before and after the BGaInAs active region. Therefore, high growth temperatures are maintained after deox during the growth of the n-type AlGaAs layer, the substrate is lowered to the cooler BGaInAs growth temperature, and then the substrate is reheated to $\sim$ 550 for the growth of the p-type AlGaAs cladding layer. The significantly hotter growth temperature can cause *in situ* annealing of the active region. The unexpected blueshift in emission wavelength observed in the EL structure is similar to the blueshift reported in dilute-nitride emitter active regions [138]–[142]. In the dilute nitrides, this shift is attributed to thermal stabilization through an increase in the N-In bonds [92], [140]. Additionally, in the dilute nitrides, thermal annealing has been shown to significantly improve the luminescence efficiency quality of the the active region [138]–[140], [142]. This improvement is attributed to both a stronger interband matrix element with increasing N-In bonds and the removal of nonradiative recombination centers [140].

Methods for investigating *in situ* and *ex situ* annealing

Intentional in situ annealing required multiple identical samples, necessitating the growth of BGaInAs QW PL structures on full 3" SI GaAs substrates. The wafers were then unloaded from the MBE system and handled cleanly in order to allow for them to be returned to the MBE system. The full wafers were cleaved into quarters, allowing for an as-grown control sample to be kept, while the remaining pieces of the sample were returned to the system, baked in the load chamber at 200

°C and baked on the bake out station at 450 °C prior to being returned to the growth chamber. They were then heated to the growth temperature of AlGaAs (580 °C) under an As overpressure to prevent As desorption from the surface for a fixed annealing time. Using this process, we confirmed the blueshift in the EL structure was caused by unintentional annealing from increased substrate temperature during the growth of the p-type cladding layer, as shown by the blueshift in the *in situ* annealed sampled compared to as-grown sample in Figure 5.2(a). However, this process is time consuming and impractical for annealing studies requiring many samples or steps. To facilitate a more exhaustive study of annealing effects in BGaInAs QW structures, the rest of the annealing studies discussed were performed using *ex situ* annealing.

Ex situ annealing was performed in a rapid thermal annealing (RTA) system, allowing for flexibility in sample size and cleanliness, as well as significantly reducing the time required. To conserve material, progressive annealing studies were performed when possible. The samples were placed on a Si wafer inside the nitrogen-purged RTA system and a GaAs capping wafer was used to prevent As desorption during the annealing process. The temperature of the backing wafer was measured by a pyrometer to determine the annealing temperature. The samples were annealed for 1 minute.

5.1.3 Potential for true 1.3 μm light emitting diode

To understand the effects of thermal annealing on BGaInAs active regions for devices, we performed *in situ* and *ex situ* annealing study on QW PL structures with nominally identical alloy composition. As shown in Figure 5.2(b), the emission wavelength blueshifts with increasing *ex situ* annealing temperature. Additionally, the photoluminesence intensity initially increases with increasing annealing temperature before ultimately decreasing.

The effects of thermal annealing on semiconductor alloys are important because unanticipated changes in alloy properties can impact device performance. Unavoidably, many optoelectronic device designs require the growth of thick cladding regions grown above the active region, grown at higher temperatures than the active region alloy. Bank *et al.* found that over-annealing of the active region, or *in situ* annealing of the active region such that no photoluminesence improvement is observed with subsequent *ex situ* annealing, could occur during this step, resulting in a higher lasing threshold current than if the alloy is not over-annealed [143]. During post-growth processing, the device structure can be *ex situ* annealed in order to exploit the improvement in PL observed with optimal thermal annealing to reduce laser threshold current [143]. Following this observation,

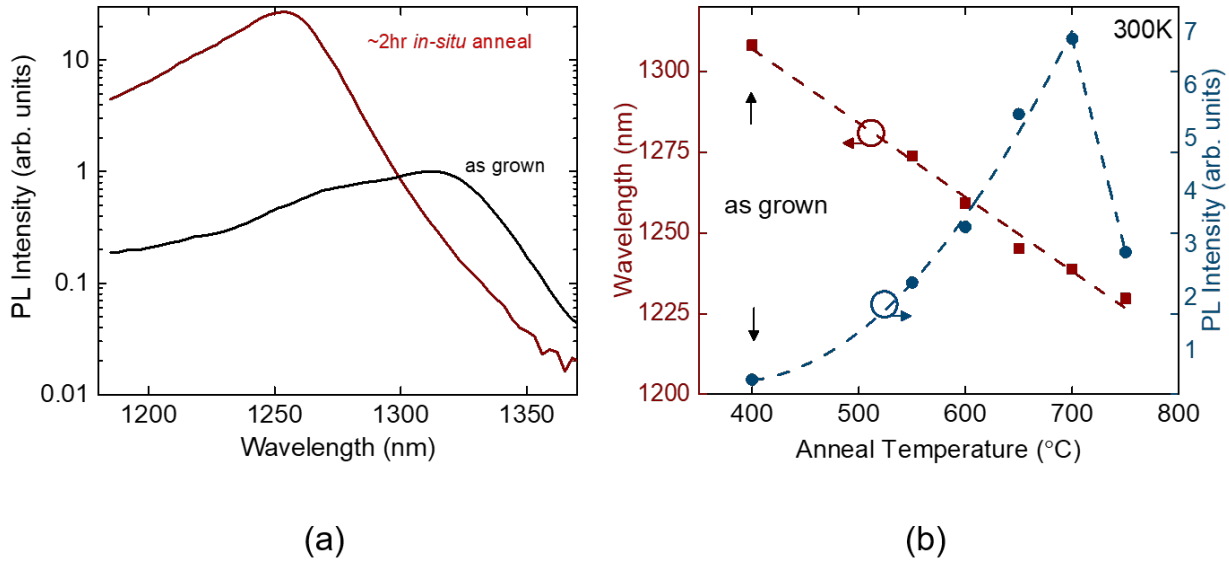

Figure 5.2: (a) *In situ* annealing of a BGaInAs QW PL structure (red) demonstrated a blueshift and improved PL intensity compared to the as grown PL structure (black). (b) *Ex situ* rapid thermal annealing of a BGaInAs QW PL similarly demonstrated a blueshift in wavelength (red) as well as an increase in PL intensity (blue) followed by a decrease in PL intensity

we performed an *ex situ* annealing study on BGaInAs QW PL structures that were first annealed *in situ* to emulate device growth. We observed no evidence of over annealing in the nominally identical BGaInAs PL structures annealed *in situ* for ~ 2 and ~ 5 hours as shown in Figure 5.3.

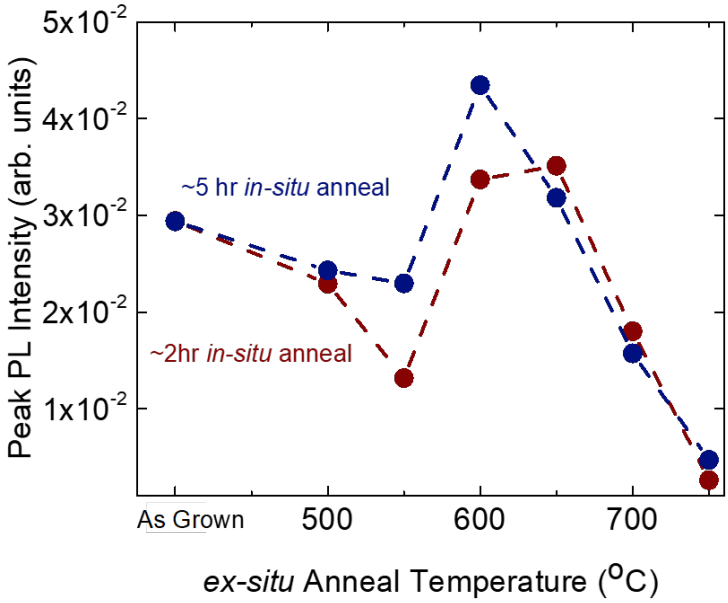

Figure 5.3: *In situ* annealed BGaInAs QW PL structures were then *ex situ* annealed to investigate overannealing. The peak PL intensity v. *ex situ* annealing of the QWs showed an increase in PL intensity indicating they were not overannealed during the *in situ* annealing.

The accompanying blueshift in emission wavelength with annealing necessitates increasing the as-grown emission wavelength in order to compensate for the wavelength shift resulting from in situ annealing of the BGaInAs layers. Increasing the as-grown emission wavelength of these QW structures requires the addition of indium, which then necessitates additional boron to compensate the additional strain from the higher In concentration. Figure 5.4 shows as-grown emission wavelength of 1.4 µm, by increasing the In concentration to 50%, and the B concentration to 5%. Performing an *ex situ* annealing step at 700 °C for 1 minute, we observed a blueshift in the peak emission wavelength to 1.3 µm and an improvement in PL efficiency as compared to the as-grown QW samples. Therefore, with careful *in situ* annealing of $B_{0.05}In_{0.50}Ga_{0.45}As$ active regions, electroluminescence at 1.3 μm on GaAs is attainable with BGaInAs alloys. However, the PL intensity of the annealed 1.4 μm QW is about one order of magnitude less than the as-grown QW structure that emitted at 1.3 μm prior to annealing. Again, we attribute this to the narrowing and possible shifting of the optimal growth conditions, which may be attributed to the more highly-mismatched nature of the alloy as demonstrated in the dilute nitrides [135] and dilute bismides, [113]. This suggests that optimization of the growth regime may be necessary at the alloy composition or wavelength of

interest.

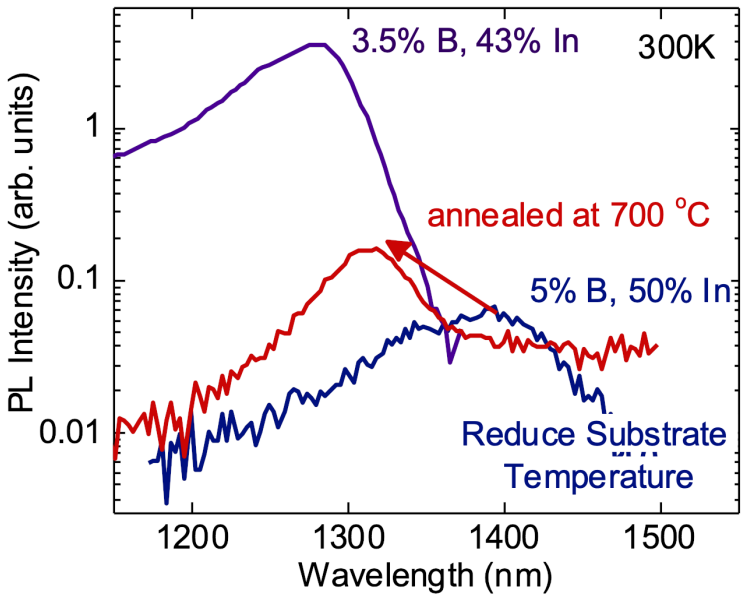

Figure 5.4: The as-grown 1.4 μm emission BGaInAs QW was *ex situ* annealed to emit at 1.3 μm. However, comparing PL intensity of the as-grown 1.3μm to the as-grown 1.4 μm QW and annealed 1.4 μm QW, we observed a 100x and 10x reduction in intensity respectively.

5.2 B-III-V alloys for GaAs-based photodiodes

The transparency of many CMOS-compatible materials in the shortwave infrared in combination with emission in the same waveband from Si-based emitter necessitates both sources nearly lattice-matched and detectors lattice-matched to Si owing to the absorption cutoff of 1 μm in Si-based detectors. The large amount of boron necessary to lattice-match B-III-V alloys to Si currently makes the investigation of BGaInAs photodetector properties prohibitively challenging on Si. Instead, we focused on BGaInAs alloys grown lattice-matched to GaAs substrates as only small amounts ($\sim$ 0.5x) of boron are necessary to compensate for the addition of indium. This investigation allowed us to understand the effects of adding boron to critical photodetector device properties, such as external quantum efficiency, multiplication gain, and excess noise. Additionally, as shown in Figure 5.5, with sufficient B and In, BGaInAs can be grown lattice-matched to GaAs with a 1 eV bandgap, providing an avenue to increase the efficiency of GaAs-based multi-junction solar cells [29].

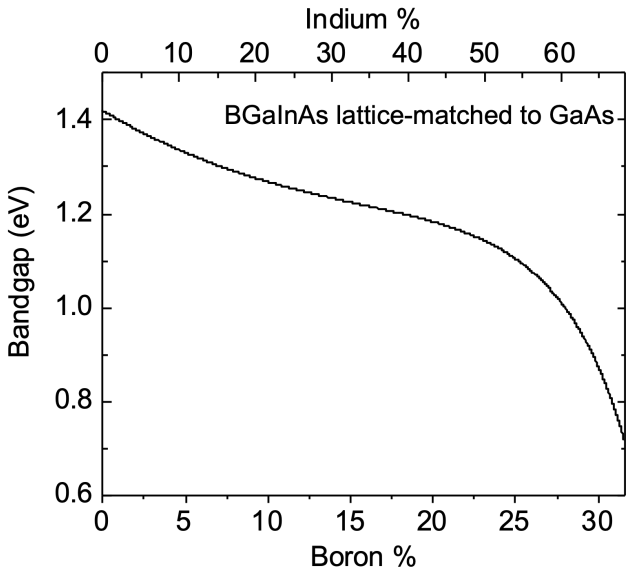

Figure 5.5: Estimated BGaInAs alloy bandgaps for lattice-matched compositions assuming a BAs bandgap of 5.8 eV.

5.2.1 Growth of p-i-n diodes

BGaInAs p-i-n junctions were grown with the same structure and under identical growth conditions as the previous BGaAs p-i-n junctions demonstrated by McNicholas [48] in order to allow for direct comparisons between device performance. N-type GaAs substrates were used. Following thermal removal of the GaAs oxide, a 200 nm Te-doped, n-type GaAs buffer was grown. Then a 150 nm Te-doped n-type BGaInAs layer was grown followed by a 400 nm intrinsic region. Finally, a 150 nm Be-doped p-type BGaInAs layer was grown followed by a highly doped 10 nm p-type BGaInAs cap. The highly-doped region thicknesses were chosen to minimize the total epitaxial thickness of the device (reducing length of growth and depletion of the boron source) while being sufficiently thick for carrier injection into the device. Similarly, the intrinsic region thickness was chosen to minimize overall epitaxial thickness of the device, while being thick enough to allow for the measurement of excess noise factor discussed in Section 5.2.5; previous investigations of "dead-space" effects, or reduced excess noise due to thin multiplication region thickness, in GaAs indicated that 400 nm is sufficiently thick to avoid such effects [144]. The growth temperature was kept at 400 °C throughout the growth of the BGaInAs layers. An As/III flux ratio of ~ 3 was used, and the BGaInAs growth rate was ~ 2 Å/s. The limited capacity of the B evaporator is not ideal for the growth of thick B-containing regions, complicating the growth of these device structures. Photodiodes with an

intrinsic region of 800 nm were grown to study the effect of increasing the i-region thickness on the multiplication gain when the devices were biased to avalanche photodiode operating voltages, but exhibited poor device characteristics, which we attribute to fluctuation in boron flux or localized strain.

The BGa(In)As photodiodes discussed in this thesis were fabricated and characterized by our collaborators at the University of Virginia in Professor Joe Campbell's group.

5.2.2 External quantum efficiency of BGaInAs photodiodes

Previous investigation of BGaAs APDs on GaAs demonstrated a decrease in external quantum efficiency with increasing boron concentration, which may be due to the formation of strain related defects resulting from the increase in tensile strain with increasing boron or an increase in B-related defects at larger boron concentrations [48]. Adding indium enabled lattice-matching of the device layers to GaAs reducing the tensile strain and likelihood of strain-driven defect formation, allowing for us to investigate if there is an inherent "B penalty" to the quantum efficiency of B-III-V based detectors. The addition of indium to lattice-match the B-containing device layers to GaAs increased the EQE significantly as shown in Figure 5.6(a). Further increasing the indium and boron concentration did not result in a significant reduction in EQE, demonstrating the viability of extended cutoff wavelength absorbers incorporating higher simultaneous B and In concentrations as shown in Figure 5.6(b). Also shown in Figure 5.6(b), as expected, the cutoff wavelength of the BGaInAs photodiodes increased as the indium concentration was increased. The bandgap of the BGaInAs alloys, estimated from the measured EQE at 50% the peak EQE, agreed well with the predicted bandgap energies for BGaInAs alloys lattice-matched to GaAs based using the direct BAs bandgap energy of 5.8 eV predicted from photoreflectance measurements of BGaAs films performed by Kudrawiec *et al.* [64].

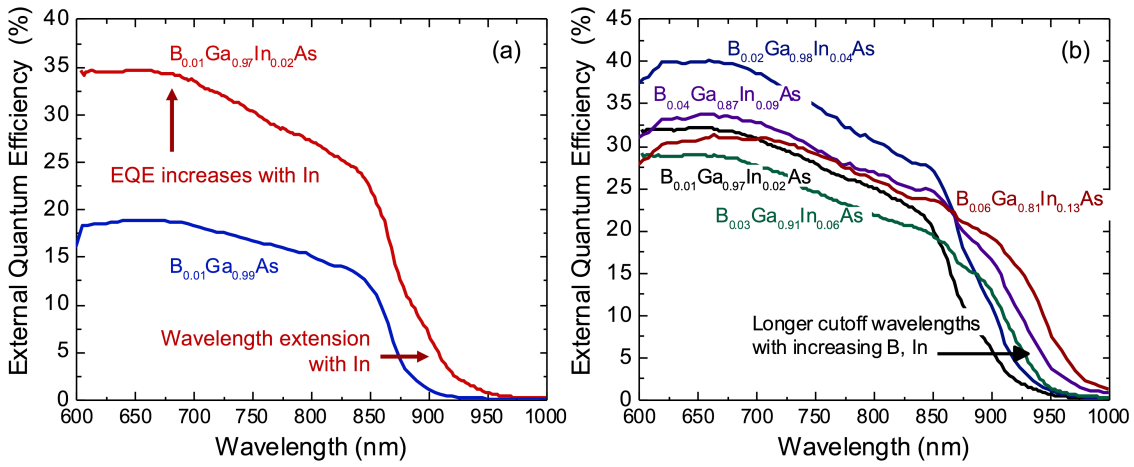

Figure 5.6: (a) External quantum efficiency of BGa(In)As p-i-n photodiodes measured at unity gain under reverse bias. The EQE is significantly higher in the BGaInAs p-i-n than in comparable In-free BGaAs p-i-n with identical B concentration and layer structure. (b) Increasing the boron and indium concentration did not significantly improve or degrade EQE. The expected increase in cutoff wavelength with increasing In content was observed.

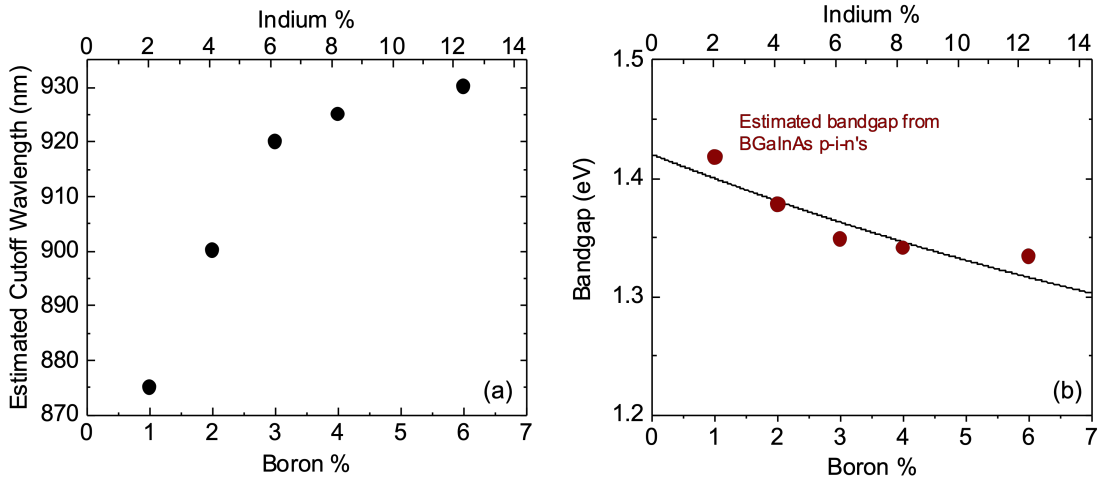

Figure 5.7: (a) Estimated cutoff wavelength from EQE measurements of BGaInAs p-i-n junctions lattice-matched to GaAs. (b) The bandgap of these alloys (red circles) agrees well with the theoretical predictions (black line) for BGaInAs alloys lattice-matched to GaAs based on a BAs bandgap of 5.8 eV.

5.2.3 Effect of annealing on BGaInAs p-i-n junctions

Similarly to the annealing benefits observed in the previous studies of highly-mismatched alloy-based optical sources, annealing of dilute-nitride photodiodes resulted in significant ($\sim$ 4x) improvement in QE [145], [146]. Volz *et al.* observed a linear relationship between the increase in PL intensity with annealing and improved EQE in InGaAsN solar cells [146]. Owing to the similar highly-mismatched nature of the dilute borides, it follows that there may be benefit to intentionally ex situ annealing BGaInAs photodetectors in order to improve their performance as discussed below. To investigate the effects of annealing on BGaInAs p-i-n junctions, we performed an *ex situ* annealing study, progressively annealing a $B_{0.03}Ga_{0.91}In_{0.06}As$ film with a GaAs cap for 30 seconds in a nitrogen-purged RTA. We observed a steady increase in PL intensity when annealing the BGaInAs film $\leq$ 650 °C. Increasing the annealing temperature beyond 650 °C resulted in a small increase in PL intensity until reaching an annealing temperature of 900 °C. We observed a small and inconsistent trend in the peak PL energy with annealing temperature. Additionally, the surface of the film became increasingly cloudy to the eye at annealing temperatures $\geq$ 700 °C. Previous investigations of BGaAs growth have shown that boron can easily surface segregate under unoptimized growth conditions, suggesting high diffusivity of B in these alloys [115]. The large shift in the peak PL energy between 850 °C and 900 °C coupled with the degradation in surface morphology at these temperatures suggests B segregation. To investigate how the improvement in PL impacted photodiode performance, while maintaining reasonable surface quality we annealed on BGaInAs p-i-n at 650 °C and 750 °C.

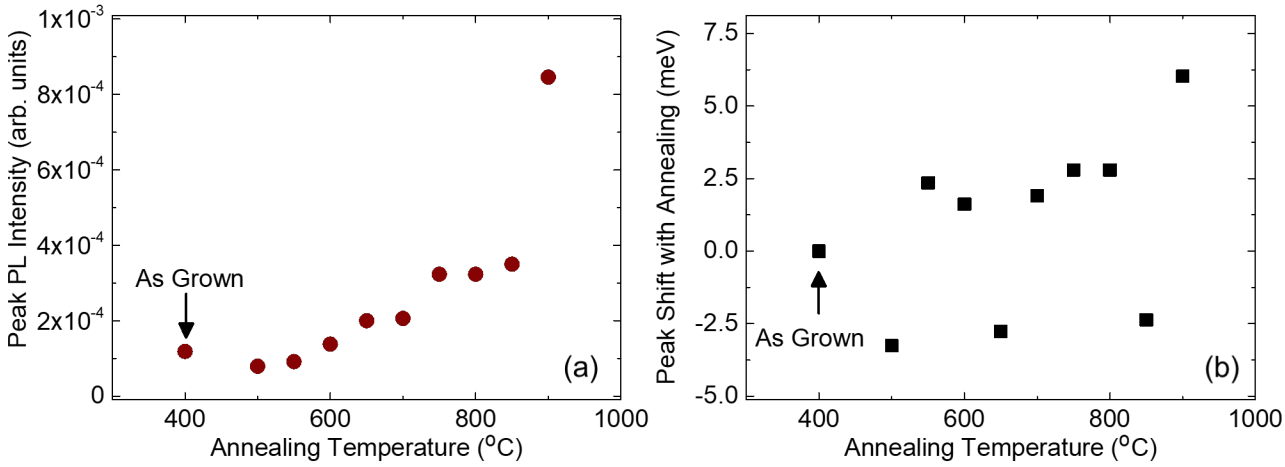

Figure 5.8: Progressive rapid thermal annealing of a 300 nm $B_{0.03}Ga_{0.91}In_{0.06}As$ film demonstrated (a) an increase PL intensity with anneal temperature and (b) no consistent trend in the change in peak PL energy with annealing temperature.

We annealed $B_{0.01}Ga_{0.97}In_{0.02}As$, $B_{0.03}Ga_{0.91}In_{0.06}As$, and $B_{0.04}Ga_{0.88}In_{0.08}As$ p-i-n junctions at 650 °C and 750 °C for 30 seconds prior to device fabrication. Nearly all of the pre-annealed device structures exhibited increased peak EQE compared to the as-grown control structures. The 1% B p-i-n demonstrated a $\sim$ 30% improvement in peak EQE with annealing at 650 °C. Annealing at 750 °C resulted in only a 12% increase in EQE, and simultaneously, increased the cutoff wavelength of the device, which may indicate out-diffusion of B from the device structure. On the other hand, the 3% B p-i-n demonstrated a $\sim$ 10% improvement in peak EQE when annealed at 650 °C and a $\sim$ 24% increase in peak EQE with no apparent wavelength shift at 750 °C, suggesting that they optimal annealing temperature may be composition dependent. The 4% B p-i-n demonstrated only slight improvement when annealed at 650 °C, and characterization of the 4% sample annealed at 750 °C was prohibited by poor device quality. The variation in EQE improvement as a function of annealing temperature suggests that the optimal annealing temperature may be alloy dependent. While the improvements in EQE observed in these dilute-boride photodiodes with annealing were not as substantial as those observed in the dilute nitrides, annealing does appear to improve BGaInAs photodiode performance. The improvement upon annealing coupled with the high EQE of as-grown BGaInAs photodiodes indicates that B-III-V alloys may be good candidates for NIR photodiodes.

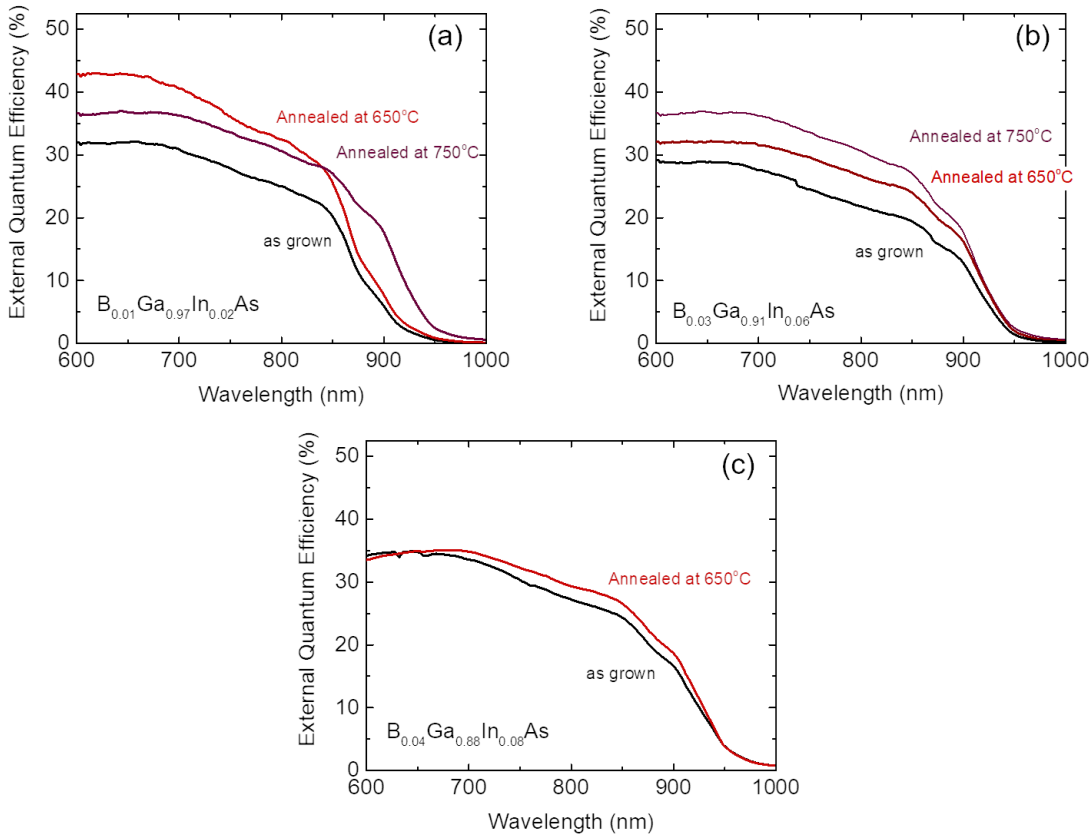

Figure 5.9: Annealing of 200 μm BGaInAs photodiodes prior to device fabrication resulted in increased EQE for nearly all of the devices measured. (a) Annealing at 650 °C resulted in the largest increase in peak EQE for the 1% device. The peak EQE decreases and the cutoff wavelength redshifts suggesting B-diffusion. (b) At 3% B annealing at 750 °C resulted in a larger improvement than at 650 °C (c) Meanwhile no significant improvement was observed in the 4% B device annealed at 650 °C. The measurement of the 750 °C APD demonstrated was prohibited by poor device quality.

5.2.4 Background doping concentration of BGaInAs photodiodes

Accurate characterization, and when possible, control of background carrier concentrations is critical for optimizing photodiode device design and operation. For example, high background carrier concentration can prohibit the depletion of multiplication layers before breakdown in avalanche photodiodes, limiting device performance. This is especially true of devices utilizing highly-mismatched alloys where unintentional doping is often observed due to intrinsic material properties or unoptimized growth limitations. As discussed in Section 4.5, unintentional p-type doping has been observed in previous reports of BGaAs growth. While, we observed no measurable unintentional doping in BGaAs and BGaInAs films using Hall effect measurements, the detection limit of the Hall system used makes accurate characterization of carrier concentrations $< 10^{16}$ cm^{-3} challenging.

Capacitance-voltage measurements performed by Professor Joe Campbell's group of the BGaInAs p-i-n diodes allowed for measurement of background carrier concentration in the intrinsic region of the devices. We observed that the background doping concentration increased in the intrinsic region of the devices with increasing B concentration. To accurately determine the polarity ofthe background carrier concentration, the p-i-n junctions were fabricated with a double mesa structure and the polarity was determined by the capacitance dependence on either the top (n-type UID) or bottom (p-type UID) mesa radius as described in [147] and [148]. While previous reports have observed unintentional p-type doping with the addition of B, we found that the 1% B APD had a n-type background concentration of 4×10^{16} cm^{-3}. Increasing the B concentration to 2% and the In concentration to 4% to maintain lattice-matching, we observed a simultaneous increase in the background carrier concentration to 5×10^{16} cm^{-3} and a change in polarity from n-type to p-type. Further increasing the B concentration to 3% B (and $\sim$ 6% In) and 4% B (and $\sim$ 8% In) increased the background carrier concentration to $\sim 8 \times 10^{16}$ cm^{-3} and $\sim 9 \times 10^{16}$ cm^{-3}, respectively. Further characterization is necessary to determine the polarity of these higher boron concentration APDs and is ongoing.

Unintentional p-type doping in BGaAs alloys has previously been attributed to B antisite incorporation [60], [149]. We note that these devices were grown using the growth regime optimized for BGaAs, to facilitate direct comparison of device performance with the BGaAs p-i-n photodiodes. The improvement in PL efficiency in BGaInAs QW structures through growth optimization suggests a reduction in native point defect density, such as B antisite. Similar growth optimization of BGaInAs photodiode device structures may enable reduced background carrier concentrations in these devices.

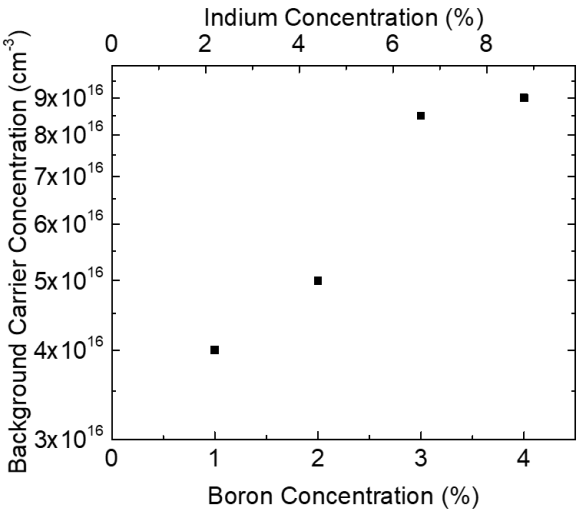

Figure 5.10: Background doping concentrations from BGaInAs p-i-n junctions with 1% to 4% B. Measurements of the background doping polarity of the 1% B p-i-n indicated n-type doping, while measurements of background doping polarity of the 2% B p-i-n indicated p-type doping.

5.2.5 Multiplication gain, dark and photo current, and excess noise performance of BGaInAs photodiodes

When biased beyond the unity gain operation voltages, multiplication gain ($\sim$ 10-20x for BGaInAs photodiodes with up to 6% B and 13% In) was observed in the BGaInAs p-i-n photodiodes, demonstrating that this material system may be useful for avalanche photodiode detectors. Moderate dark currents were observed under reverse-bias, current-voltage measurements. The dark currents may be reduced with future growth regime advancements similar to those discussed in Section 4.3 as the 1% B and 2% In BGaInAs photodiode demonstrated the lowest dark currents and the dark current increased at higher B concentrations.

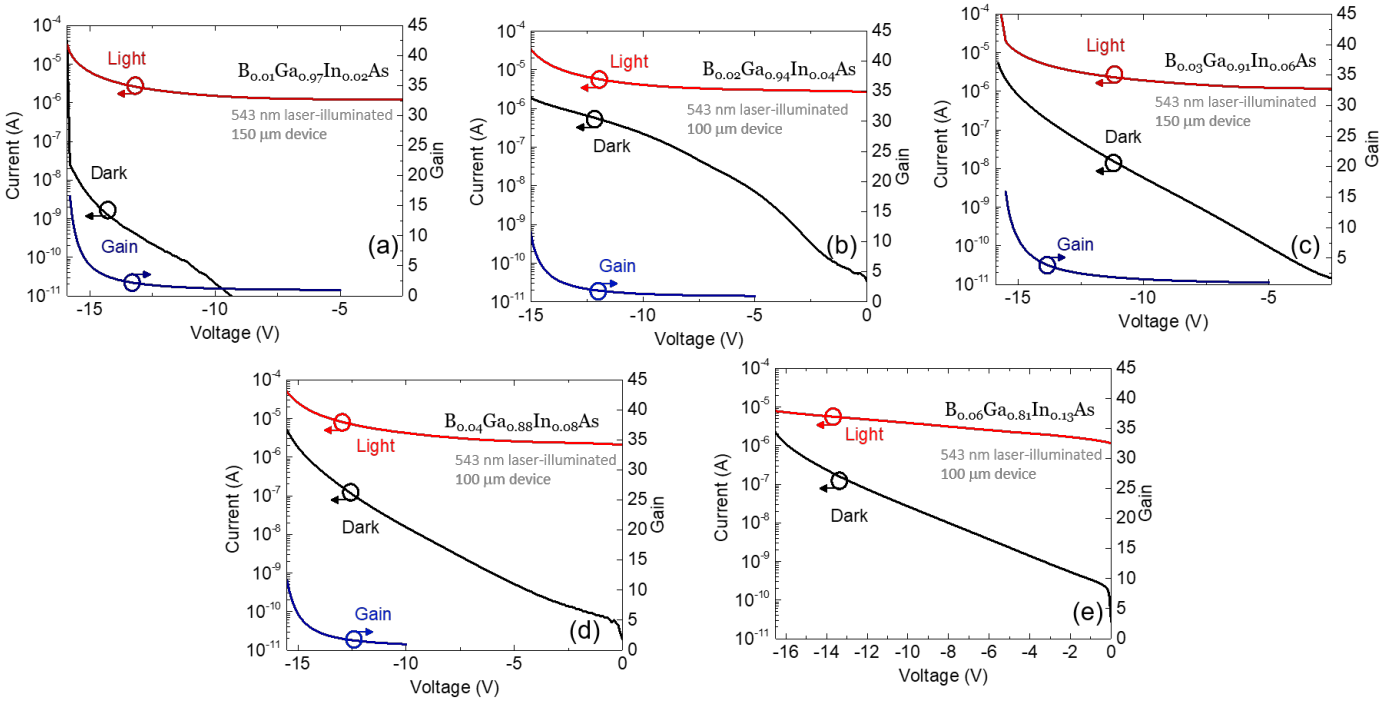

Figure 5.11: Light and dark current versus voltage measurements for BGaInAs p-i-n's with increasing simultaneous B and In concentrations while remaining lattice-matched to GaAs. Compared to (a) $B_{0.01}Ga_{0.97}In_{0.02}As$, dark currents increased in (b) $B_{0.02}Ga_{0.94}In_{0.04}As$, (c) $B_{0.03}Ga_{0.91}In_{0.06}As$, (d) $B_{0.04}Ga_{0.88}In_{0.08}As$ and (e) $B_{0.06}Ga_{0.81}In_{0.13}As$. Multiplication gains of $\sim$ 10-20x were observed for the devices shown in a-d and no gain was observed in (e).

In avalanche photodiodes, multiplication gain results from charge carrier multiplication through impact ionization of high-energy carriers in the multiplication region of the device. As discussed in Section 1.2.3, few materials for avalanche photodiodes exist where the increase in internal gain does not lead to a simultaneous increase in device excess noise due to the stochastic nature of impact ionization. In hole-injected multiplication regions, the carrier ionization ratio, k, is defined as k=α/β and in electron-injected multiplication regions, k=β/α. The excess noise factors of BGaInAs p-i-n APDs were measured under electron injection. The addition of just 1% B reduced the excess noise factor below that of a GaAs p-i-n with a comparable i-region thickness of 0.5 µm [144]. Further increasing the B concentration to 3% with an In concentrations 6%, resulted in further reduction of excess noise factor, achieving a k-value between 0.1 and 0.2 with only slight changes to the alloy composition. The "dead space" effect has been shown to decrease excess noise by decreasing the multiplication region thickness such that it is thinner than a few multiples of

the impact ionization distance [144]. This work chose multiplier regions thin enough to overcome the difficult growth of the alloys, but thicker than the thin regions demonstrated to reduce excess noise in GaAs diodes by Hu *et al.* [144], suggesting that the changes in noise performance were achieved primarily through modification of the impact ionization coefficients through alloying. The significant change observed in noise performance with only slight changes to the alloy composition indicates that further reductions in excess noise may be possible through growth optimization of alloys incorporation larger boron concentrations.

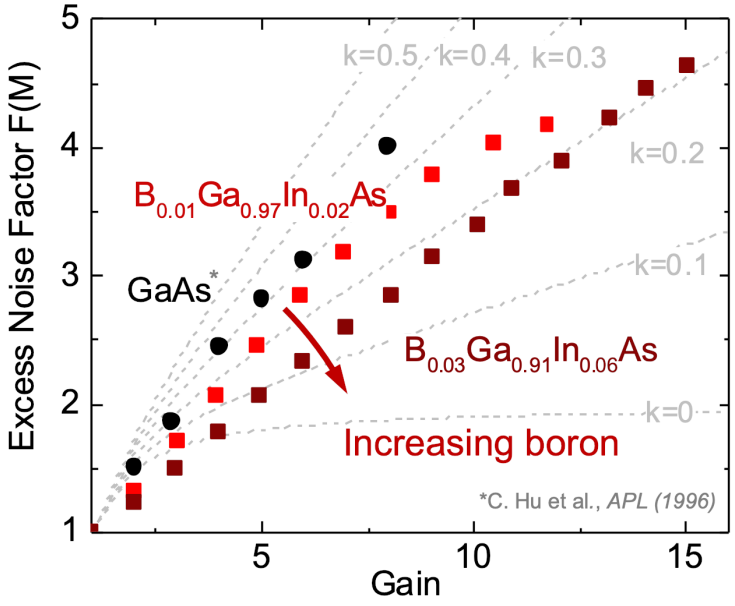

Figure 5.12: Excess noise factor versus multiplication gain for BGaInAs APDs. The k-value decreased for a BGaInAs APD with 1% B and 2% In compared to a GaAs control [144]. Further increasing the B and In concentrations to 3% and 6% respectively, resulted in a further decrease in the k-value.

The impact ionization coefficients for electrons (α) and holes (β) were determined from gain versus voltage measurements of the BGaInAs p-i-n photodiodes using a method similar to that of Yuan *et al.* [150]. Highly mismatched alloys like dilute-nitrides [42] and -borides have been theorized to suppress the electron-initiated impact ionization coefficient (α) through perturbation of the conduction band edge arising from band anticrossing interactions with resonant defect states introduced by the incorporation of the highly-mismatched element. In dilute-nitride based APDs, the reduction in α was not substantial enough to significantly reduce excess noise factors at the limited achievable nitrogen concentrations [44]. Our measurements indicated both an increase in

the electron-initiated ionization coefficient and a decrease in the hole-initiated ionization coefficient with dilute boron concentrations, compared to a GaAs control [151], suggesting that perturbation of the conduction band is not the primary origin of the overall reduction in excess noise observed in these devices. While preliminary predictions from theory suggest perturbation of the conduction band with the introduction of B, the effects of B incorporation on the full band structure of BGaInAs alloys have not yet been studied in significant detail and may enable a more through understanding of the reduction in hole-initiated impact ionization. Nevertheless, the significant change in excess noise observed at these dilute B concentrations, in concert with the larger B concentrations achievable in these alloys paint a favorable picture for further improving the noise performance of dilute-boride APDs through further growth optimization.

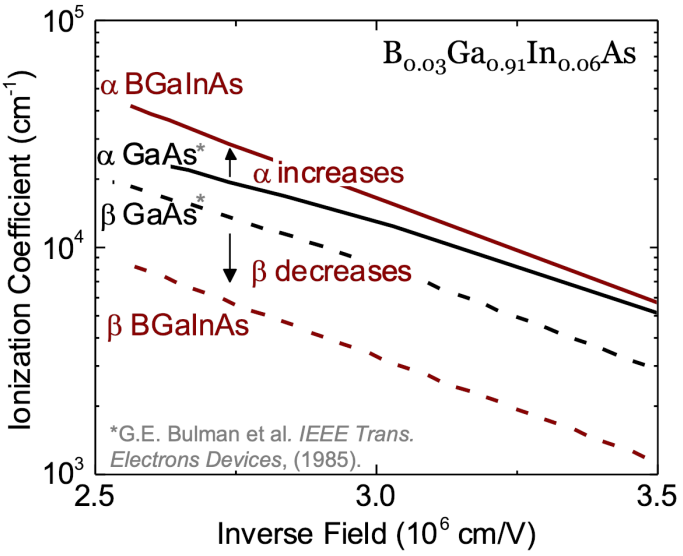

Figure 5.13: Hole and electron impact ionization coefficients of a $B_{0.03}Ga_{0.91}In_{0.06}As$ APD were determined using a method similar to that of Yuan *et al.* [150]. These measurements indicated both an increase in the electron impact ionization coefficient and a decrease in the hole impact ionization coefficient compared to GaAs control [151].

Chapter 6

Conclusions

The challenging synthesis of boron-pnictides and their alloys has thus far prevented the investigation of the effects of boron incorporation on many material properties which are critical for optoelectronic device design. The recent development of a highly-kinetically limited MBE growth regime for the ternary alloy BGaAs enabled higher boron concentrations than previously realized. Extending this growth regime to the quaternary alloy BGaInAs, we used boron to strain-engineer extended wavelength emitters and lattice-matched absorbers on GaAs. We demonstrated the first BGaInAs active region light-emitting diode, the first all-BGaInAs avalanche photodiodes, and the highest simultaneous B and In concentration alloys to date, $B_{0.1}Ga_{0.4}In_{0.5}As$. During our investigation of extended wavelength BGaInAs emitters, we observed a "boron penalty" to luminescence efficiency under unoptimized growth conditions analogous to the decrease in optical quality observed in other highly-mismatched alloys. We then demonstrated how this apparent boron penalty at increased boron concentration can be overcome through optimization of the growth regime. In addition to the significant improvement in optical quality compared to a nominally identical BGaInAs emitter grown under unoptimized growth conditions, the optimized growth regime demonstrated significant improvement in optical quality as compared to the highest In concentration, boron-free InGaAs QW control structures grown coherently-strained on GaAs. In emitter structures, we investigated properties of these alloys critical to the design of optical sources using these alloys including the blueshift in wavelength and improvement in PL intensity of emitters when thermally annealed, the blueshift in wavelength with increasing boron content, and the potential to improve optical quality by optimizing the growth regime of the alloy at the wavelength of interest. In photodiode devices, we demonstrated multiplication gain, highlighting the potential for BGaInAs alloys for

use in avalanche photodiodes. Furthermore, we demonstrated a reduction in excess noise with increasing boron concentration, suggesting that adding boron may be a materials-based approach to decreasing excess noise in APDs. We also observed a growth temperature-dependency on electron carrier concentration in doped BGaInAs films suggesting further growth optimization is necessary.

The method through which we improved the optical quality of these alloys, identifying, isolating, and controlling individual MBE growth parameters to control surface kinetics during growth, can be extended to BGaInAs alloy growth for all compositions and device structures. In this work, we identified the dependency of optical quality on growth rate, growth temperature, and As_2/III flux. The impact of varying the Bi on surfactant flux was not investigated here and may provide further opportunity for growth improvement, with the opportunity to investigate surfactant atoms beyond Bi, such as Sb. The electron-beam evaporator used for supplying boron for this project does not currently enable *in situ* flux measurements. A system through which the electron-beam power to flux relationship can be measured at the beginning of the growth day would reduce calibration growths necessary and conserve material, extending growth campaigns and increasing day-to-day reproducibility. Furthermore, the electron-beam evaporator uses a tilted hearth due to the geometry of the source ports on the MBE system, limiting the amount of material that can be loaded and leading to shadowing of the hearth as material is depleted. The current electron-beam evaporator flux and crucible size is limited by the geometry of the system. An MBE system compatible with a larger electron-beam evaporator without a tilted hearth would increase the amount of source material that could be loaded, eliminate shadowing, and provide more stable fluxes for thicker epitaxial layers. These improvements could reduce day to day variability in boron flux, while enabling thicker intrinsic-region APDs for higher multiplication gain and reduce machine downtime.

The addition of boron to III-V alloys was investigated as a potential path towards III-V optoelectronic integration on Si. Through the investigation of B-III-V alloys on GaAs, we demonstrated optoelectronic devices with B-III-V active regions and a method for increasing the incorporation of B and the material quality through control of their molecular beam epitaxy growth. Combined with the demonstration of BGaAs growth on GaP-on-Si substrates by McNicholas [48], this work could lead to the realization of B-III-V optoelectronic devices on Si.

Appendix A

Boron growth

Before touching any part of the electron beam evaporator new users must read the associated manuals to ensure proper usage and prevent damage to the vacuum system and/or themselves.

A.1 General overview of the e-beam evaporator

The e-beam evaporator used in this project is necessary for high boron fluxes. Electrons are accelerated onto the surface of the source charge, heating and evaporating the source material. The electrons are accelerated through a large potential difference applied across the filament. The electrons are directed towards the evaporator hearth with a magnet, while electromagnets are used to control the raster of the electron beam in the hearth. The figure-8 raster pattern was chosen to provide a consistent B flux and depleting the source material within the hearth evenly.

The operation of the e-beam, with accelerating voltages on the order of 4-10 kV, requires high-voltage power supplies. Therefore safety protocols and interlocks (outlined in detail in [48]) are necessary to protect the user and the vacuum system. A ceramic insulator insulates the high-voltage power supply from the chamber. This ceramic insulator is very fragile, requiring careful removal and attachment of the high-voltage power supply during maintenance. Failure to remove or attach the power supply carefully can damage the ceramic and create vacuum leaks. Additional concern is the failure of the beam-steering electromagnets, which can result in drift of the electron path to outside of the hearth, causing heating of the chamber walls and vacuum failure.

A.2 Initial out-gassing of the e-beam

[48] details the process of removing the e-beam from the chamber and reloading source material. Careful intial out-gassing of the e-beam is crucial as the large amounts of hydrogen generated could trip the chamber pressure interlocks if the e-beam power is increased too rapidly.

- Make sure a residual-gas analyzer scan is started to monitor the gas load generated.
- Turn off the beam flux gauge
- Move car so that the substrate points towards the sump
- Turn on HV power supply (power switch on the front of the unit) and the e-beam controller (power switch on the back of the unit)
- Enable the e-beam interlocks (key on the front of the interlock box). The e-beam controller will the status of the interlocks.
  - Water Interlock, 3.350 (V) SRS Channel 5
  - Pressure Interlock, 1e-5 SRS Channel 6
- Open the boron shutter
- Turn on the HV
- Check filament turns on (should be visible after $\sim$ 30 seconds)
- Turn on emission current to 1 mA. Wait for chamber to pump out
- Continue to ramp the emission current by 1 mA, waiting for the chamber to pump out after each step.
- Turn off the raster after 8 mA and let chamber fully pump out
- Reduce the raster size to $\sim \frac{1}{4}$ of hearth size
- Ramp the emission current to 6 mA
- Raster around the perimeter, watching how the pressure increases at each point. Increase the emission current if the pressure stops changing as the raster is moved.

- If the chamber pressure is in the high 10^{-7} Torr, turn off the high voltage and let the chamber pump out
- Around 12-14 mA, increase the raster size back to the full hearth, ramp up to $\sim$ 20 mA (depending on the highest emission current necessary for the campaign) and actuate the e-beam cell shutter (slowly)
- Cool down slowly ("popping" will occur if the emission current is decreased too quickly)
- turn off HV, close B shutter

A.3 Check e-beam alignment prior to growth day

An important note is that the e-beam controller cannot detect short circuit failure of the deflection coils. Therefore, it is important to verify the beam position in the hearth prior to every growth day.

- Turn off beam flux gauge
- Move car so substrate points towards the sump
- Turn on HV supply (power switch on the front of the unit) and the e-beam controller (power switch on the back of the unit)
- Enable the e-beam interlocks (key on the front of the interlock box). The e-beam controller will the status of the interlocks.
  - Water Interlock, 3.350 (V) SRS Channel 5
  - Pressure Interlock, 1e-5 SRS Channel 6
- Open the boron shutter
- Turn on the HV
- Check filament turns on (should be visible after $\sim$ 30 seconds)
- Turn on emission current (1.5-2 mA)
- Check e-beam that the spot is in the center of the hearth. If no spot is observed, do not increase the e-beam emission $>$ 6 mA.
- Reduce the emission current to 0 mA, turn off the HV, and close the B shutter

A.4 E-beam operation during growth

- The high voltage of the e-beam interferes with RHEED
- After the boron-free buffer layer, turn on HV, ramp to growth in 5 mA increments, soaking for 1 minute at each power. Let it to sit at growth current for at least a minute before B-containing layer
- The emergency button on the interlock box instantly switches off the high-voltage in case of vacuum failure or large variations in e-beam power.

Bibliography

[1] J. W. Matthews and A. E. Blakeslee, "ŋƉßSSþÞDefects in epitaxial multilayers: I. Misfit dislocations," *Journal of Crystal Growth*, vol. 27, pp. 118–125, Dec. 1974, ISSN: 0022-0248. DOI: 10.1016/S0022-0248(74)80055-2.

[2] R. People and J. C. Bean, "ŋƉßSSþÞCite as," *Appl. Phys. Lett*, vol. 47, p. 322, 1985. DOI: 10.1063/1.96206. [Online]. Available: https://doi.org/10.1063/1.96206.

[3] K. N. Tu, J. W. Mayer, and L. C. Feldman, "ŋƉßSSþÞElectronic thin film science : for electrical engineers and materials scientists," p. 428, 1992.

[4] K. Kim and A. Zunger, "ŋƉßSSþÞSpatial Correlations in GaInAsN Alloys and their Effects on Band-Gap Enhancement and Electron Localization," 2001. DOI: 10.1103/PhysRevLett.86.2609.

[5] X. Kong, A. Trampert, E. Tournié, and K. H. Ploog, "ŋƉßSSþÞDecomposition in as-grown (Ga,In)(N,As) quantum wells," *Applied Physics Letters*, vol. 87, no. 17, p. 171 901, Oct. 2005. DOI: 10.1063/1.2108108.

[6] S. Takeda and A. Furusawa, "ŋƉßSSþÞToward large-scale fault-tolerant universal photonic quantum computing," *APL Photonics*, vol. 4, no. 6, 2019, ISSN: 23780967. DOI: 10.1063/1.5100160. [Online]. Available: http://dx.doi.org/10.1063/1.5100160.

[7] D. Kang, M. Kim, H. He, and A. S. Helmy, "ŋƉßSSþÞTwo polarization-entangled sources from the same semiconductor chip," *Physical Review A - Atomic, Molecular, and Optical Physics*, vol. 92, no. 1, pp. 1–7, 2015, ISSN: 10941622. DOI: 10.1103/PhysRevA.92.013821.

[8] N. Jones, *ŋƉßSSþÞHow to stop data centres from gobbling up the world's electricity*, Sep. 2018. DOI: 10.1038/d41586-018-06610-y.

[9] E. Masanet, A. Shehabi, N. Lei, S. Smith, and J. Koomey, "ŋƉßSSþÞRecalibrating global data center energy-use estimates," DOI: 10.1007/s12053-019-09809-8. [Online]. Available: www.iea.org/tcep/..

[10] A. Shehabi, S. J. Smith, D. A. Sartor, R. E. Brown, M. Herrlin, J. G. Koomey, E. R. Masanet, N. Horner, I. L. Azevedo, and W. Lintner, "ŋƉßSSþÞUnited States Data Center Energy Usage Report," *Berkeley Lab*, no. June, p. 65, 2016, ISSN: 1002087x. [Online]. Available: https://www.osti.gov/servlets/purl/1372902/%20https://eta.lbl.gov/publications/united-states-data-center-energy.

[11] N. Margalit, C. Xiang, S. M. Bowers, A. Bjorlin, R. Blum, and J. E. Bowers, *ŋƉßSSþÞPerspective on the future of silicon photonics and electronics*, 2021. DOI: 10.1063/5.0050117. [Online]. Available: https://doi.org/10.1063/5.0050117.

[12] M.R. Watts, "ŋƉßSSþÞSilicon Photonic Phased Array LiDAR," in *Analog Photonics: AutoSens Conference*, 2018.

[13] D. L. Huffaker, G. Park, Z. Zou, O. B. Shchekin, and D. G. Deppe, "ŋƉßSSþÞ1.3 m room-temperature GaAs-based quantum-dot laser," *Applied Physics Letters*, vol. 73, no. 18, pp. 2564–2566, Nov. 1998. DOI: 10.1063/1.122534.

[14] K. Nakahara, M. Kondow, T. Kitatani, M. C. Larson, and K. Uomi, "ŋƉßSSþÞ1.3-m continuous-wave lasing operation in GaInNAs quantum-well lasers," *IEEE Photonics Technology Letters*, vol. 10, no. 4, pp. 487–488, Apr. 1998. DOI: 10.1109/68.662569.

[15] S. R. Bank, H. Bae, S. Member, L. L. Goddard, H. B. Yuen, M. a. Wistey, R. Kudrawiec, and J. S. Harris Jr, "ŋƉßSSþÞRecent Progress on 1 . 55-um Dilute-Nitride Lasers," *Ieee Journal of Quantum Electronics*, vol. 43, no. 9, pp. 773–785, 2007, ISSN: 1476-4687. DOI: 10.1038/nature20792.

[16] R. McIntyre, "ŋƉßSSþÞMultiplication Noise in Uniform Avalanche Diodes," *IEEE Transactions on Electron Devices*, vol. ED-13, no. 1, pp. 164–168, 1966, ISSN: 15579646. DOI: 10.1109/T-ED.1966.15651.

[17] J. C. Campbell, S. Demiguel, F. Ma, A. Beck, X. Guo, S. Wang, X. Zheng, X. Li, J. D. Beck, M. A. Kinch, A. Huntington, L. A. Coldren, J. Decobert, and N. Tscherptner, "ŋƉßSSþÞRecent advances in avalanche photodiodes," *IEEE Journal on Selected Topics in Quantum Electronics*, vol. 10, no. 4, pp. 777–787, Jul. 2004, ISSN: 1077260X. DOI: 10.1109/JSTQE.2004.833971.

[18] J. Beck, C. Wan, M. Kinch, J. Robinson, P. Mitra, R. Scritchfield, F. Ma, and J. Campbell, "ŋƉßSSþÞThe HgCdTe Electron Avalanche Photodiode,"

[19] A. R. J. Marshall, C. H. Tan, M. J. Steer, and J. P. R. David, "ŋƉßSSþÞElectron dominated impact ionization and avalanche gain characteristics in InAs photodiodes," *Applied Physics Letters*, vol. 93, no. 11, p. 111 107, Sep. 2008, ISSN: 0003-6951. DOI: 10.1063/1.2980451. [Online]. Available: https://aip.scitation.org/doi/abs/10.1063/1.2980451.

[20] M. E. Woodson, M. Ren, S. J. Maddox, Y. Chen, S. R. Bank, and J. C. Campbell, "ŋƉßSSþÞLow-noise AlInAsSb avalanche photodiode," *Citation: Applied Physics Letters*, vol. 108, p. 81 102, 2016. DOI: 10.1063/1.4942372. [Online]. Available: http://dx.doi.org/10.1063/1.4942372http://scitation.aip.org/content/aip/journal/apl/108/8?ver=pdfcov.

[21] A. K. Rockwell, M. Ren, M. Woodson, A. H. Jones, S. D. March, Y. Tan, Y. Yuan, Y. Sun, R. Hool, S. J. Maddox, M. L. Lee, A. W. Ghosh, J. C. Campbell, and S. R. Bank, "ŋƉßSSþÞToward deterministic construction of low noise avalanche photodetector materials," *Applied Physics Letters*, vol. 113, no. 10, p. 102 106, Sep. 2018, ISSN: 0003-6951. DOI: 10.1063/1.5040592. [Online]. Available: https://aip.scitation.org/doi/abs/10.1063/1.5040592.

[22] S. Francoeur, M. J. Seong, A. Mascarenhas, S. Tixier, M. Adamcyk, and T. Tiedje, "ŋƉßSSþÞBand gap of GaAs1-xBix, 0<x< 3.6%," *Applied Physics Letters*, vol. 82, no. 22, pp. 3874–3876, 2003, ISSN: 00036951. DOI: 10.1063/1.1581983. [Online]. Available: https://doi.org/10.1063/1.1581983.

[23] G. Jaschke, R. Averbeck, L. Geelhaar, and H. Riechert, "ŋƉßSSþÞLow threshold InGaAsN/GaAs lasers beyond 1500 nm," in *Journal of Crystal Growth*, vol. 278, North-Holland, May 2005, pp. 224–228. DOI: 10.1016/j.jcrysgro.2004.12.059.

[24] S. Sato and S. Satoh, "ŋƉßSSþÞRoom-temperature continuous-wave operation of 1.24-μm GaInNAs lasers grown by metal-organic chemical vapor deposition," *IEEE Journal on Selected Topics in Quantum Electronics*, vol. 5, no. 3, pp. 707–710, 1999, ISSN: 1077260X. DOI: 10.1109/2944.788439.

[25] V. Gambin, W. Ha, M. Wistey, H. Yuen, S. R. Bank, S. M. Kim, and J. S. Harris, "ŋƉßSSþÞ-GaInNAsSb for 1.3-1.6-μm-long wavelength lasers grown by molecular beam epitaxy," *IEEE Journal on Selected Topics in Quantum Electronics*, vol. 8, no. 4, pp. 795–800, Jul. 2002, ISSN: 1077260X. DOI: 10.1109/JSTQE.2002.800843.

[26] S. R. Bank, M. A. Wistey, L. L. Goddard, H. B. Yuen, V. Lordi, and J. S. Harris, "ŋƉßSSþÞLow-threshold continuous-wave 1.5-/spl mu/m GaInNAsSb lasers grown on GaAs," *IEEE Journal of Quantum Electronics*, vol. 40, no. 6, pp. 656–664, Jun. 2004. DOI: 10.1109/jqe.2004.828249.

[27] S. R. Kurtz, D. Myers, and J. M. Olson, "ŋƉßSSþÞProjected performance of three- and four-junction devices using GaAs and GaInP," *Conference Record of the IEEE Photovoltaic Specialists Conference*, pp. 875–878, 1997, ISSN: 01608371. DOI: 10.1109/PVSC.1997.654226.

[28] A. J. Ptak, D. J. Friedman, S. Kurtz, and R. C. Reedy, "ŋƉßSSþÞLow-acceptor-concentration GaInNAs grown by molecular-beam epitaxy for high-current p-i-n solar cell applications," *Journal of Applied Physics*, 2005, ISSN: 00218979. DOI: 10.1063/1.2113414.

[29] D. Jackrel, A. Ptak, S. Bank, H. Yuen, M. Wistey, D. Friedman, S. Kurtz, and J. S. Harris, "ŋƉßSSþÞGaInNAsSb solar cells grown by molecular beam epitaxy," *Conference Record of the 2006 IEEE 4th World Conference on Photovoltaic Energy Conversion, WCPEC-4*, vol. 1, pp. 783–786, 2006. DOI: 10.1109/WCPEC.2006.279573.

[30] P. Ludewig, N. Knaub, N. Hossain, S. Reinhard, L. Nattermann, I. P. Marko, S. R. Jin, K. Hild, S. Chatterjee, W. Stolz, S. J. Sweeney, and K. Volz, "ŋƉßSSþÞElectrical injection Ga(AsBi)/(AlGa)As single quantum well laser," *Applied Physics Letters*, vol. 102, no. 24, 2013, ISSN: 00036951. DOI: 10.1063/1.4811736. [Online]. Available: http://dx.doi.org/10.1063/1.4811736].

[31] R. B. Lewis, D. A. Beaton, X. Lu, and T. Tiedje, "ŋƉßSSþÞGaAs1-xBix light emitting diodes," *Journal of Crystal Growth*, vol. 311, no. 7, pp. 1872–1875, Mar. 2009, ISSN: 0022-0248. DOI: 10.1016/J.JCRYSGRO.2008.11.093.

[32] N. Hossain, I. P. Marko, S. R. Jin, K. Hild, S. J. Sweeney, R. B. Lewis, D. A. Beaton, and T. Tiedje, "ŋƉßSSþÞRecombination mechanisms and band alignment of GaAs1xBix/GaAs light emitting diodes," *Applied Physics Letters*, vol. 100, no. 5, p. 051 105, Jan. 2012, ISSN: 0003-6951. DOI: 10.1063/1.3681139. [Online]. Available: https://aip.scitation.org/doi/abs/10.1063/1.3681139.

[33] T. Lu, Z. Ma, C. Du, Y. Fang, H. Wu, Y. Jiang, L. Wang, L. Dai, H. Jia, W. Liu, and H. Chen, "ŋƉßSSþÞTemperature-dependent photoluminescence in light-emitting diodes," *Scientific Reports 2014 4:1*, vol. 4, no. 1, pp. 1–7, Aug. 2014, ISSN: 2045-2322. DOI: 10.1038/srep06131. [Online]. Available: https://www.nature.com/articles/srep06131.

[34] I. P. Marko, S. R. Jin, K. Hild, Z. Batool, Z. L. Bushell, P. Ludewig, W. Stolz, K. Volz, R. Butkutė, V. Pačebutas, A. Geizutis, A. Krotkus, and S. J. Sweeney, "ŋƉßSSþÞProperties of hybrid MOVPE/MBE grown GaAsBi/GaAs based near-infrared emitting quantum well lasers," *Semiconductor Science and Technology*, vol. 30, no. 9, p. 094 008, Jun. 2015, ISSN: 0268-1242. DOI: 10.1088/0268-1242/30/9/094008. [Online]. Available: https://iopscience.iop.org/article/10.1088/0268-1242/30/9/094008%20https://iopscience.iop.org/article/10.1088/0268-1242/30/9/094008/meta.

[35] R. D. Richards, C. J. Hunter, F. Bastiman, A. R. Mohmad, and J. P. R. David, "ŋƉßSSþÞTelecommunication wavelength GaAsBi light emitting diodes," *IET Optoelectronics*, vol. 10, no. 2, pp. 34–38, Apr. 2016, ISSN: 1751-8776. DOI: 10.1049/IET-OPT.2015.0051. [Online]. Available: https://ietresearch.onlinelibrary.wiley.com/doi/full/10.1049/iet-opt.2015.0051%20https://ietresearch.onlinelibrary.wiley.com/doi/abs/10.1049/iet-opt.2015.0051%20https://ietresearch.onlinelibrary.wiley.com/doi/10.1049/iet-opt.2015.0051.

[36] P. K. Patil, E. Luna, T. Matsuda, K. Yamada, K. Kamiya, F. Ishikawa, and S. Shimomura, "ŋƉßSSþÞGaAsBi/GaAs multi-quantum well LED grown by molecular beam epitaxy using a two-substrate-temperature technique," *Nanotechnology*, vol. 28, no. 10, p. 105 702, Feb. 2017, ISSN: 0957-4484. DOI: 10.1088/1361-6528/AA596C. [Online]. Available: https://iopscience.iop.org/article/10.1088/1361-6528/aa596c%20https://iopscience.iop.org/article/10.1088/1361-6528/aa596c/meta.

[37] T. Fuyuki, K. Yoshida, R. Yoshioka, and M. Yoshimoto, "ŋƉßSSþÞElectrically pumped room-temperature operation of GaAs1xBix laser diodes with low-temperature dependence of oscillation wavelength," *Applied Physics Express*, vol. 7, no. 8, p. 082 101, Jul. 2014, ISSN: 1882-0786. DOI: 10.7567/APEX.7.082101. [Online]. Available: https://iopscience.iop.org/article/10.7567/APEX.7.082101%20https://iopscience.iop.org/article/10.7567/APEX.7.082101/meta.

[38] X. Wu, W. Pan, Z. Zhang, Y. Li, C. Cao, J. Liu, L. Zhang, Y. Song, H. Ou, and S. Wang, "ŋƉßSSþÞ1.142 μm GaAsBi/GaAs Quantum Well Lasers Grown by Molecular Beam Epitaxy," *ACS Photonics*, vol. 4, no. 6, pp. 1322–1326, 2017, ISSN: 23304022. DOI: 10.1021/acsphotonics.7b00240. [Online]. Available: https://pubs.acs.org/sharingguidelines.

[39] H. Kim, Y. Guan, S. E. Babcock, T. F. Kuech, and L. J. Mawst, "ŋƉßSSþÞCharacteristics of OMVPE grown GaAsBi QW lasers and impact of post-growth thermal annealing," DOI: 10.1063/1.5017965. [Online]. Available: https://doi.org/10.1063/1.5017965.

[40] C. J. Hunter, F. Bastiman, A. R. Mohmad, R. Richards, J. S. Ng, S. J. Sweeney, and J. P. David, "ŋƉßSSþÞAbsorption characteristics of GaAs1?xBix/GaAs diodes in the near-infrared," *IEEE Photonics Technology Letters*, vol. 24, no. 23, pp. 2191–2194, 2012, ISSN: 10411135. DOI: 10.1109/LPT.2012.2225420.

[41] T. B. Rockett, R. D. Richards, Y. Gu, F. Harun, Y. Liu, Z. Zhou, and J. P. David, "ŋƉßSSþÞInfluence of growth conditions on the structural and opto-electronic quality of GaAsBi," *Journal of Crystal Growth*, vol. 477, pp. 139–143, Nov. 2017, ISSN: 00220248. DOI: 10.1016/j.jcrysgro.2017.02.004.

[42] A. Adams, "ŋƉßSSþÞBand-structure engineering to control impact ionisation and related high-field processes," *Electronics Letters*, vol. 40, no. 17, p. 1086, 2004, ISSN: 00135194. DOI: 10.1049/el:20046315. [Online]. Available: https://digital-library.theiet.org/content/journals/10.1049/el_20046315.

[43] A. Lindsay and E. P. O'Reilly, "ŋƉßSSþÞTheory of electronic structure of BGaAs and related alloys," *Physica Status Solidi (C) Current Topics in Solid State Physics*, vol. 5, no. 2, pp. 454–459, Feb. 2008, ISSN: 18626351. DOI: 10.1002/pssc.200777456.

[44] S. L. Tan, W. M. Soong, J. E. Green, M. J. Steer, S. Zhang, L. J. Tan, J. S. Ng, I. P. Marko, S. J. Sweeney, A. R. Adams, J. Allam, and J. P. David, "ŋƉßSSþÞExperimental evaluation of impact ionization in dilute nitride GaInNAs diodes," *Applied Physics Letters*, vol. 103, no. 10, pp. 0–4, 2013, ISSN: 00036951. DOI: 10.1063/1.4819846.

[45] Y. Liu, X. Yi, N. J. Bailey, Z. Zhou, T. B. Rockett, L. W. Lim, C. H. Tan, R. D. Richards, and J. P. David, "ŋƉßSSþÞValence band engineering of GaAsBi for low noise avalanche photodiodes," *Nature Communications*, vol. 12, no. 1, pp. 1–8, Aug. 2021, ISSN: 20411723. DOI: 10.1038/s41467-021-24966-0. [Online]. Available: https://www.nature.com/articles/s41467-021-24966-0.

[46] F. V. Williams and R. A. Ruehrwein, "ŋƉßSSþÞThe Preparation and Properties of Boron Phosphides and Arsenides1," *Journal of the American Chemical Society*, vol. 82, no. 6, pp. 1330–1332, Mar. 1960. DOI: 10.1021/ja01491a014.

[47] J. Perri, S. La Placa, B. Post, and IUCr, "ŋƉßSSþÞNew group III-group V compounds: BP and BAs," *urn:issn:0365-110X*, vol. 11, no. 4, pp. 310–310, Apr. 1958, ISSN: 0365-110X. DOI: 10.1107/S0365110X58000827. [Online]. Available: //scripts.iucr.org/cgi-bin/paper?a02241.

[48] K. McNicholas, "ŋƉßSSþÞEmerging Epitaxial Materials for Coherent III-V (Opto)electronic Heterostructure Devices," Ph.D. dissertation, University of Texas, 2019.

[49] J. F. Geisz, D. J. Friedman, S. Kurtz, J. M. Olson, A. B. Swartzlander, R. C. Reedy, and A. G. Norman, "ŋƉßSSþÞEpitaxial growth of BGaAs and BGaInAs by MOCVD," *Journal of Crystal Growth*, vol. 225, no. 2-4, pp. 372–376, May 2001. DOI: 10.1016/s0022-0248(01)00883-1.

[50] M. E. Groenert, R. Averbeck, W. Hösler, M. Schuster, and H. Riechert, "ŋƉßSSþÞOptimized growth of BGaAs by molecular beam epitaxy," *Journal of Crystal Growth*, vol. 264, no. 1-3, pp. 123–127, Mar. 2004. DOI: 10.1016/j.jcrysgro.2004.01.010.

[51] K. M. Yu, S. V. Novikov, R. Broesler, I. N. Demchenko, J. D. Denlinger, Z. Liliental-Weber, F. Luckert, R. W. Martin, W. Walukiewicz, and C. T. Foxon, "ŋƉßSSþÞHighly mismatched crystalline and amorphous GaN1-x As x alloys in the whole composition range," *Journal of Applied Physics*, vol. 106, no. 10, 2009, ISSN: 00218979. DOI: 10.1063/1.3259434.

[52] J. Geisz, D. Friedman, and S. Kurtz, "ŋƉßSSþÞBGaInAs solar cells lattice-matched to GaAs," in *Conference Record of the Twenty-Eighth IEEE Photovoltaic Specialists Conference - 2000 (Cat. No.00CH37036)*, vol. 76, IEEE, Mar. 2000, pp. 990–993, ISBN: 0-7803-5772-8. DOI: 10.1109/PVSC.2000.916052. [Online]. Available: http://ieeexplore.ieee.org/document/916052/.

[53] W. Shan, W. Walukiewicz, J. Wu, K. M. Yu, J. W. Ager, S. X. Li, E. E. Haller, J. F. Geisz, D. J. Friedman, and S. R. Kurtz, "ŋƉßSSþÞBand-gap bowing effects in BxGa1-xAs alloys," *Journal of Applied Physics*, vol. 93, no. 5, pp. 2696–2699, Mar. 2003. DOI: 10.1063/1.1540230.

[54] G. L. W. Hart and A. Zunger, "ŋƉßSSþÞElectronic structure of BAs and boride III-V alloys," *Physical Review B*, vol. 62, no. 20, pp. 13 522–13 537, Nov. 2000, ISSN: 0163-1829. DOI: 10.1103/PhysRevB.62.13522. [Online]. Available: https://link.aps.org/doi/10.1103/PhysRevB.62.13522.

[55] M. P. Surh, S. G. Louie, and M. L. Cohen, "ŋƉßSSþÞQuasiparticle energies for cubic BN, BP, and BAs," Tech. Rep. 11, 1991.

[56] B. A. Zaoui, F. El, and H. Hassan, "ŋƉßSSþÞFull potential linearized augmented plane wave calculations of structural and electronic properties of BN," Tech. Rep., 2001, pp. 253–262. [Online]. Available: www.iop.org/Journals/cmPII:S0953-8984.

[57] T. L. Chu and A. E. Hyslop, "ŋƉßSSþÞPreparation and Properties of Boron Arsenide Films," *Journal of The Electrochemical Society*, vol. 121, no. 3, p. 412, 1974, ISSN: 00134651. DOI: 10.1149/1.2401826.

[58] S. M. Ku, "ŋƉßSSþÞPreparation and Properties of Boron Arsenides and Boron Arsenide-Gallium Arsenide Mixed Crystals," *Journal of The Electrochemical Society*, vol. 113, no. 8, p. 813, 1966, ISSN: 00134651. DOI: 10.1149/1.2424125.

[59] D. J. Srvxzr, "ŋƉßSSþÞElectronic Structure and Optical Spectrum of Boron Arsenide," Tech. Rep. 8, 1970.

[60] V. K. Gupta, M. W. Koch, N. J. Watkins, Y. Gao, and G. W. Wicks, "ŋƉßSSþÞMolecular beam epitaxial growth of BGaAs ternary compounds," *Journal of Electronic Materials*, vol. 29, no. 12, pp. 1387–1391, Dec. 2000, ISSN: 03615235. DOI: 10.1007/s11664-000-0123-3. [Online]. Available: http://link.springer.com/10.1007/s11664-000-0123-3.

[61] M. Guemou, B. Bouhafs, A. Abdiche, R. Khenata, Y. Al Douri, and S. Bin Omran, "ŋƉßSSþÞFirst-principles calculations of the structural, electronic and optical properties of cubic B xGa 1-xAs alloys," *Physica B: Condensed Matter*, vol. 407, no. 8, pp. 1292–1300, Apr. 2012, ISSN: 09214526. DOI: 10.1016/j.physb.2012.01.132.

[62] S. Ilahi, F. Saidi, R. Hamila, N. Yacoubi, H. Maaref, and L. Auvray, "ŋƉßSSþÞShift of the gap energy and thermal conductivity in BGaAs/GaAs alloys," *Physica B: Condensed Matter*, vol. 421, pp. 105–109, Jul. 2013, ISSN: 09214526. DOI: 10.1016/j.physb.2013.03.045.

[63] S. Azzi, A. Zaoui, and M. Ferhat, "ŋƉßSSþÞOn the importance of the band gap bowing in Boron-based III-V ternary alloys," *Solid State Communications*, vol. 144, no. 5-6, pp. 245–248, Nov. 2007, ISSN: 00381098. DOI: 10.1016/j.ssc.2007.08.017.

[64] R. Kudrawiec, M. P. Polak, K. M. Mcnicholas, J. Kopaczek, M. A. Wistey, and S. R. Bank, "ŋƉßSSþÞBowing of the band gap and spin-orbit splitting energy in BGaAs," *Mater. Res. Express*, vol. 6, p. 125 913, 2019. DOI: 10.1088/2053-1591/ab62e9. [Online]. Available: https://doi.org/10.1088/2053-1591/ab62e9.

[65] R. Hamila, F. Saidi, A. Fouzri, L. Auvray, Y. Monteil, and H. Maaref, "ŋƉßSSþÞClustering effects in optical properties of BGaAs/GaAs epilayers," *Journal of Luminescence*, vol. 129, no. 9, pp. 1010–1014, Sep. 2009, ISSN: 00222313. DOI: 10.1016/j.jlumin.2009.04.013.

[66] K. M. McNicholas, R. H. El-Jaroudi, and S. R. Bank, "ŋƉßSSþÞKinetically Limited Molecular Beam Epitaxy of B x Ga 1– x As Alloys," *Crystal Growth & Design*, vol. 22, p. 59, 2021, ISSN: 1528-7483. DOI: 10.1021/acs.cgd.1c00291.

[67] V. Gottschalch, G. Leibiger, and G. Benndorf, "ŋƉßSSþÞMOVPE growth of B x Ga 1Àx As, B x Ga 1ÀxÀy In y As, and B x Al 1Àx As alloys on (0 0 1) GaAs," Tech. Rep., 2003, pp. 468–473.

[68] R. Hamila, F. Saidi, P. H. Rodriguez, L. Auvray, Y. Monteil, and H. Maaref, "ŋƉßSSþÞ-Growth temperature effects on boron incorporation and optical properties of BGaAs/GaAs grown by MOCVD," *Journal of Alloys and Compounds*, vol. 506, no. 1, pp. 10–13, Sep. 2010, ISSN: 09258388. DOI: 10.1016/j.jallcom.2010.06.169.

[69] R. Hamila, F. Saidi, H. Maaref, P. Rodriguez, and L. Auvray, "ŋƉßSSþÞPhotoluminescence properties and high resolution x-ray diffraction investigation of BInGaAs/GaAs grown by the metalorganic vapour phase epitaxy method," *Journal of Applied Physics*, vol. 112, no. 6, p. 063 109, Sep. 2012, ISSN: 0021-8979. DOI: 10.1063/1.4752031. [Online]. Available: http://aip.scitation.org/doi/10.1063/1.4752031.

[70] F. Saidi, F. Hassen, H. Maaref, H. Dumont, and Y. Monteil, "ŋƉßSSþÞOptical study of BxGa1-xAs/GaAs epilayers," in *Materials Science and Engineering C*, vol. 26, Elsevier BV, Mar. 2006, pp. 236–239. DOI: 10.1016/j.msec.2005.10.056.

[71] Q. Wang, Z. Jia, X. Ren, Y. Yan, Z. Bian, X. Zhang, S. Cai, and Y. Huang, "ŋƉßSSþÞEffect of boron incorporation on the structural and photoluminescence properties of highly-strained InxGa1-xAs/GaAs multiple quantum wells," *AIP Advances*, vol. 3, no. 7, p. 72 111, Jul. 2013. DOI: 10.1063/1.4815971.

[72] Q. Wang, X. Ren, X. Guo, T. Li, P. Wang, X. Zhang, Y. Huang, X. Duan, and S. Cai, "ŋƉßSSþÞOver 1.3 μm emission from (B) InAs/GaAs quantum dots capped by InGaAs strain-reducing layer," in *19th In Symposium Nanostructures: Physics and Technology*, 2011, p. 85.

[73] T. Hidouri, F. Saidi, H. Maaref, P. Rodriguez, and L. Auvray, "ŋƉßSSþÞLSE investigation of the thermal effect on band gap energy and thermodynamic parameters of BInGaAs/GaAs Single Quantum Well," *Optical Materials*, vol. 62, pp. 267–272, Dec. 2016, ISSN: 09253467. DOI: 10.1016/j.optmat.2016.10.010. [Online]. Available: https://linkinghub.elsevier.com/retrieve/pii/S0925346716305596.

[74] T. Hidouri, R. Hamila, I. Fraj, F. Saidi, H. Maaref, P. Rodriguez, and L. Auvray, "ŋƉßSSþÞInvestigation of the localization phenomenon in quaternary BInGaAs/GaAs for optoelectronic applications," *Superlattices and Microstructures*, vol. 103, pp. 386–394, 2017, ISSN: 10963677. DOI: 10.1016/j.spmi.2016.10.021. [Online]. Available: http://dx.doi.org/10.1016/j.spmi.2016.10.021.

[75] G. B. Stringfellow and G. S. Chen, "ŋƉßSSþÞAtomic ordering in III/V semiconductor alloys," *Citation: Journal of Vacuum Science & Technology B: Microelectronics and Nanometer Structures Processing*, vol. 9, p. 2182, 1991. DOI: 10.1116/1.585761. [Online]. Available: https://doi.org/10.1116/1.585761.

[76] G. B. Stringfellow, "ŋƉßSSþÞThermodynamic considerations for epitaxial growth of III/V alloys," *Journal of Crystal Growth*, vol. 468, no. November 2016, pp. 11–16, 2017, ISSN: 00220248. DOI: 10.1016/j.jcrysgro.2016.11.062. [Online]. Available: http://dx.doi.org/10.1016/j.jcrysgro.2016.11.062.

[77] A. J. Springthorpe and P. Mandeville, "ŋƉßSSþÞMass spectrometry during molecular-beam epitaxy: An alternative to reflection high-energy electron diffraction," *Citation: Journal of Vacuum Science & Technology B: Microelectronics Processing and Phenomena*, vol. 6, p. 754, 1988. DOI: 10.1116/1.584366. [Online]. Available: https://doi.org/10.1116/1.584366.

[78] A. Jasik, A. Wnuk, J. Gaca, M. Wójcik, A. Wójcik-Jedlińska, J. Muszalski, and W. Strupiński, "ŋƉßSSþÞThe influence of the growth rate and V/III ratio on the crystal quality of InGaAs/GaAs QW structures grown by MBE and MOCVD methods," *Journal of Crystal Growth*, vol. 311, no. 19, pp. 4423–4432, Sep. 2009, ISSN: 00220248. DOI: 10.1016/j.jcrysgro.2009.07.032.

[79] T. Nishinaga, X. Q. Shen, and D. Kishimoto, "ŋƉßSSþÞSurface diffusion length of cation incorporation studied by microprobe-RHEED/SEM MBE," *Journal of Crystal Growth*, vol. 163, no. 1-2, pp. 60–66, May 1996, ISSN: 00220248. DOI: 10.1016/0022-0248(95)01050-5.

[80] A. Yamashiki and T. Nishinaga, "ŋƉßSSþÞArsenide pressure dependence of incorporation diffusion length on (0 0 1) and (1 1 0) surfaces and inter-surface diffusion in MBE of GaAs," *Journal of Crystal Growth*, vol. 198-199, no. pt 2, pp. 1125–1129, Mar. 1999, ISSN: 00220248. DOI: 10.1016/S0022-0248(98)01135-X.

[81] O. A. Ageev, M. S. Solodovnik, S. V. Balakirev, I. A. Mikhaylin, and M. M. Eremenko, "ŋƉßSSþÞMonte Carlo simulation of the kinetic effects on GaAs/GaAs(001) MBE growth," *Journal of Crystal Growth*, vol. 457, pp. 46–51, Jan. 2017, ISSN: 00220248. DOI: 10.1016/j.jcrysgro.2016.05.039.

[82] R. F. C. Farrow, "ŋƉßSSþÞMolecular beam epitaxy : applications to key materials," p. 772, 1995.

[83] T. Nishinaga and X. Shen, *Advances in the Understanding of Crystal Growth Mechanisms*. Elsevier, 1999, pp. 117–130, ISBN: 9780444825049. DOI: 10.1016/c2009-0-13276-2. [Online]. Available: https://books.google.com/books?hl=en&lr=&id=GyTqxnr-uc8C&oi=fnd&pg=PA117&dq=Nishinaga+Shen+Inter-surface+diffusion+of+cation+incorporation+in+MBE&ots=ROa5hqles0&sig=z31CJ5Kdb0c7DEdS_zI8g69pp0c#v=onepage&q=Nishinaga%2520Shen%2520Inter-surface%2520diffusion.

[84] J. H. Neave, P. J. Dobson, J. J. Harris, P. Dawson, and B. A. Joyce, "ŋƉßSSþÞSilicon doping of MBE-grown GaAs films," *Applied Physics A Solids and Surfaces*, vol. 32, no. 4, pp. 195–200, 1983, ISSN: 07217250. DOI: 10.1007/BF00820260.

[85] T. Ogura, D. Kishimoto, and T. Nishinaga, "ŋƉßSSþÞEffect of As molecular species on inter-surface diffusion in GaAs MBE for ridge structure fabrication," *Journal of Crystal Growth*, vol. 226, no. 2-3, pp. 179–184, Jun. 2001, ISSN: 00220248. DOI: 10.1016/S0022-0248(01)01020-X.

[86] H. S. Loka, S. D. Benjamin, and P. W. Smith, "ŋƉßSSþÞOptical characterization of low-temperature-grown GaAs for ultrafast all-optical switching devices," *IEEE Journal of Quantum Electronics*, vol. 34, no. 8, pp. 1426–1436, 1998, ISSN: 00189197. DOI: 10.1109/3.704335.

[87] N. Q. Thinh, I. A. Buyanova, W. M. Chen, H. P. Xin, and C. W. Tu, "ŋƉßSSþÞFormation of nonradiative defects in molecular beam epitaxial GaNxAs1x studied by optically detected magnetic resonance," *Applied Physics Letters*, vol. 79, no. 19, pp. 3089–3091, Nov. 2001, ISSN: 0003-6951. DOI: 10.1063/1.1416155. [Online]. Available: http://aip.scitation.org/doi/10.1063/1.1416155.

[88] S. R. Bank, H. B. Yuen, M. A. Wistey, V. Lordi, H. P. Bae, and J. S. Harris, "ŋƉßSSþÞEffects of growth temperature on the structural and optical properties of 1.55μm GaInNAsSb quantum wells grown on GaAs," *Applied Physics Letters*, vol. 87, no. 2, p. 021 908, Jul. 2005, ISSN: 0003-6951. DOI: 10.1063/1.1993772. [Online]. Available: http://apl.aip.org/about/rights_and_permissions%20http://aip.scitation.org/doi/10.1063/1.1993772.

[89] M. Copel, M. C. Reuter, M. Horn Von Hoegen, and R. M. Tromp, "ŋƉßSSþÞInfluence of surfactants in Ge and Si epitaxy on Si(001)," vol. 42, pp. 15–1990,

[90] J. Massies and N. Grandjean, "ŋƉßSSþÞSurfactant effect on the surface diffusion length in epitaxial growth," *Physical Review B*, vol. 48, no. 11, pp. 8502–8505, 1993, ISSN: 01631829. DOI: 10.1103/PhysRevB.48.8502.

[91] S. Iwanari and K. Takayanagi, "ŋƉßSSþÞSurfactant epitaxy of Si on Si(111) surface mediated by a Sn layer I. Reflection electron microscope observation of the growth with and without a Sn layer mediate the step flow," *Journal of Crystal Growth*, vol. 119, no. 3-4, pp. 229–240, May 1992, ISSN: 0022-0248. DOI: 10.1016/0022-0248(92)90675-9.

[92] K. Volz, V. Gambin, W. Ha, M. A. Wistey, H. Yuen, S. Bank, and J. S. Harris, "ŋƉßSSþÞThe role of Sb in the MBE growth of (GaIn)(NAsSb)," *Journal of Crystal Growth*, vol. 251, no. 1-4, pp. 360–366, Apr. 2003, ISSN: 0022-0248. DOI: 10.1016/S0022-0248(02)02198-X.

[93] M. Copel, M. C. Reuter, E. Kaxiras, and R. M. Tromp, "ŋƉßSSþÞPHYSICAL REVIEW LETTERS Snrfactants in Epitaxial Growth," vol. 63, no. 6, 1989.

[94] H. J. Osten, J. Klatt, G. Lippert, E. Bugiel, and S. Higuchi, "ŋƉßSSþÞSurfactant-mediated growth of germanium on silicon (001) with submonolayer coverage of Sb and Te," *Journal of Applied Physics*, vol. 74, no. 4, pp. 2507–2511, 1993, ISSN: 00218979. DOI: 10.1063/1.354690. [Online]. Available: https://doi.org/10.1063/1.354690.

[95] H. Nakahara and M. Ichikawa, "ŋƉßSSþÞMolecular beam epitaxial growth of Si on Ga-activated Si(111) surface," *Appl. Phys. Lett*, vol. 61, p. 1531, 1992. DOI: 10.1063/1.107538. [Online]. Available: https://doi.org/10.1063/1.107538.

[96] J. Massies, N. Grandjean, and V. H. Etgens, "ŋƉßSSþÞSurfactant mediated epitaxial growth of InxGa1-xAs on GaAs (001)," *Applied Physics Letters*, vol. 61, no. 1, pp. 99–101, Jun. 1992, ISSN: 00036951. DOI: 10.1063/1.107626. [Online]. Available: https://aip.scitation.org/doi/abs/10.1063/1.107626.

[97] M. R. Pillai, S.-S. Kim, S. T. Ho, and S. A. Barnett, "ŋƉßSSþÞGrowth of In[sub x]Ga[sub 1x]As/GaAs heterostructures using Bi as a surfactant," *Journal of Vacuum Science & Technology B: Microelectronics and Nanometer Structures*, vol. 18, no. 3, p. 1232, 2000, ISSN: 0734211X. DOI: 10.1116/1.591367.

[98] G. S. Petrich, A. M. Dabiran, J. E. Macdonald, and P. I. Cohen, "ŋƉßSSþÞThe effect of submonolayer Sn δ-doping layers on the growth of InGaAs and GaAs The effect of submonolayer Sn S
doping layers on the growth of InGaAs and GaAs," *Citation: Journal of Vacuum Science & Technology B: Microelectronics and Nanometer Structures Processing*, vol. 9, p. 2150, 1991. DOI: 10.1116/1.585755. [Online]. Available: https://doi.org/10.1116/1.585755.

[99] S. Tixier, M. Adamcyk, E. Young, J. Schmid, and T. Tiedje, "ŋƉßSSþÞSurfactant enhanced growth of GaNAs and InGaNAs using bismuth," *Journal of Crystal Growth*, vol. 1-4, no. 251, pp. 449–454, Apr. 2003, ISSN: 0022-0248. DOI: 10.1016/S0022-0248(02)02217-0. [Online]. Available: https://www.infona.pl//resource/bwmeta1.element.elsevier-3cf43060-8c45-34b6-9c89-e9fd0a970838.

[100] A. Ptak, D. Beaton, and A. Mascarenhas, "ŋƉßSSþÞGrowth of BGaAs by molecular-beam epitaxy and the effects of a bismuth surfactant," *Journal of Crystal Growth*, vol. 351, no. 1, pp. 122–125, Jul. 2012, ISSN: 00220248. DOI: 10.1016/j.jcrysgro.2012.04.026. [Online]. Available: https://linkinghub.elsevier.com/retrieve/pii/S0022024812002928.

[101] S. Tixier, M. Adamcyk, T. Tiedje, S. Francoeur, A. Mascarenhas, P. Wei, and F. Schiettekatte, "ŋƉßSSþÞMolecular beam epitaxy growth of GaAs1-xBix," *Applied Physics Letters*, vol. 82, no. 14, pp. 2245–2247, Apr. 2003, ISSN: 00036951. DOI: 10.1063/1.1565499.

[102] M. Kondow, K. Uomi, A. Niwa, T. Kitatani, S. Watahiki, and Y. Yazawa, "ŋƉßSSþÞ-GaInNAs: A Novel Material for Long-Wavelength-Range Laser Diodes with Excellent High-Temperature Performance," *Japanese Journal of Applied Physics*, vol. 35, no. Part 1, No. 2B, pp. 1273–1275, Feb. 1996. DOI: 10.1143/jjap.35.1273.

[103] S. Fahy and E. P. O'Reilly, "ŋƉßSSþÞIntrinsic limits on electron mobility in dilute nitride semiconductors," *Applied Physics Letters*, vol. 83, no. 18, pp. 3731–3733, 2003, ISSN: 00036951. DOI: 10.1063/1.1622444. [Online]. Available: https://doi.org/10.1063/1.1622444.

[104] D. A. Beaton, R. B. Lewis, M. Masnadi-Shirazi, and T. Tiedje, "ŋƉßSSþÞTemperature dependence of hole mobility in GaAs1-xBix alloys," *Journal of Applied Physics*, vol. 108, no. 8, p. 83 708, 2010, ISSN: 00218979. DOI: 10.1063/1.3493734. [Online]. Available: https://doi.org/10.1063/1.3493734.

[105] R. N. Kini, A. J. Ptak, B. Fluegel, R. France, R. C. Reedy, and A. Mascarenhas, "ŋƉßSSþÞ-Effect of Bi alloying on the hole transport in the dilute bismide alloy GaAs1-xBix," *Physical Review B - Condensed Matter and Materials Physics*, vol. 83, no. 7, pp. 1–6, 2011, ISSN: 10980121. DOI: 10.1103/PhysRevB.83.075307.

[106] R. Mouillet, L. A. De Vaulchier, E. Deleporte, Y. Guldner, L. Travers, and J. C. Harmand, "ŋƉßSSþÞRole of nitrogen in the mobility drop of electrons in modulation-doped GaAsN/AlGaAs heterostructures," *Solid State Communications*, vol. 126, no. 6, pp. 333–337, 2003, ISSN: 00381098. DOI: 10.1016/S0038-1098(03)00140-6. [Online]. Available: www.elsevier.com/locate/ssc.

[107] D. G. Cooke, F. A. Hegmann, E. C. Young, and T. Tiedje, "ŋƉßSSþÞElectron mobility in dilute GaAs bismide and nitride alloys measured by time-resolved terahertz spectroscopy," *Applied Physics Letters*, vol. 89, no. 12, p. 122 103, 2006, ISSN: 00036951. DOI: 10.1063/1.2349314. [Online]. Available: https://doi.org/10.1063/1.2349314.

[108] G. Vardar, S. W. Paleg, M. V. Warren, M. Kang, S. Jeon, and R. S. Goldman, "ŋƉßSSþÞMechanisms of droplet formation and Bi incorporation during molecular beam epitaxy of GaAsBi," *Applied Physics Letters*, vol. 102, no. 4, p. 042 106, Jan. 2013, ISSN: 0003-6951. DOI: 10.1063/1.4789369. [Online]. Available: https://aip.scitation.org/doi/abs/10.1063/1.4789369.

[109] X. Lu, D. A. Beaton, R. B. Lewis, T. Tiedje, and M. B. Whitwick, "ŋƉßSSþÞEffect of molecular beam epitaxy growth conditions on the Bi content of GaAs 1x Bi x," 2008. DOI: 10.1063/1.2918844.

[110] M. Yoshimoto, S. Murata, A. Chayahara, Y. Horino, J. Saraie, and K. Oe, "ŋƉßSSþÞMetastable GaAsBi Alloy Grown by Molecular Beam Epitaxy," *Japanese Journal of Applied Physics*, vol. 42, no. 10B, p. L1235, Oct. 2003, ISSN: 1347-4065. DOI: 10.1143/JJAP.42.L1235. [Online]. Available: https://iopscience.iop.org/article/10.1143/JJAP.42.L1235%20https://iopscience.iop.org/article/10.1143/JJAP.42.L1235/meta.

[111] A. J. Ptak, R. France, D. A. Beaton, K. Alberi, J. Simon, A. Mascarenhas, and C.-S. Jiang, "ŋƉßSSþÞKinetically limited growth of GaAsBi by molecular-beam epitaxy," *Journal of Crystal Growth*, vol. 338, no. 1, pp. 107–110, Jan. 2012. DOI: 10.1016/j.jcrysgro.2011.10.040.

[112] S. G. Spruytte, M. C. Larson, W. Wampler, C. W. Coldren, H. E. Petersen, and J. S. Harris, "ŋƉßSSþÞNitrogen incorporation in group IIInitridearsenide materials grown by elemental source molecular beam epitaxy," *Journal of Crystal Growth*, vol. 227-228, pp. 506–515, Jul. 2001. DOI: 10.1016/s0022-0248(01)00757-6.

[113] A. J. Ptak, D. A. Beaton, and A. Mascarenhas, "ŋƉßSSþÞGrowth of BGaAs by molecular-beam epitaxy and the effects of a bismuth surfactant," *Journal of Crystal Growth*, vol. 351, no. 1, pp. 122–125, Jul. 2012. DOI: 10.1016/j.jcrysgro.2012.04.026.

[114] H. Detz, D. MacFarland, T. Zederbauer, S. Lancaster, A. M. Andrews, W. Schrenk, and G. Strasser, "ŋƉßSSþÞGrowth rate dependence of boron incorporation into BxGa1xAs layers," *Journal of Crystal Growth*, vol. 477, pp. 77–81, Nov. 2017, ISSN: 00220248. DOI: 10.1016/j.jcrysgro.2017.02.043.

[115] H. Dumont, D. Rutzinger, C. Vincent, J. Dazord, Y. Monteil, F. Alexandre, and J. L. Gentner, "ŋƉßSSþÞSurface segregation of boron in BxGa1-xAs/GaAs epilayers studied by x-ray photoelectron spectroscopy and atomic force microscopy," *Applied Physics Letters*, vol. 82, no. 12, pp. 1830–1832, Mar. 2003, ISSN: 00036951. DOI: 10.1063/1.1561164. [Online]. Available: http://aip.scitation.org/doi/10.1063/1.1561164.

[116] Y. P. Varshni, "ŋƉßSSþÞTemperature dependence of the energy gap in semiconductors," *Physica*, vol. 34, no. 1, pp. 149–154, Jan. 1967, ISSN: 0031-8914. DOI: 10.1016/0031-8914(67)90062-6.

[117] A. Polimeni, M. Capizzi, M. Geddo, M. Fischer, M. Reinhardt, and A. Forchel, "ŋƉßSSþÞEffect of temperature on the optical properties of (InGa)(AsN)/GaAs single quantum wells," *Applied Physics Letters*, vol. 77, no. 18, p. 2870, Oct. 2000, ISSN: 0003-6951. DOI: 10.1063/1.1320849. [Online]. Available: https://aip.scitation.org/doi/abs/10.1063/1.1320849.

[118] R. A. Mair, J. Y. Lin, H. X. Jiang, E. D. Jones, A. A. Allerman, and S. R. Kurtz, "ŋƉßSSþÞTime-resolved photoluminescence studies of InxGa1xAs1yNy," *Applied Physics Letters*, vol. 76, no. 2, p. 188, Jan. 2000, ISSN: 0003-6951. DOI: 10.1063/1.125698. [Online]. Available: https://aip.scitation.org/doi/abs/10.1063/1.125698.

[119] S. Shirakata, M. Kondow, and T. Kitatani, "ŋƉßSSþÞTemperature-dependent photoluminescence of high-quality GaInNAs single quantum wells ARTICLES YOU MAY BE INTERESTED IN," *Cite as: Appl. Phys. Lett*, vol. 80, p. 2087, 2002. DOI: 10.1063/1.1463208. [Online]. Available: https://doi.org/10.1063/1.1463208.

[120] R. Kudrawiec and J. Misiewicz, "ŋƉßSSþÞPhotoreflectance and contactless electroreflectance measurements of semiconductor structures by using bright and dark configurations ARTICLES YOU MAY BE INTERESTED IN," *Rev. Sci. Instrum*, vol. 80, p. 96 103, 2009. DOI: 10.1063/1.3213613. [Online]. Available: https://doi.org/10.1063/1.3213613.

[121] A. H. Jones, "ŋƉßSSþÞAlxIn1-xAsySb1-y Digital Alloy Avalanche Photodiodes for Low-Noise Applications," Ph.D. dissertation, University of Virginia, 2020.

[122] M. H. Woods, W. C. Johnson, and M. A. Lampert, "ŋƉßSSþÞUse of a Schottky barrier to measure impact ionization coefficients in semiconductors," *Solid-State Electronics*, vol. 16, no. 3, pp. 381–394, Mar. 1973, ISSN: 0038-1101. DOI: 10.1016/0038-1101(73)90013-0.

[123] National Institute of Standards and Technology, *ŋƉßSSþÞHall Effect Measurements*, 2008. [Online]. Available: https://www.nist.gov/pml/nanoscale-device-characterization-division/popular-links/hall-effect.

[124] G. E. Stillman, M. Kim, B. Lee, and T. Low, "ŋƉßSSþÞCharacterization and Properties of Semiconductors," in *Handbook on Semiconductors*, T. Moss and S. Mahajan, Eds., 3rd ed., Elsevier Science B.V., 1994, ch. 10, pp. 783–994.

[125] H. Duschanek and P. Rogl, "ŋƉßSSþÞCritical Assessment and Thermodynamic Calculation of the Binary System Boron-Tunsten (B-W)," *Journal of Phase Equilibria*, vol. 16, no. 2, pp. 150–161, 1995.

[126] H. Ye, Y. Song, Y. Gu, and S. Wang, "ŋƉßSSþÞLight emission from InGaAs:Bi/GaAs quantum wells at 1.3 m," *AIP Advances*, vol. 2, no. 4, p. 42 158, Dec. 2012. DOI: 10.1063/1.4769102.

[127] N. Tansu, Y.-L. Chang, T. Takeuchi, D. P. Bour, S. W. Corzine, M. R. T. Tan, and L. J. Mawst, "ŋƉßSSþÞTemperature analysis and characteristics of highly strained InGaAs-GaAsP-GaAs (&lt 1.17 m) quantum-well lasers," *IEEE Journal of Quantum Electronics*, vol. 38, no. 6, pp. 640–651, Jun. 2002. DOI: 10.1109/jqe.2002.1005415.

[128] A. J. Ptak, S. W. Johnston, S. Kurtz, D. J. Friedman, and W. K. Metzger, "ŋƉßSSþÞA comparison of MBE- and MOCVD-grown GaInNAs," *Journal of Crystal Growth*, vol. 251, no. 1-4, pp. 392–398, Apr. 2003. DOI: 10.1016/s0022-0248(02)02201-7.

[129] E. C. Larkins and J. S. Harris, "ŋƉßSSþÞMolecular Beam Epitaxy of High-Quality GaAs and AlGaAs," in *Molecular Beam Epitaxy*, Elsevier, 1995, pp. 114–274. DOI: 10.1016/B978-081551371-1.50004-4. [Online]. Available: https://linkinghub.elsevier.com/retrieve/pii/B9780815513711500044.

[130] J. M. Moison, F. Houzay, F. Barthe, J. M. Gérard, B. Jusserand, J. Massies, and F. S. Turco-Sandroff, "ŋƉßSSþÞSurface segregation in 111—V alloys," *Journal of crystal growth*, vol. 111, pp. 144–150, 1991.

[131] K. Akimoto, M. Kamada, K. Taira, M. Arai, and N. Watanabe, "ŋƉßSSþÞPhotoluminescence killer center in AlGaAs grown by molecular-beam epitaxy," *Journal of Applied Physics*, vol. 59, no. 8, p. 2833, Aug. 1998, ISSN: 0021-8979. DOI: 10.1063/1.336938. [Online]. Available: https://aip.scitation.org/doi/abs/10.1063/1.336938.

[132] T. Hayakawa, M. Kondo, T. Suyama, K. Takahashi, S. Yamamoto, S. Yano, and T. Hijikata, "ŋƉßSSþÞEffect of group V/III flux ratio on deep electron traps in AlxGa1xAs (x=0.7) grown by molecular beam epitaxy," *Applied Physics Letters*, vol. 49, no. 13, p. 788, Jun. 1998, ISSN: 0003-6951. DOI: 10.1063/1.97547. [Online]. Available: https://aip-scitation-org.ezproxy.lib.utexas.edu/doi/abs/10.1063/1.97547.

[133] C. E. C. Wood, D. V. Morgan, and L. Rathbun, "ŋƉßSSþÞMolecular-beam epitaxial group III arsenide alloys: Effect of substrate temperature on composition," *Journal of Applied Physics*, vol. 53, no. 6, p. 4524, Jun. 1998, ISSN: 0021-8979. DOI: 10.1063/1.331195. [Online]. Available: https://aip-scitation-org.ezproxy.lib.utexas.edu/doi/abs/10.1063/1.331195.

[134] H. H. Tan, P. Lever, and C. Jagadish, "ŋƉßSSþÞGrowth of highly strained InGaAs quantum wells on GaAs substrates - Effect of growth rate," *Journal of Crystal Growth*, vol. 274, no. 1-2, pp. 85–89, Jan. 2005, ISSN: 00220248. DOI: 10.1016/j.jcrysgro.2004.10.031.

[135] S. R. Bank, M. A. Wistey, H. B. Yuen, L. L. Goddard, H. Bae, and J. S. Harris, "ŋƉßSSþÞMolecular-beam epitaxy growth of low-threshold cw GaInNAsSb lasers at 1.5 μm," *Journal of Vacuum Science & Technology B: Microelectronics and Nanometer Structures*, vol. 23, no. 3, p. 1337, 2005, ISSN: 0734211X. DOI: 10.1116/1.1914825.

[136] J. Teubert, P. J. Klar, W. Heimbrodt, V. Gottschalch, A. Lindsay, and E. P. O'Reilly, "ŋƉßSSþÞEffect of localized B and N states on the magneto-transport of (B,Ga,In)As and (Ga,In)(N,As)," *physica status solidi (b)*, vol. 244, no. 1, pp. 431–436, Jan. 2007, ISSN: 03701972. DOI: 10.1002/pssb.200672540. [Online]. Available: http://doi.wiley.com/10.1002/pssb.200672540.

[137] E. F. Schubert, "ŋƉßSSþÞDoping in III-V Semiconductors," *Doping in III-V Semiconductors*, Sep. 1993. DOI: 10.1017/CBO9780511599828. [Online]. Available: https://www.cambridge.org/core/books/doping-in-iiiv-semiconductors/F05AEE3D3139B07CE4F3556B1360B869.

[138] H. P. Xin, K. L. Kavanagh, M. Kondow, and C. W. Tu, "ŋƉßSSþÞEffects of rapid thermal annealing on GaInNAs/GaAs multiple quantum wells," *Journal of Crystal Growth*, vol. 201-202, pp. 419–422, May 1999. DOI: 10.1016/s0022-0248(98)01366-9.

[139] K. Volz, J. Koch, B. Kunert, I. Nemeth, and W. Stolz, "ŋƉßSSþÞInfluence of annealing on the optical and structural properties of dilute N-containing III/V semiconductor heterostructures," *Journal of Crystal Growth*, vol. 298, pp. 126–130, Jan. 2007, ISSN: 00220248. DOI: 10.1016/j.jcrysgro.2006.10.014. [Online]. Available: https://linkinghub.elsevier.com/retrieve/pii/S0022024806009572.

[140] V. Lordi, H. B. Yuen, S. R. Bank, M. A. Wistey, J. S. Harris, and S. Friedrich, "ŋƉßSSþÞNearest-neighbor distributions inGa1-xInxNyAs1-yandGa1-xInxNyAs1-y-zSbzthin films upon annealing," *Physical Review B*, vol. 71, no. 12, Mar. 2005. DOI: 10.1103/physrevb.71.125309.

[141] E. V. K. Rao, A. Ougazzaden, Y. L. Bellego, and M. Juhel, "ŋƉßSSþÞOptical properties of low band gap GaAs(1-x)Nx layers: Influence of post-growth treatments," *Applied Physics Letters*, vol. 72, no. 12, pp. 1409–1411, Mar. 1998. DOI: 10.1063/1.120579.

[142] T. Kageyama, T. Miyamoto, S. Makino, F. Koyama, and K. Iga, "ŋƉßSSþÞThermal Annealing of GaInNAs/GaAs Quantum Wells Grown by Chemical Beam Epitaxy and Its Effect on Photoluminescence," *Japanese Journal of Applied Physics*, vol. 38, no. Part 2, No. 3B, pp. L298–L300, Mar. 1999. DOI: 10.1143/jjap.38.l298.

[143] S. R. Bank, H. B. Yuen, H. Bae, M. A. Wistey, and J. S. Harris, "ŋƉßSSþÞOverannealing effects in GaInNAs(Sb) alloys and their importance to laser applications," *Applied Physics Letters*, vol. 88, no. 22, p. 221 115, May 2006. DOI: 10.1063/1.2208375.

[144] C. Hu, K. A. Anselm, B. G. Streetman, and J. C. Campbell, "ŋƉßSSþÞNoise characteristics of thin multiplication region GaAs avalanche photodiodes," *Applied Physics Letters*, vol. 69, no. 24, pp. 3734–3736, Jun. 1996, ISSN: 00036951. DOI: 10.1063/1.117205. [Online]. Available: https://aip.scitation.org/doi/abs/10.1063/1.117205.

[145] T. H. Wu, Y. K. Su, R. W. Chuang, C. Y. Cheng, and Y. C. Lin, "ŋƉßSSþÞCharacterization of the post-thermal annealing effect for p-GaAs/i-InGaAsN/n-GaAs hetero-junction solar cells," *Solar Energy Materials and Solar Cells*, vol. 107, pp. 344–347, 2012, ISSN: 09270248. DOI: 10.1016/j.solmat.2012.07.010. [Online]. Available: http://dx.doi.org/10.1016/j.solmat.2012.07.010.

[146] K. Volz, D. Lackner, I. Németh, B. Kunert, W. Stolz, C. Baur, F. Dimroth, and A. W. Bett, "ŋƉßSSþÞOptimization of annealing conditions of (GaIn)(NAs) for solar cell applications," *Journal of Crystal Growth*, vol. 310, no. 7-9, pp. 2222–2228, 2008, ISSN: 00220248. DOI: 10.1016/j.jcrysgro.2007.11.199.

[147] D. R. Fink, S. Lee, S. H. Kodati, V. Rogers, T. J. Ronningen, M. Winslow, C. H. Grein, A. H. Jones, J. C. Campbell, J. F. Klem, and S. Krishna, "ŋƉßSSþÞDetermination of background doping polarity of unintentionally doped semiconductor layers," *Applied Physics Letters*, vol. 116, no. 7, p. 72 103, 2020, ISSN: 00036951. DOI: 10.1063/1.5142377. [Online]. Available: https://doi.org/10.1063/1.5142377.

[148] D. Chen, J. A. McArthur, S. D. March, X. Xue, A. H. Jones, A. A. Dadey, S. R. Bank, and J. C. Campbell, "ŋƉßSSþÞComparison and analysis of Al0.7InAsSb avalanche photodiodes with different background doping polarities," *Applied Physics Letters*, vol. 119, no. 3, p. 32 101, 2021, ISSN: 00036951. DOI: 10.1063/5.0056300. [Online]. Available: https://doi.org/10.1063/5.0056300.

[149] S. K. Brierley, H. T. Hendriks, W. E. Hoke, P. J. Lemonias, and D. G. Weir, "ŋIJßSSþÞObservation of boron-related photoluminescence in GaAs layers grown by molecular beam epitaxy," *Applied Physics Letters*, vol. 63, no. 6, pp. 812–814, Jun. 1993, ISSN: 00036951. DOI: 10.1063/1.109916. [Online]. Available: https://aip.scitation.org/doi/abs/10.1063/1.109916.

[150] Y. Yuan, J. Zheng, Y. Tan, Y. Peng, A.-K. Rockwell, S. R. Bank, A. Ghosh, and J. C. Campbell, "ŋIJßSSþÞTemperature dependence of the ionization coefficients of InAlAs and AlGaAs digital alloys," *Photonics Research*, vol. 6, no. 8, p. 794, Aug. 2018, ISSN: 2327-9125. DOI: 10.1364/prj.6.000794. [Online]. Available: https://www.osapublishing.org/viewmedia.cfm?uri=prj-6-8-794&seq=0&html=true%20https://www.osapublishing.org/abstract.cfm?uri=prj-6-8-794%20https://www.osapublishing.org/prj/abstract.cfm?uri=prj-6-8-794.

[151] G. E. Bulman, V. M. Robbins, and G. E. Stillman, "ŋIJßSSþÞThe Determination of Impact Ionization Coefficients in (100) Gallium Arsenide Using Avalanche Noise and Photocurrent Multiplication Measurements," *IEEE Transactions on Electron Devices*, vol. 32, no. 11, pp. 2454–2466, 1985. DOI: 10.1109/T-ED.1985.22295.

...